TUDelft

Delft University of Technology

Catalytic ceramic nanofiltration for direct surface water treatment and fenton cleaning

Lin, B.

DOI

10.4233/uuid:aabdc210-7b2a-4e28-808b-9dce5c3b9a43

Publication date

2023

Document Version

Final published version

Citation (APA)

Lin, B. (2023). *Catalytic ceramic nanofiltration for direct surface water treatment and fenton cleaning.* [Dissertation (TU Delft), Delft University of Technology]. https://doi.org/10.4233/uuid:aabdc210-7b2a-4e28-808b-9dce5c3b9a43

Important note

To cite this publication, please use the final published version (if applicable).
Please check the document version above.

CATALYTIC CERAMIC NANOFILTRATION FOR DIRECT SURFACE WATER TREATMENT AND FENTON CLEANING

Bin LIN

Propositions accompanying the dissertation

CATALYTIC CERAMIC NANOFILTRATION FOR DIRECT SURFACE WATER TREATMENT AND FENTON CLEANING

by

Bin LIN

1. Pre-filtration with iron-based catalyst suspensions pre-coats the catalyst on the ceramic nanofiltration membrane surface and not within the inner pores (this thesis).

2. The combination of Fenton oxidation and oxalic acid relaxation fully removes both the cake and adsorptive fouling on an iron oxide pre-coated ceramic nanofiltration membrane (this thesis).

3. Fenton cleaning alone completely removes the cake layer fouling of an iron oxychloride pre-coated ceramic nanofiltration membrane, while partially removing the adsorptive fouling (this thesis).

4. The total permeate production of ceramic nanofiltration is not influenced by the remaining adsorptive fouling after cleaning, since the adsorptive fouling always only occurs at the beginning of the cycle (this thesis).

5. Cleaning efficacy of a membrane process should be evaluated according to the flux recovery measured with a foulant solution rather than measured with pure water.

6. The design and operation of a surface water treatment plant using membrane technologies should not only focus on the rejection of the pollutants, but also on the efficient and eco-friendly cleaning of the membranes.

7. When designing a hybrid water treatment process for removing organic matter, the synergistic effect should be considered in relation to the specific characteristics of the organic matter.

8. Multi-stage pre-treatment of surface water is unnecessary for drinking water production, when an alternative single-step method has the ability to adapt to the complex water matrix.

9. During the development of an international PhD candidate, research institutions should consider his/her future career competitiveness in his/her country of origin.

10. Never let yourself fall down only for a tough moment in your life, since being alive as the sun rises is the best news and power for your days.

These propositions have been approved by the promotors Prof. dr. ir. L.C. Rietveld and Dr. ir. S.G.J. Heijman, and are regarded as opposable and defendable.

CATALYTIC CERAMIC NANOFILTRATION FOR DIRECT SURFACE WATER TREATMENT AND FENTON CLEANING

DISSERTATION

for the purpose of obtaining the degree of doctor
at Delft University of Technology
by the authority of the Rector Magnificus, prof. dr. ir. T.H.J.J. van der Hagen,
chair of the Board for Doctorates
to be defended publicly on
Tuesday 27 June 2023 at 10:00 o'clock

by

Bin LIN

Master of Environmental Engineering, Nanjing University, China
born in Huangshan, China

This dissertation has been approved by the promotors.

Composition of the doctoral committee:

Rector Magnificus	Chairperson
Prof. dr. ir. L.C. Rietveld	Delft University of Technology, promotor
Dr. ir. S.G.J. Heijman	Delft University of Technology, promotor

Independent members:

Prof. dr. M.D. Kennedy	Delft University of Technology / IHE Delft, the Netherlands
Prof. dr. N. Z-X. Low	Nanjing Tech University, China
Prof. dr. ir. J.A.H. Hofman	University of Bath, United Kingdom
Dr. A. Haidari	Brabant Water, the Netherlands
Dr. M.B. Tanis-Kanbur	Technical University of Denmark, Denmark
Prof. dr. ir. J.B. van Lier	Delft University of Technology, reserve member

Printed by: proefschrift-aio.nl

Cover by: Bin LIN

An electronic version of this dissertation is available at https://repository.tudelft.nl/

谨以此书献给我的孩子林霏开，愿你在成长的道路上，勇敢、坚毅、沉着、明智。

CONTENTS

SUMMARY

Over the past decades, direct nanofiltration (NF) without pre-treatment has been widely recognized as an alternative for conventional membrane technologies in both drinking water and wastewater treatment, owing to its advantages in energy saving, low chemical usage and high permeate purity. As an alternative, ceramic NF has received growing attention in recent years, given its good robustness and stable separation capabilities as compared to polymeric NF membranes. Organic fouling of ceramic NF membranes remains the key problem affecting the performance of the membranes in water treatment. However, conventional forward flush with pure water is not effective for removing the organic fouling due to its sticky nature. Backwash with pure water has to be applied at high pressures, thereby having a risk of damaging the structure of the membranes. Therefore, chemical forward flush with strong acids, bases or chlorine is frequently required as a substitute for backwash and conventional forward flush, leading to more consumption of the chemicals. To apply innovative ceramic NF in direct surface water treatment, an eco-friendly cleaning strategy of using Fenton-based oxidation was studied in relation to the fouling characteristic of the membrane.

A literature study was done to review the present knowledge on using oxidation methods for fouling mitigation of ceramic membranes. It was found that existing studies predominantly were focused on direct oxidation of organic substances in feed water of ceramic membrane filtration. This kind of oxidation strategies could mainly reduce cake layer fouling of the membranes, while in many cases aggravating pore clogging due to an oxidation-induced conversion of large-sized organic molecules into smaller ones. Additionally, there is a risk of secondary pollution by using oxidation in the feed water, since the oxidants and potentially produced oxidation by-products can penetrate the membranes into permeate. However, little knowledge is available on using oxidation for cleaning fouling layers, in particular, on a ceramic NF membrane, in terms of the impact of its fouling characteristics on the efficacy of oxidative cleaning. It was thus recommended that, investigating the efficacy and mechanisms of an oxidative cleaning method for ceramic NF membranes, should be based on an in-depth understanding of fouling of the membranes.

To improve the mass transfer efficacy of Fenton oxidation reactions, an integration of oxalic acid chelation and Fenton oxidation was proposed for cleaning alginate fouling of an iron oxide (Fe_3O_4) pre-coated ceramic NF membrane. A synergistic effect of oxalic acid relaxation and Fenton oxidation over the alginate fouling layer was proved to act as a main mechanism for the membrane cleaning, presumably due to improved diffusion of hydrogen peroxide (H_2O_2) through the relaxed fouling layer onto the active sites of the catalyst pre-coat layer. Based on this mechanism, cleaning of the pre-coated membrane using an oxalic acid/H_2O_2 solution for 15 min resulted in stable initial normalized

fluxes (83.33–90.15%) during five repeated fouling/cleaning cycles, without renewing the pre-coat layer between the cycles.

To explore the relation between Fenton cleaning efficacy and different fouling types of an iron oxychloride (FeOCl) pre-coated ceramic NF membrane, an adsorption experiment and cake filtration model fitting were separately executed to distinguish between adsorption and cake layer fouling. The results showed that the flux evolution during filtration with alginate solutions consisted of an initial sharp flux decline, due to rapid adsorption of the foulants (adsorptive fouling), and a subsequent gradual flux decline, resulting from progressive cake build-up on the membrane (cake layer fouling). The efficacy of Fenton cleaning predominantly depended on the cake layer fouling (above the adsorptive fouling layer), where the flux recovery at thin cake layer fouling (98.5%) was higher than at thick cake layer fouling (65.4%). Fenton cleaning was mainly effective for cake layer fouling compared to adsorptive fouling. The total permeate production during ceramic NF was not influenced by the remaining adsorptive fouling (after cleaning), since the adsorptive fouling always only occurs at the beginning of each cycle. Therefore, the removal of the adsorptive fouling was of minor importance for the overall performance of the pre-coated ceramic NF membrane using Fenton cleaning.

To investigate the potential of applying the FeOCl pre-coated ceramic NF membranes for direct surface (canal) water treatment, constant-flux filtration and Fenton cleaning experiments were performed at a bench scale. It was found that the dependence of fouling during ceramic NF on the pre-coat layer and the feed pH was mainly associated with adsorption capabilities of the membrane under the individual conditions. The FeOCl layer was uniformly pre-coated on top of the membrane by means of crossflow pre-filtration with a FeOCl suspension, only resulting in a minimal decrease (<4%) of the membrane permeance. A large-sized fraction (3–30 μm) of the colloids in the canal water, in combination with an operating flux of about $46 \, L \, m^{-2} \, h^{-1}$, contributed to faster pore clogging in the pre-coat layer (with the transmembrane pressure (TMP) increasing from 10.0 to 21.0 bar within 1 h) than in the pristine membrane (with the TMP increasing from 8.0 to 21.0 bar within 4 h). However, the pristine and pre-coated membranes fouled comparably at a flux of around $23 \, L \, m^{-2} \, h^{-1}$ (with the TMP increasing from 5.0 to 11.0 bar and from 5.0 to 9.5 bar, respectively, within 4 h). The catalytic pre-coat layer facilitated the restoration of filtration resistances of the fouled membrane through Fenton cleaning, while the separation layer of the membrane maintained high rejections (approximately 90%) of the natural organic matter (NOM) over five one-day fouling/cleaning cycles.

The pre-coat layer remained reproducible over the five long-running cycles, having a minor loss of 15.6% in its thickness.

Overall, it can be concluded that ceramic NF membranes, containing an iron-based catalyst pre-coat layer (Fe_3O_4 or FeOCl) on top of the membranes, were able to remove the fouling, formed by a highly concentrated alginate solution or NOM/colloids in surface (canal) water, on/in the pre-coated membranes by Fenton cleaning. However, the efficacy of Fenton cleaning varied depending on fouling types (adsorptive and cake layer fouling) and characteristics of the FeOCl pre-coated membranes filtering the alginate solution. The cake layer fouling was almost completely removed by Fenton cleaning in contrast to the adsorptive fouling. A combination of Fenton oxidation and oxalic acid relaxation over the fouling layers improved the overall cleaning efficacy due to a potentially promoted mass transfer of H_2O_2 through the fouling layers onto the active sites of the (Fe_3O_4) pre-coat layer. The FeOCl pre-coated ceramic NF membrane was verified to be applicable in direct surface (canal) water treatment with respect to both rejection of NOM and Fenton cleaning.

Chapter 1

INTRODUCTION

1.1 Surface water treatment for drinking water production

1.1.1 Conventional multiple-stage treatment procedure

Safe and adequate drinking water is one of the basic requirements for the health of human beings. Conventional drinking water treatment contains multiple processing units involving coagulation, flocculation, sedimentation, sand filtration and disinfection (Chang et al., 2017; Ho et al., 2012). The conventional treatment procedure is able to readily meet the criteria of drinking water quality with relatively clean drinking water sources, while being inapplicable to handling water with various organic micro-pollutants (OMPs) and a high concentration of natural organic matter (NOM) due to a potential risk in the formation of disinfection by-products during post-chlorination (Fujioka et al., 2021). Moreover, the cost and quality of drinking water production, using the conventional treatment procedure, often vary with the fluctuations of NOM in its composition and concentration in surface waters (Köhler et al., 2016; Sillanpää et al., 2018). In addition, the conventional multiple-stage drinking water treatment results in a large footprint, complicated operations and large consumption of chemicals (e.g. coagulants and flocculants). Hence, these drawbacks of the conventional treatment procedure call for an urgent need to develop more compact, efficient and eco-friendly drinking water treatment technologies.

1.1.2 Direct nanofiltration as advanced treatment

Direct nanofiltration (NF) is a promising option for treating surface waters without any pre-treatment, in order to perform water treatment processes by a single-step, chemical-free operation (Futselaar et al., 2002). NF membranes typically enables the removal of most organic matter including OMPs (>200–300 Da), a fraction of hardness-causing compounds and multivalent ions, and almost all microbes from surface water (Liikanen et al., 2003; Siddiqui et al., 2000). However, most commercially available NF membranes, e.g. polymeric spiral-wound membranes, are susceptible to biofouling and spacer clogging by colloids in the feed water, which need to be prevented by pre-treatment (e.g. sand filtration, micro- and ultrafiltration (MF/UF)) of the feed water (Dreszer et al., 2014; Wibisono et al., 2015). As an alternative, polyamide thin-film composite membranes can only be operated at a very low flux (e.g. 4 L m^{-2} h^{-1}) to maintain a stable operation during direct surface water treatment (Fujioka et al., 2021). Apart from their high fouling propensity, polymeric NF membranes are sensitive to the use of extreme chemical concentrations, pH and temperature during chemical cleaning (Chen et al., 2003).

1.2 Ceramic nanofiltration membranes

1.2.1 Characteristics and application status in water treatment

Ceramic NF has emerged as a promising substitute for polymeric NF in water treatment, given its good chemical resistance and long lifespan (>15 years) (Kramer et al., 2015; López et al., 2020; Puthai et al., 2016). The commercialization of ceramic NF membranes has been realized by Rauschert (Inopor, Germany). Present studies have also demonstrated the ability of commercial ceramic NF membranes with a molecular weight cut-off (MWCO) of <1 kDa for effectively removing a broad variety of pollutants (e.g. multivalent ions, pathogens, NOM and colloids) while exerting relatively less removal of inorganic salts and low molecular weight OMPs (<200 Da) (Árki et al., 2019; Caltran et al., 2020; Chen et al., 2017; Fujioka et al., 2014).

Currently, applications of ceramic NF membranes have been tested on a lab scale in direct water reclamation from sewage and secondary wastewater effluent (Fujioka et al., 2018; Kramer et al., 2015). A pilot-scale plant of industrial ceramic NF, containing a total filtration area of about 234 m^2, was established on an oil field in Canada and ran for more than 12500 h to treat the wastewater directly on a daily basis (Cabrera et al., 2022). In this pilot application, according to Motta Cabrera et al. (2021), the capital investment was approximately 5% higher in the ceramic NF system than in the polymeric NF system at similar capacities, but the annual operating cost was around 55% less for the ceramic NF system because of its lower maintenance cost. However, studies or applications regarding ceramic NF in surface water treatment for drinking water production do not exist by far.
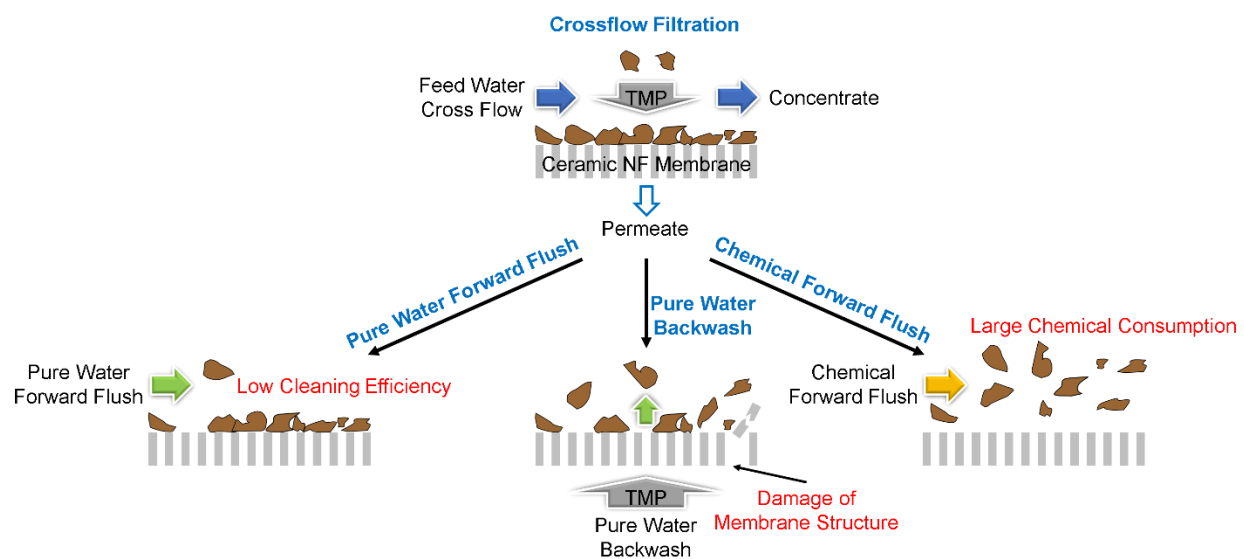
1.2.2 Organic fouling

According to the nature of foulants, membrane fouling is classified into (i) organic fouling, (ii) inorganic fouling/scaling, (iii) particulate/colloidal fouling and (iv) biofouling (microbial growth and adhesion). In particular, organic fouling of ceramic NF membranes by organic molecules/colloids, can lead to a substantial reduction in water production, which remains one of the major obstacles to upscaling the current implementation of the membranes in water treatment (Kramer et al., 2015). Organic foulants in source waters (e.g. surface water), present as NOM and organic colloids, typically comprise polysaccharides, humic substances and proteins (Van Geluwe et al., 2011). Among these, the polysaccharides, as the main component of biopolymers (>100 kDa), have been considered the key fouling-causing organic matter during low-pressure membrane filtration (e.g. MF and UF) (Meng et al., 2017).

Earlier research (Kuzmenko et al., 2005) has reported that organic fouling of MF and UF processes occurs mainly through internal adsorption, pore blocking and cake build-up, which could be

influenced by physicochemical properties of both the organic foulants (e.g. charge, size, hydrophobicity and conformation) and the membranes (e.g. surface charge, pore size and hydrophobicity). In addition, several studies (Mustafa et al., 2016a; b) have demonstrated that organic fouling of ceramic NF membranes mainly depends on the entire surface chemistry (e.g. functionalities, hydrophilicity and charge) of the membranes, determining the types and strength of potential foulant-membrane interactions (e.g. hydrogen bonding, ion and electrostatic interactions). However, a clear understanding of fouling characteristics and mechanisms during ceramic NF in water treatment is still lacking.

1.2.3 Problems with conventional hydraulic and chemical cleaning methods

Figure 1.1 *Basic scenarios of pure water forward flush, pure water backwash and chemical forward flush in response to organic fouling of ceramic nanofiltration membranes in a crossflow filtration mode.*

The lack of cost-effective and eco-friendly cleaning methods is another important factor affecting the up-scaling application of ceramic NF membranes for water treatment. Figure 1.1 illustrates the basic scenarios of pure water forward flush, pure water backwash and chemical forward flush in response to organic fouling of ceramic NF membranes in a crossflow filtration mode. Forward flush with pure water has proven to be ineffective for organic fouling of ceramic NF membranes, due to strong adherence of the organic foulants to the membranes, especially in the presence of calcium ions in the solution (Mustafa et al., 2016b; Zhao et al., 2018). Backwash at high pressures has been found to cause damages to the structure of ceramic NF membranes (Kramer et al., 2020). Therefore, frequent chemical forward flush with a strong acid (e.g. hydrochloric acid) or base (e.g. sodium hydroxide)

needs to be used offline, resulting in a long downtime of filtration and an increase in the chemical consumption (Kramer et al., 2015). An effective and mild cleaning approach in response to the organic fouling of the ceramic NF membranes, in order to improve their applicability in water treatment, is still missing.

1.3 Oxidation in fouling control and cleaning of ceramic membranes

1.3.1 Types and mechanisms of oxidation for fouling mitigation

In literature, oxidation processes in combination with ceramic membrane filtration for the fouling control can be classified into (i) oxidation of the feed water (Jiang et al., 2022; Sun et al., 2018; Winter et al., 2016; Zhu et al., 2022) and (ii) oxidative cleaning of the fouled membranes (Alresheedi et al., 2019b; De Angelis and de Cortalezzi, 2016). Here, the fouling control of the ceramic membranes through oxidation mainly aims at (i) mineralization of the feed organics to reduce the organic loading before filtration, (ii) alterations in physicochemical properties (e.g. molecular/colloidal sizes, hydrophilicity and charge properties) of the foulants to restrict their attachment onto the membranes, and (iii) degradation/transformation of the foulants on/in the membranes to facilitate their removal or detachment from the membranes (Rosman et al., 2018; Zhou et al., 2017).

1.3.2 Oxidation of organic matter in feed water

Dosing oxidants in the feed water of ceramic membrane filtration has a risk of secondary pollution resulting from a potential passage of the residual oxidants into the permeate. Moreover, there is a trade-off between decreased reversible fouling, as a result of oxidation of the feed organics, and an increased passage of the oxidized organics into the permeate, due to decomposition of the organics into smaller-sized fractions (Wei et al., 2016). In addition, irreversible fouling of ceramic membranes can be aggravated after oxidation of the feed organics, attributed to an increase in pore blockage (Ibn Abdul Hamid et al., 2017; Im et al., 2019; Winter et al., 2016).

1.3.3 Oxidation as a cleaning method for fouled ceramic membranes

Oxidative cleaning of fouled ceramic membranes, e.g. using Fenton reactions (De Angelis and de Cortalezzi, 2016), forward flush with ozonated water (Fujioka et al., 2018), immersed cleaning by sodium hypochlorite (Alresheedi et al., 2019a; Alresheedi et al., 2019b), has been counted as an effective means of removing fouling from the membranes, without causing the aforementioned secondary pollution in the permeate and extra irreversible fouling of the membranes. Nevertheless, to obtain ozonated water, having adequate ozone in the water phase, for achieving steady cleaning

efficacy is energy intensive, since ozone is unstable in water. In addition, oxidative cleaning using sodium hypochlorite damages the end sealing layers of ceramic NF membranes, thereby causing a defect on the membranes (Kramer et al., 2019).

A Fenton reaction between heterogeneous catalysts and hydrogen peroxide (H_2O_2) is able to generate reactive hydroxyl radicals ($^\bullet$OH) for efficiently oxidizing organic matter on the surface of the catalysts (He et al., 2016). Lin and Gurol (1998) proposed the basic routes of Fenton reactions initiated by iron-based catalysts, as shown in Equations (1.1)–(1.3):

$$\equiv\text{Fe(II)-OH} + H_2O_2 \rightarrow \equiv\text{Fe(III)-OH} + {}^\bullet\text{OH} \tag{1.1}$$

$$\equiv\text{Fe(III)-OH} + H_2O_2 \rightarrow \equiv\text{Fe(II)} + H_2O + HO_2{}^\bullet \tag{1.2}$$

$$\equiv\text{Fe(III)-OH} + HO_2{}^\bullet \rightarrow \equiv\text{Fe(II)} + H_2O + O_2 \tag{1.3}$$

Hence, coating Fenton catalysts on and/or within ceramic membranes enables oxidative removal of the deposited foulants from the membrane surface (Sun et al., 2018; Zhang et al., 2021). Studies on catalytic ceramic MF and UF have indicated that fouling of the membranes (e.g. accumulation of organic foulants on the surface and/or in the pores) can impede the mass transfer of H_2O_2 and $^\bullet$OH radicals, thereby influencing the efficacy of Fenton cleaning (De Angelis and de Cortalezzi, 2016). Further attention thus needs to be paid to investigating oxidative cleaning of ceramic NF membranes in relation to their specific fouling characteristics.

1.4 Thesis research framework

The main objective of this research was to probe into the relation between the efficacy/mechanisms of Fenton cleaning of a catalytic ceramic NF membrane and its fouling types/characteristics in direct surface water treatment. To achieve the objective, research questions were proposed as listed below and studied in the chapters of the thesis.

Research question 1: *What is the current understanding of fouling characteristics of ceramic membranes and the effect of oxidation on fouling mitigation?*

Chapter 2 reflects a literature study focusing on the current knowledge on using oxidation methods for fouling control of ceramic membranes. Surface properties and interactions of ceramic membranes, related to fouling mechanisms and characteristics of the membranes, were described. By reviewing the present publications, the effect of oxidation on fouling characteristics of ceramic membranes was

discussed. Given the available knowledge, therefore, how to effectively use oxidation for fouling control of ceramic membranes was suggested.

Research question 2: *How to improve the efficacy of Fenton cleaning over an alginate fouling layer on ceramic NF membranes?*

Chapter 3 introduces an integration of oxalic acid chelation and Fenton oxidation for cleaning alginate fouled ceramic NF membranes. A synergistic effect of relaxation and oxidation over the fouling layers was proved to act as the main mechanism for the membrane cleaning.

Research question 3: *How is Fenton cleaning related to fouling types of a ceramic NF membrane?*

Chapter 4 describes the relationship between the efficacy of Fenton cleaning and the fouling types of a ceramic NF membrane. Adsorptive and cake layer fouling were separately identified during alginate fouling of the membrane, and were studied in terms of their individual effect on Fenton cleaning. This chapter provided new insights into the criteria for optimizing oxidative (Fenton) cleaning during ceramic NF in water treatment.

Research question 4: *What are the fouling characteristics and Fenton cleaning efficacy of a ceramic NF membrane in direct surface water treatment?*

Chapter 5 demonstrates the potential of using an FeOCl pre-coated ceramic NF membrane with Fenton cleaning for direct surface water treatment. Fouling characteristics of the membrane were studied in terms of the impact of feed pH, FeOCl pre-coat layer and permeate flux. The efficacy of Fenton cleaning for the fouled membrane was evaluated over multiple cycles.

References

Alresheedi, M.T., Barbeau, B., Basu, O.D., 2019a. Comparisons of NOM fouling and cleaning of ceramic and polymeric membranes during water treatment. Separation and Purification Technology 209, 452-460.

Alresheedi, M.T., Basu, O.D., Barbeau, B., 2019b. Chemical cleaning of ceramic ultrafiltration membranes – Ozone versus conventional cleaning chemicals. Chemosphere 226, 668-677.

Árki, P., Hecker, C., Tomandl, G., Joseph, Y., 2019. Streaming potential properties of ceramic nanofiltration membranes – Importance of surface charge on the ion rejection. Separation and Purification Technology 212, 660-669.

Cabrera, S.M., Winnubst, L., Richter, H., Voigt, I., McCutcheon, J., Nijmeijer, A., 2022. Performance evaluation of an industrial ceramic nanofiltration unit for wastewater treatment in oil production. Water Research 220, 118593.

Caltran, I., Rietveld, L.C., Shorney-Darby, H.L., Heijman, S.G.J., 2020. Separating NOM from salts in ion exchange brine with ceramic nanofiltration. Water Research 179, 115894.

Chang, H., Liang, H., Qu, F., Liu, B., Yu, H., Du, X., Li, G., Snyder, S.A., 2017. Hydraulic backwashing for low-pressure membranes in drinking water treatment: A review. Journal of Membrane Science 540, 362-380.

Chen, J.P., Kim, S.L., Ting, Y.P., 2003. Optimization of membrane physical and chemical cleaning by a statistically designed approach. Journal of Membrane Science 219(1), 27-45.

Chen, P., Ma, X., Zhong, Z., Zhang, F., Xing, W., Fan, Y., 2017. Performance of ceramic nanofiltration membrane for desalination of dye solutions containing NaCl and Na_2SO_4. Desalination 404, 102-111.

De Angelis, L., de Cortalezzi, M.M.F., 2016. Improved membrane flux recovery by Fenton-type reactions. Journal of Membrane Science 500, 255-264.

Dreszer, C., Flemming, H.C., Zwijnenburg, A., Kruithof, J.C., Vrouwenvelder, J.S., 2014. Impact of biofilm accumulation on transmembrane and feed channel pressure drop: Effects of crossflow velocity, feed spacer and biodegradable nutrient. Water Research 50, 200-211.

Fujioka, T., Hoang, A.T., Okuda, T., Takeuchi, H., Tanaka, H., Nghiem, L.D., 2018. Water reclamation using a ceramic nanofiltration membrane and surface flushing with ozonated water. International Journal of Environmental Research and Public Health 15(4), 799.

Fujioka, T., Khan, S.J., McDonald, J.A., Nghiem, L.D., 2014. Nanofiltration of trace organic chemicals: A comparison between ceramic and polymeric membranes. Separation and Purification Technology 136, 258-264.

Fujioka, T., Ngo, M.T.T., Makabe, R., Ueyama, T., Takeuchi, H., Nga, T.T.V., Bui, X.-T., Tanaka, H., 2021. Submerged nanofiltration without pre-treatment for direct advanced drinking water treatment. Chemosphere 265, 129056.

Futselaar, H., Schonewille, H., van der Meer, W., 2002. Direct capillary nanofiltration – a new high-grade purification concept. Desalination 145(1), 75-80.

He, J., Yang, X., Men, B., Wang, D., 2016. Interfacial mechanisms of heterogeneous Fenton reactions catalyzed by iron-based materials: A review. Journal of Environmental Sciences 39, 97-109.

Ho, L., Braun, K., Fabris, R., Hoefel, D., Morran, J., Monis, P., Drikas, M., 2012. Comparison of drinking water treatment process streams for optimal bacteriological water quality. Water Research 46(12), 3934-3942.

Ibn Abdul Hamid, K., Sanciolo, P., Gray, S., Duke, M., Muthukumaran, S., 2017. Impact of ozonation and biological activated carbon filtration on ceramic membrane fouling. Water Research 126, 308-318.

Im, D., Nakada, N., Kato, Y., Aoki, M., Tanaka, H., 2019. Pretreatment of ceramic membrane microfiltration in wastewater reuse: A comparison between ozonation and coagulation. Journal of Environmental Management 251, 109555.

Jiang, T., Tian, T., Guan, Y.-F., Yu, H.-Q., 2022. Contrasting behaviors of pre-ozonation on ceramic membrane biofouling: Early stage vs late stage. Water Research 220, 118702.

Köhler, S.J., Lavonen, E., Keucken, A., Schmitt-Kopplin, P., Spanjer, T., Persson, K., 2016. Upgrading coagulation with hollow-fibre nanofiltration for improved organic matter removal during surface water treatment. Water Research 89, 232-240.

Kramer, F.C., Shang, R., Heijman, S.G.J., Scherrenberg, S.M., van Lier, J.B., Rietveld, L.C., 2015. Direct water reclamation from sewage using ceramic tight ultra- and nanofiltration. Separation and Purification Technology 147, 329-336.

Kramer, F.C., Shang, R., Rietveld, L.C., Heijman, S.J.G., 2020. Fouling control in ceramic nanofiltration membranes during municipal sewage treatment. Separation and Purification Technology 237, 116373.

Kramer, F.C., Shang, R., Scherrenberg, S.M., Rietveld, L.C., Heijman, S.J.G., 2019. Quantifying defects in ceramic tight ultra- and nanofiltration membranes and investigating their robustness. Separation and Purification Technology 219, 159-168.

Kuzmenko, D., Arkhangelsky, E., Belfer, S., Freger, V., Gitis, V., 2005. Chemical cleaning of UF membranes fouled by BSA. Desalination 179(1), 323-333.

Liikanen, R., Miettinen, I., Laukkanen, R., 2003. Selection of NF membrane to improve quality of chemically treated surface water. Water Research 37(4), 864-872.

Lin, S.-S., Gurol, M.D., 1998. Catalytic decomposition of hydrogen peroxide on iron oxide: Kinetics, mechanism, and implications. Environmental Science & Technology 32(10), 1417-1423.

López, J., Reig, M., Vecino, X., Gibert, O., Cortina, J.L., 2020. Comparison of acid-resistant ceramic and polymeric nanofiltration membranes for acid mine waters treatment. Chemical Engineering Journal 382, 122786.

Meng, F., Zhang, S., Oh, Y., Zhou, Z., Shin, H.-S., Chae, S.-R., 2017. Fouling in membrane bioreactors: An updated review. Water Research 114, 151-180.

Motta Cabrera, S., Winnubst, L., Richter, H., Voigt, I., Nijmeijer, A., 2021. Industrial application of ceramic nanofiltration membranes for water treatment in oil sands mines. Separation and Purification Technology 256, 117821.

Mustafa, G., Wyns, K., Buekenhoudt, A., Meynen, V., 2016a. Antifouling grafting of ceramic membranes validated in a variety of challenging wastewaters. Water Research 104, 242-253.

Mustafa, G., Wyns, K., Buekenhoudt, A., Meynen, V., 2016b. New insights into the fouling mechanism of dissolved organic matter applying nanofiltration membranes with a variety of surface chemistries. Water Research 93, 195-204.

Puthai, W., Kanezashi, M., Nagasawa, H., Tsuru, T., 2016. Nanofiltration performance of SiO_2-ZrO_2 membranes in aqueous solutions at high temperatures. Separation and Purification Technology 168, 238-247.

Rosman, N., Salleh, W.N.W., Mohamed, M.A., Jaafar, J., Ismail, A.F., Harun, Z., 2018. Hybrid membrane filtration-advanced oxidation processes for removal of pharmaceutical residue. Journal of Colloid and Interface Science 532, 236-260.

Siddiqui, M., Amy, G., Ryan, J., Odem, W., 2000. Membranes for the control of natural organic matter from surface waters. Water Research 34(13), 3355-3370.

Sillanpää, M., Ncibi, M.C., Matilainen, A., Vepsäläinen, M., 2018. Removal of natural organic matter in drinking water treatment by coagulation: A comprehensive review. Chemosphere 190, 54-71.

Sun, S., Yao, H., Fu, W., Hua, L., Zhang, G., Zhang, W., 2018. Reactive Photo-Fenton ceramic membranes: Synthesis, characterization and antifouling performance. Water Research 144, 690-698.

Van Geluwe, S., Braeken, L., Van der Bruggen, B., 2011. Ozone oxidation for the alleviation of membrane fouling by natural organic matter: A review. Water Research 45(12), 3551-3570.

Wei, D., Tao, Y., Zhang, Z., Zhang, X., 2016. Effect of pre-ozonation on mitigation of ceramic UF membrane fouling caused by algal extracellular organic matters. Chemical Engineering Journal 294, 157-166.

Wibisono, Y., Yandi, W., Golabi, M., Nugraha, R., Cornelissen, Emile R., Kemperman, A.J.B., Ederth, T., Nijmeijer, K., 2015. Hydrogel-coated feed spacers in two-phase flow cleaning in spiral wound membrane elements: A novel platform for eco-friendly biofouling mitigation. Water Research 71, 171-186.

Winter, J., Uhl, W., Bérubé, P.R., 2016. Integrated oxidation membrane filtration process – NOM rejection and membrane fouling. Water Research 104, 418-424.

Zhang, S., Hedtke, T., Zhu, Q., Sun, M., Weon, S., Zhao, Y., Stavitski, E., Elimelech, M., Kim, J.-H., 2021. Membrane-confined iron oxychloride nanocatalysts for highly efficient heterogeneous Fenton water treatment. Environmental Science & Technology 55(13), 9266-9275.

Zhao, Y.-y., Wang, X.-m., Yang, H.-w., Xie, Y.-f.F., 2018. Effects of organic fouling and cleaning on the retention of pharmaceutically active compounds by ceramic nanofiltration membranes. Journal of Membrane Science 563, 734-742.

Zhou, Z., He, X., Zhou, M., Meng, F., 2017. Chemically induced alterations in the characteristics of fouling-causing bio-macromolecules – Implications for the chemical cleaning of fouled membranes. Water Research 108, 115-123.

Zhu, L., Wang, W., Zhao, P., Wang, S., Yang, K., Shi, H., Xu, M., Dong, Y., 2022. Silicon carbide catalytic ceramic membranes with nano-wire structure for enhanced anti-fouling performance. Water Research 226, 119209.

Chapter 2

EFFECT OF OXIDATION ON SURFACE INTERACTIONS IN RELATION TO

FOULING BEHAVIOUR OF CERAMIC MEMBRANES: A REVIEW

Abstract

Ceramic membrane technologies have made rapid progress in drinking water and industrial/municipal wastewater treatment, owing to their chemical robustness, good recoverability and long lifetime. Fouling by organic substances is one of the main problems that impede the application of ceramic membranes in water treatment. Oxidation of organic foulants is able to change surface interactions between the foulants and ceramic membranes, thereby affecting fouling behaviour of the membranes. This chapter presents a state-of-the-art overview of the surface interactions in relation to the fouling behaviour of ceramic membranes, together with in-depth discussion about the effect of oxidation on the membrane fouling. The results show that the researchers have employed a variety of oxidation processes, focusing on modifying physicochemical characteristics of organic foulants in feed water, mainly for fouling control of ceramic MF/UF membranes. However, knowledge gaps must be addressed to overcome the lack of: (i) a clear understanding of fouling behaviour and characteristics of ceramic NF membranes in water treatment, and (ii) studies of using (catalytic) oxidation methods for cleaning the membranes. Therefore, we advocate for investigations of the efficacy and mechanisms of oxidative cleaning methods for a ceramic NF membrane in relation to its specific fouling characteristics.

2.1 Introduction

Ceramic membranes have emerged as a promising alternative to their polymeric counterparts for water treatment, given their better robustness and longer service life. Among current studies, ceramic membranes have served as a water purification unit in sole filtration (Barredo-Damas et al., 2012) as well as in combination with oxidation processes (Guo et al., 2016). Implementation of ceramic membranes has, by far, been limited to water treatment mostly at a lab or pilot scale. A clear understanding of fouling/separation characteristics of ceramic membranes, in particular when used in filtration/oxidation hybrid processes, is lacking.

Present knowledge framework is mainly focused on polymeric membranes, which has suggested surface properties of the membranes, amongst other parameters (e.g. solution chemistry and operating conditions), can play a significant role in fouling and separation behaviour of the membranes (Childress and Elimelech, 1996). Different surface properties (e.g. surface charges, functionalities and hydrophilicity) of ceramic and polymeric membranes, may correspond to distinct fouling and/or retention mechanisms, making it unreliable to directly translate polymeric membrane related principles to the understanding of filtration behaviour of ceramic membranes (Lee et al., 2013;

Lee and Kim, 2014; Liu et al., 2019b). Among current studies, of particular interest is solute-membrane interactions, resulting from unique surface properties of a ceramic membrane (Arndt et al., 2016; Fujioka et al., 2014; Hofs et al., 2011; Nagasawa et al., 2020; Zhang et al., 2009). However, state-of-the-art knowledge concerning surface properties and interactions of ceramic membranes, and their underlying relation with filtration behaviour of the membranes, have not been systematically reviewed to date.

Over the past few decades, growing attention has been paid to a combined use of ceramic membranes with oxidation processes, aiming at retarding membrane fouling and/or enhancing pollutant removal from a broad range of water matrices, including municipal wastewater (Asif et al., 2021; Guo et al., 2018; Ibn Abdul Hamid et al., 2017), pharmaceutical wastewater (Li et al., 2022; Wang et al., 2020; Wu et al., 2019), surface water (Cheng et al., 2017; Zhang et al., 2020a), dyestuff wastewater (Zhang et al., 2016a; Zhao et al., 2019), and oily water (Li et al., 2015; Xue et al., 2016). Given the good robustness of ceramic membranes against an oxidizing environment, oxidation/ceramic membrane filtration hybrid systems have flexible options serving as the oxidation treatment unit, involving ozonation (Lee et al., 2019; Song et al., 2018; Szymanska et al., 2014), ferrate-based oxidation (Liu et al., 2019a; Liu et al., 2018), Fenton reactions (Plakas et al., 2019; Sun et al., 2018; Zhang et al., 2021), PMS activation (Cheng et al., 2018; Zhang et al., 2020b; Zhao et al., 2020), photo-catalysis (Nyamutswa et al., 2020; Yang et al., 2019; Zhang et al., 2020a) and electrochemical oxidation (Fu et al., 2019; Geng and Chen, 2017; Zheng et al., 2018).

As compared to sole filtration, integration of ceramic membranes with oxidation processes, can result in more complicated fouling and/or separation behaviour. Diverse physicochemical characteristics (e.g. molecular/colloidal sizes, charges and hydrophilicity) of organic pollutants, upon exposure to an oxidizing environment, tend to vary simultaneously and interplay with each other. For instance, some researchers reported that SA, HA and BSA molecules, following ozonation or PMS-based oxidation at certain doses, could re-aggregate into larger flocs with their zeta potential being changed in the meantime (Song et al., 2018; Yu et al., 2017; Zhao et al., 2020). Wei et al. (2016) and Zhang et al. (2013b) demonstrated that ozonation was able to convert large-sized hydrophobic organics into smaller hydrophilic fragments. Many efforts have been dedicated to investigating the changes in physicochemical characteristics of organic matter by oxidation in relation to filtration behaviour of ceramic membranes. One of the unsolved problems is that, oxidative cleavage of organic pollutants into smaller-sized and more hydrophilic intermediate products, results in a trade-off between decreased accumulation of the foulants on membrane surfaces and increased passage of the

intermediate products into permeate, due to weakened steric exclusion and low hydrophobic attraction (Chen and Columbia, 2011; Cheng et al., 2017; Kim et al., 2008; Park et al., 2012). Moreover, there remains a considerable doubt about the relation between electrostatic interactions and filtration behaviour of ceramic membranes, which lies in that, for instance, charge properties of organics often vary depending on oxidizing degrees (Song et al., 2018; Tang et al., 2017) and are accompanied with changes in their particle sizes and conformation (Asif et al., 2021; Kampf et al., 2015; Wang et al., 2019; Zhao et al., 2020).

Therefore, this chapter aims to present state-of-the-art knowledge on filtration behaviour of ceramic membranes in relation to their surface interactions in the absence and presence of oxidation. Firstly, studies on typical physicochemical properties and surface interactions of ceramic membranes, are discussed to help readers understand how fouling and separation behaviour correlates to surface properties and interactions of the membranes. Secondly, attempts on the integration of oxidation and ceramic membrane filtration in water treatment are reviewed, focusing on clarifying how changes in physicochemical characteristics of organic substances as a result of oxidation influence the performance of fouling mitigation and pollutant retention of the membrane.

2.2 Surface properties and interactions on ceramic membranes

2.2.1 Fundamentals of typical surface properties of ceramic membranes
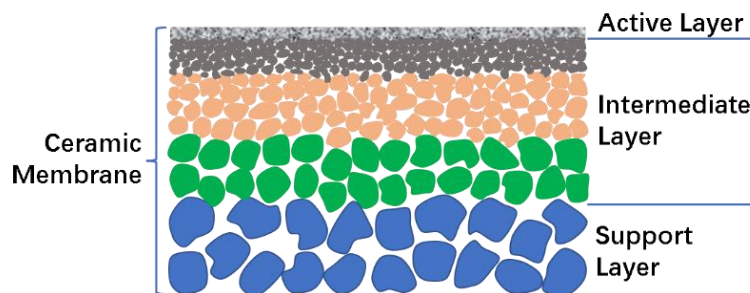
Figure 2.1 *Cross-sectional schematic of an asymmetrical ceramic membrane.*

Based on the distinction in pore sizes, ceramic membranes are classified into MF, UF and NF. RO is currently applied in polymeric membranes. Typically, ceramic membranes consist of an asymmetric multilayer of a three-dimensional interconnected network, including thick support/intermediate layers and a thin active separation layer (Figure 2.1). The multilayer is mostly made from (non)metal oxides, including ZrO_2 (Gao et al., 2020), TiO_2 (Chen et al., 2017; Song et al., 2016), Al_2O_3 (Gu et al.,

2020; Qin et al., 2015; Wang et al., 2016), SiO_2 (Puthai et al., 2017; Zhao et al., 2018a), or non-oxide materials, involving SiC (Hofs et al., 2011) and α-Si_3N_4 (Li et al., 2017).

**Table 2.1** *Surface properties of ceramic membranes*

No.	Active layer material	Pore size/ MWCO[a]	ZP (mV)[b]/pH_IEP[c]	R (nm)[d]	CA (°)[e]	Ref.
1	α-Al_2O_3	210 nm	-	122	24	(Gu et al., 2020)
2	ZrO_2	200 nm	+4.1 (pH6.0)	-	37	(Gao et al., 2020)
3	SiO_2	1.5 nm	−5.7 (pH8.1)	2	40	(Zhao et al., 2018a)
4	TiO_2	1.4 nm	−12.3 (pH8.1)	20	16	(Zhao et al., 2018a)
5	TiO_2	1.5 nm	−7.2 (pH8.1)	30	19	(Zhao et al., 2018a)
6	TiO_2	1 nm	−9.6 (pH8.1)	8	31	(Zhao et al., 2018a)
7	α-Al_2O_3	100 nm	-	-	67	(He et al., 2011)
8	TiO_2	512 Da	-	-	20	(Mustafa et al., 2014)
9	TiO_2	30 nm	pH_IEP: 4.2	-	-	(Moritz et al., 2001b)
10	ZrO_2	5 nm	pH_IEP: 4.6	-	-	(Moritz et al., 2001b)
11	α-Al_2O_3	60 nm	pH_IEP: 4.3	-	-	(Moritz et al., 2001b)
12	γ-Al_2O_3	5 nm	pH_IEP: 6.0	-	-	(Moritz et al., 2001b)
13	SiC	960 nm	pH_IEP: 2.6	-	-	(Hofs et al., 2011)
14	Al_2O_3	200 nm	pH_IEP: 8.3	-	27	(Zhang et al., 2009)
15	TiO_2	200 nm	pH_IEP: 6.1	-	20	(Zhang et al., 2009)
16	Al_2O_3	195 nm	pH_IEP: 5.0	68	-	(Chong and Wang, 2019)
17	γ-Al_2O_3	1–2 nm	-	-	30–60	(Wang et al., 2016)
18	TiO_2	2–4 nm	-	45	40	(Kujawa et al., 2017)
19	TiO_2	200 nm	-	61	40	(Kujawa et al., 2017)
20	TiO_2-ZrO_2	8.6 nm	−24.8 (pH6.0)	-	-	(Lu et al., 2015)

[a] MWCO: molecular weight cut-off; [b] ZP: zeta potential; [c] pH_IEP: isoelectric point; [d] R: roughness; [e] CA: contact angle.

Homogeneity of surface hydroxyl group

Surface properties of a ceramic membrane, such as charges and hydrophilicity, are dependent on surface chemistry of the membrane. Unlike the heterogeneity in chemical functionalities (e.g. hydroxyl, carboxyl and phenyl groups) of polymeric membranes, surface functionalities of ceramic membranes are more homogeneous in (non-)metallic hydroxyl groups (Árki et al., 2019; Lee et al., 2013; Lee and Kim, 2014). Apart from hydroxyl groups, Zhao et al. (2018a) probed the presence of a small number of carboxylic groups in ceramic membranes, deriving from structural impurities during a sol-gel synthesis process of commercial ceramic membranes, while the percentages of carbon atoms (<30%) and carboxylic groups (<8%) of the ceramic membranes were much smaller than those (~70% and 15%, respectively) of polymeric ones (Tang et al., 2009).
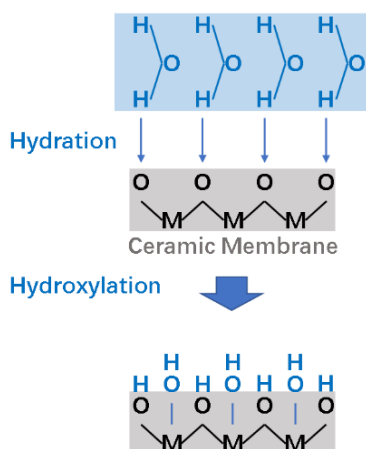

Figure 2.2 *Formation mechanism and types of hydroxyl groups on the surface of ceramic membranes.*

Hydroxyl groups of a ceramic membrane are supposed to form through dissociative chemisorption of water molecules, involving hydration and hydroxylation, as illustrated in Figure 2.2 (Tamura et al., 2001). The hydration process occurs on coordinatively unsaturated surface lattice metal ions of ceramic membranes as a strong Lewis acid site for water adsorption to form a coordination shell, where the oxide cations bind to a hydroxyl group of water molecules and the lattice oxygen ions bind to a water proton in aqueous phase (Kasprzyk-Hordern, 2004; Shirai et al., 2016). Thereafter, the surfaces of ceramic particles undergo the hydroxylation process through dissociation of the chemisorbed water molecules and forms two types of hydroxyl groups, i.e. $O_{ads}H$ (O_{ads}: water oxygen) and O_sH (O_s: oxide surface oxygen) (Hass et al., 1998; Tamura et al., 2001; Yopps and Fuerstenau, 1964). Different properties of the adsorbed water and the $O_{ads}H$ and O_sH groups have been previously characterized by −OH stretching in the range of 3450−3650 cm^{-1} and at around 3780 and 3430 cm^{-1},

respectively (Hass et al., 1998). Another study about TiO_2 oxides indicated that molecularly adsorbed water on the TiO_2 surface accounted for 80% of −OH stretching band intensity, whereas the percentage of 20% was attributed to surface hydroxyl groups (Nosaka et al., 2006).

Surface hydrophilicity

Surface hydrophilicity is counted as an important parameter for predicting fouling propensity of ceramic membranes. Hydrophilicity of a ceramic membrane is measured in terms of a static or dynamic contact angle using a liquid droplet (e.g. water) on the membrane surface, whereby either a smaller contact angle or a faster reduction in the dynamic contact angle corresponds to a more hydrophilic membrane surface (Dobrak et al., 2010; Zhang et al., 2009). The contact angles of ceramic membranes, composed of different (non)metal oxide materials, are summarized in Table 2.1. The water contact angles typically range from 10° to 60° on ceramic membranes (He et al., 2011; Mustafa et al., 2016a; b; Puthai et al., 2016), while covering a much broader range of 10−160° on polymeric membranes (Gray et al., 2007; Lee and Kim, 2014; Park et al., 2005; Qu et al., 2014; Shan et al., 2016). It is therefore not reliable to claim that ceramic membranes are more hydrophilic than polymeric ones.
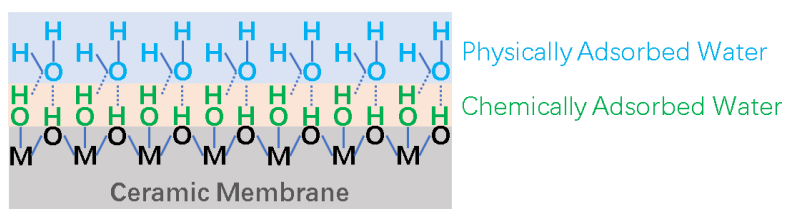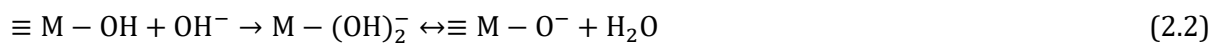

Figure 2.3 *Possible structure of adsorbed water multilayer on the surface of ceramic membranes.*

The abundance of hydroxyl groups on ceramic membranes has been considered the main cause for hydrophilic surface chemistry of the membranes (Sah et al., 2004). Surface hydroxyl groups on a ceramic powder or membrane, arising from hydroxylation of a chemically adsorbed monolayer of water molecules, are able to further interact with water molecules by means of hydrogen bonding and thus form a physically absorbed water multilayer on the membrane surface (Al-Abadleh and Grassian, 2003a; Al-Abadleh and Grassian, 2003b; Lu et al., 2016; Sneh et al., 1996; Takeuchi et al., 2005; Tuladhar et al., 2016). The structural model of the physically and chemically adsorbed multilayer of water molecules on the ceramic membrane is illustrated in Figure 2.3. Surface hydrophilicity of ceramic membranes has been considered to mainly depend on chemical properties of the hydroxyl groups (e.g. density and O−H bond strength) on the membranes (Zaouri et al., 2017).

According to Lu et al. (2016), a stronger O−H bond on the surface of different metal oxide membranes corresponded to larger electron density of O−H groups and a stronger hydrogen bonding affinity between the O−H groups and water molecules, whereby the resultant stronger hydrophilic character on the membrane surfaces rendered the membranes less prone to irreversible fouling in oil/water emulsion treatment.

Surface charge

Ceramic membranes tend to be electrically charged upon contact with a polar liquid (e.g. water), owing to the amphoteric character of their surface hydroxyl groups (Herbig et al., 2003). The surface charges on a ceramic membrane are formed as a result of association/dissociation of protons onto/from the hydroxyl groups of the membrane, which are often called protonation and deprotonation, respectively (Zhang et al., 2008). The amphoteric properties of hydroxyl groups on ceramic membranes enable the protonation and deprotonation depending on the solution pH, as can be expressed in Equation (2.1) and (2.2) (Árki et al., 2019; Larbot et al., 1988; Moritz et al., 2001a).

$$\equiv M - OH + H^+ \rightarrow \equiv M - OH_2^+ \leftrightarrow M^+ + H_2O \tag{2.1}$$

$$\equiv M - OH + OH^- \rightarrow M - (OH)_2^- \leftrightarrow \equiv M - O^- + H_2O \tag{2.2}$$

One hydroxyl group ($\equiv$M−OH) on the membranes associates a proton (H^+) from the solution to obtain a positive charge ($\equiv$M−OH$_2^+$) at pH < pH$_{PZC}$ (point of zero charge, a pH value at which the net surface charge is zero), while disassociating a H^+ to acquire a negative charge ($\equiv$M−O$^-$) at pH > pH$_{PZC}$ (Zhu et al., 2016). Therefore, an increase in pH with crossing the pH$_{PZC}$ leads to a transition of the surface charges of the ceramic membrane from positive to negative values.
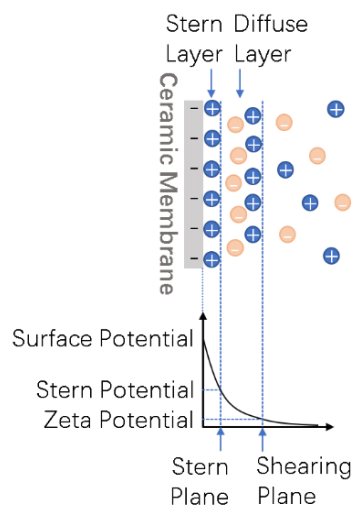
Figure 2.4 *Schematic of electric double layer on the surface of ceramic membranes.*

In addition, physical or chemical adsorption of potential-determining ions may behave as another cause for surface charging on ceramic membranes. To neutralize the surface charges on a ceramic membrane, co- and counter ions in the vicinity of the membrane pore walls incline to reorganize via ion-membrane interactions causing the formation of an electric double layer at the solution-membrane interface, where the potential varies progressively from the membrane surface to the bulk solution (Árki et al., 2019; Moritz et al., 2001b). The electric double layer is schematically illustrated in Figure 2.4. The zeta potential represents a potential at the shearing plane between the compact layer (strongly bound to the pore walls) and the mobile diffuse layer, which acts as an indication of net surface charges and charge distribution within the electric double layer (Fievet et al., 2001; Szymczyk et al., 1997). The influence of ion adsorption on the zeta potential of ceramic membranes primarily depends on the concentration and nature of co- and counter ions and their binding affinity towards the membranes. Widely accepted is that an increase in ion strength reduces the zeta potential of ceramic membranes, resulting from compression of the diffuse layer on the membrane surface (Nazzal and Wiesner, 1994; Sbaï et al., 2003; Zaouri et al., 2017). As earlier documented (Moritz et al., 2001a; Mullet et al., 1997; Mullet et al., 1999; Szymczyk et al., 1997; Van Gestel et al., 2002; Zhao et al., 2005), increasing ion strength by an indifferent NaCl or KCl electrolyte hardly changed the pH_{IEP} (isoelectric point, a pH value where the zeta potential is zero) of a ceramic membrane, whilst an exposure of the membrane to a $CaCl_2$ or Na_2SO_4 solution shifted the pH_{IEP} toward a higher or lower pH, respectively, due to specific adsorption of the Ca^{2+} or SO_4^{2-} ions onto the membrane. Previous studies (Zhang et al., 2009; Zhang et al., 2008) revealed a shift of pH_{IEP} from 8.3 to 4.1 when increasingly doping TiO_2 (5–60%) into an Al_2O_3 membrane, attributing to a stronger adsorption affinity of the TiO_2 hydroxyl groups toward OH^- ions than that of the Al_2O_3 hydroxyl groups.

2.2.2 Surface interactions of ceramic membranes in water treatment

Categories of surface interactions on ceramic membranes

Given that both ceramic and polymeric membranes have porous channels for water permeation, one can anticipate similar physical interactions (e.g. steric/size exclusion) and hydrodynamic forces (e.g. permeation-derived drag) for both membrane types (Arndt et al., 2016; Lee and Kim, 2014). Widely accepted is that, regardless of ceramic or polymeric membranes, particles with a size smaller than or comparable to the pore sizes of the membranes often result in pore narrowing or blocking, whilst particles having a size larger than the membrane pores form a cake layer on the membrane surface (Van Geluwe et al., 2011; Wei et al., 2016; Yin et al., 2013). An exception to this rule is that oil droplets

in oil–water emulsions, notwithstanding their larger sizes in comparison with the pore diameters of a ceramic membrane, could be squeezed into or through the membrane pores by permeation drag forces due to a deformation of the oil droplets (Tummons et al., 2016; Zhou et al., 2010).

The unique physicochemical properties of a ceramic membrane, with respect to its surface hydroxyl groups, charge and hydrophilicity, typically correspond to hydrogen bonding, van der Waals forces, electrostatic/ionic and hydrophobic/hydrophilic interactions (Fujioka et al., 2014; Lee and Kim, 2014; Lu et al., 2016; Mustafa et al., 2016b; Wang et al., 2017; Zaouri et al., 2017; Zhao et al., 2018a). The surface hydroxyl groups and/or adsorbed water molecules of a ceramic membrane, are apt to form hydrogen bonds with polar functional groups (e.g. carboxylic and phenolic groups) of amphipathic (e.g. HA) or hydrophilic (e.g. polysaccharides and proteins) substances (Zaouri et al., 2017; Zhao et al., 2018a). Electrostatic interactions between ionized organic matter and ceramic membranes rely on the difference between the membrane pH_{IEP} and solution pH (pH_S), whereby the adsorption of anion (A^-) or cation (C^+) is favoured at $pH_S < pH_{IEP}$ or $pH_S > pH_{IEP}$ with the acid ($\equiv M{-}OH_2^+$) or base ($\equiv M{-}O^-$) hydroxyl group and being the electrostatic attraction sites, respectively, as described in Equation (2.3) and (2.4).

$$\equiv M - OH_2^+ + A^- \xleftrightarrow{pH_S < pH_{IEP}} \equiv M - OH_2^+ \cdots A^- \qquad (2.3)$$

$$\equiv M - O^- + C^+ \xleftrightarrow{pH_S > pH_{IEP}} \equiv M - O^- \cdots C^+ \qquad (2.4)$$

Multivalent cations (e.g. Ca^{2+}, Mg^{2+} and Fe^{3+}) are believed to facilitate adsorption of foulants onto a ceramic membrane via ionic interactions, such as cation bridging between the negatively charged membrane surface and the anionic functionalities (e.g. carboxylic and phenolic groups) of the organic substances and charge neutralization (Kim et al., 2009; Mustafa et al., 2016b). This, nonetheless, does not mean that fouling of ceramic membranes must be aggravated, since cation bridging can occur between the anionic organics as well and thus promotes aggregation of the particles into larger-sized ones with the formation of a more porous cake layer (Arndt et al., 2016). Owing to the hydrophilic nature of most ceramic membranes, hydrophobic interactions can play a minor role in adsorption of organic pollutants (Fujioka et al., 2014; Zhao et al., 2018a). A hydration layer is apt to form on the external and internal surfaces of the ceramic membranes, functioning as a barrier to repel hydrophobic substances from adhering to the membranes. Son et al. (2017) reported that hydrophilic interactions may act as an important pathway for adsorption of hydrophilic substances onto ceramic membranes.

Techniques for characterizing membrane-foulant and foulant-foulant interactions

The interactive forces between the membrane and the foulant as well as those between the foulant in the fouling layer and the foulant in the bulk solution during ceramic membrane filtration can be directly probed by an AFM measurement in a tapping mode, using a SiN cantilever loaded with the foulant colloid as the modified colloid probe (Lee and Kim, 2014; Lu et al., 2016). For instance, Li and Elimelech (2004) and Lee and Kim (2014) employed a carboxylate modified latex colloid as the surrogate for HA, since carboxylic groups are the typical functional groups of HA. Lu et al. (2016) investigated the interactive forces between ceramic membranes and oil droplets using an oil-coated colloid probe during AFM measurement. Therefore, the interactive forces of a probe colloid toward the clean or fouled surface of ceramic membranes can be measured to reflect the fouling rate/extent at the beginning or later stage of filtration, respectively. The normalized interactive forces (F/R) are calculated based on the deflection of the cantilever, as shown in Equation (2.5) (Li and Elimelech, 2004):

$$F(d)/R = 2\pi W(d) \tag{2.5}$$

where $F(d)$ and $W(d)$ are the interactive force (N) and the interactive energy per unit area (J m^{-2}), respectively, between the probe colloid and the membrane surface separated by a distance of d (m), R is the radius (m) of the probe colloid. However, with AFM measurement, different types of interactive forces are always counted as a whole, making it hard to understand how each interactive force contributes to the fouling of ceramic membranes.

In addition, the XDLVO theory enables the calculation of surface free energy of foulant-foulant and foulant-membrane interactions on ceramic membranes, wherein van der Waals force, electrostatic double layer force and Lewis acid-base force are taken into account for the calculation (Bai et al., 2022; Kim et al., 2009; Zhao et al., 2020). The surface free energy per unit area, due to van der Waals forces, electrostatic double layer forces and Lewis acid-base forces, respectively, is calculated with Equation (2.6), (2.7) and (2.8):

$$\Delta G^{LW} = 2\left(\sqrt{\gamma_w^{LW}} - \sqrt{\gamma_m^{LW}}\right) \cdot \left(\sqrt{\gamma_f^{LW}} - \sqrt{\gamma_w^{LW}}\right) \tag{2.6}$$

$$\Delta G^{EL} = \varepsilon_0 \varepsilon_r \cdot \zeta_f \zeta_m / \lambda_{EL} \tag{2.7}$$

$$\Delta G^{AB} = 2\sqrt{\gamma_w^+}\left(\sqrt{\gamma_m^-} + \sqrt{\gamma_f^-} - \sqrt{\gamma_w^-}\right) + 2\sqrt{\gamma_w^-}\left(\sqrt{\gamma_m^+} + \sqrt{\gamma_f^+} - \sqrt{\gamma_w^+}\right)$$
$$- 2\left(\sqrt{\gamma_m^+\gamma_f^-} + \sqrt{\gamma_m^-\gamma_f^+}\right)$$

(2.8)

where ΔG is the surface free energy, with its superscripts, *LW*, *EL* and *AB*, representing the van der Waals force, electrostatic double layer force and Lewis acid-base force, respectively. γ^{LW}, γ^+ and γ^- are the *LW*, electron acceptor and electron donor components of surface tension, respectively, with their subscripts, *f*, *w* and *m*, denoting the foulant, water and membrane, correspondingly. $\varepsilon_0\varepsilon_r$ is the dielectric permittivity of water. ζ_f and ζ_m are the zeta potentials of the foulant and membrane, respectively. λ_{EL} is the characteristic decay length for *EL* interactions in aqueous phase. The surface tension parameters of the foulant (γ_f^+, γ_f^- and γ_f^{LW}) and membrane (γ_m^+, γ_m^- and γ_m^{LW}) can be determined by measuring the contact angle values of three probe liquids with known surface tension (γ_P^+, γ_P^- and γ_P^{LW}) based on the extended Young equation (van Oss, 2007), as presented in Equation (2.9):

$$\left(\gamma_P^{LW} + 2\sqrt{\gamma_P^+\gamma_P^-}\right)(1 + \cos\theta) = 2\left(\sqrt{\gamma_T^{LW}\gamma_P^{LW}} + \sqrt{\gamma_T^+\gamma_P^-} + \sqrt{\gamma_T^-\gamma_P^+}\right)$$

(2.9)

where θ is the contact angle measured with each probe liquid on the clean or foulant-deposited membrane. Subscript *P* represents each given probe liquid, while subscript *T* is the tested foulant or membrane. Water, formamide and diiodomethane with known surface tension parameters have been widely used as the probe liquids for the measurement of surface free energy of ceramic membranes (Zhao et al., 2018b; Zhao et al., 2020).

The strength of surface interactions during ceramic membrane filtration can also be assessed by means of a batch adsorption experiment in the absence of a permeate flow (Doneva et al., 2001; Lee and Kim, 2014). Therefore, adsorption capacities/kinetics of foulants onto the membrane and a permeance decline due to adsorption are counted as indicators for the magnitudes of the interactive forces, since no convection-induced deposition is present at the membrane surface (Martínez et al., 2000). Lee and Kim (2014) reported a much smaller adsorption capacity of HA on ceramic membranes than on polymeric membranes, which was in agreement with smaller adhesion forces of HA toward the ceramic membranes than toward the polymeric membranes as measured by AFM technology. Likewise, the fouling reversibility of a fouled ceramic membrane in a hydraulic cleaning experiment depends on the strength of surface interactions, wherein the permeance recovery with backwash or forward flush is another criterion for evaluating the adhesion forces (Mustafa et al.,

2016a). As such, the hydraulic cleaning experiment is able to distinguish between surface interactions contributing to either hydraulically reversible or irreversible fouling (Alresheedi et al., 2019; Hofs et al., 2011).

2.2.3 Surface interactions in relation to fouling/separation behaviour of ceramic membranes

Effect of surface interactions on fouling behaviour of ceramic membranes

Foulant deposition on/in ceramic membranes occurs as a result of a combination of multiple surface interactions. A number of researchers (Alresheedi et al., 2019; Hofs et al., 2011; Lee et al., 2013; Murić et al., 2014) agreed that, notwithstanding filtration with natural waters and wastewaters under comparable size exclusion (i.e. pore size) conditions, hydrophilic ceramic (e.g. SiC, ZrO_2, TiO_2 and Al_2O_3) membranes developed less fouling and higher cleanability in terms of backwash than hydrophobic polymeric (e.g. PES, PES/PVP, PC, PVDF and PVC) membranes. Some researchers (Mustafa et al., 2016b; Mustafa et al., 2018; Mustafa et al., 2014) grafted hydrophobic functional groups (methyl, phenyl or propyl) on TiO_2 membranes to replace the hydroxyl groups, nonetheless, the fouling was instead reduced with an increase in the membrane hydrophobicity. It seems that high hydrophilicity of a ceramic membrane cannot behave as a sole criterion accounting for its decreased fouling, but rather the whole of surface chemistry determines the fouling. Chen et al. (2022) and (Xu et al., 2020) demonstrated that the lower fouling of SiC membranes than that of Al_2O_3 membranes during filtration with oil-in-water emulsions was attributed to the stronger electrostatic repulsion and weaker hydrophobic attraction of the SiC membranes toward the foulants. Also, a combined effect exists between size exclusion and electrostatic interactions during fouling of ceramic membranes. An example is that surface charges of a ceramic membrane can reduce its effective pore diameters through the formation of an electric double layer on the pore walls, whereby electrostatic interactions between charged pore surfaces and charged organics become more important for smaller pore-sized (e.g. NF) membranes (Lee et al., 2002; Moritz et al., 2001a; Moritz et al., 2001b; Van Gestel et al., 2002). For ceramic membranes with pore sizes comparable to oil droplet sizes, electrostatic repulsion in combination with size exclusion played a synergetic role in preventing the penetration of SDS-surrounded droplets into the pores, while electrostatic attraction promoted the deformation and penetration of DTAB-surrounded droplets into/through the pores and thus weakened the size exclusion (Nagasawa et al., 2020). A new combined effect between electrostatic attraction and size exclusion has been elucidated by Lu et al. (2015): electrostatic adsorption of the CTAB surfactant, out of CTAB-stabilized oil droplets, onto pore walls of a TiO_2 membrane, reduced

the effective pore sizes and, meanwhile, enlarged the destabilized droplets, thereby causing improved size exclusion and less pore blocking. Shang et al. (2015) found that ceramic MF/UF permeate of surface water, when fed to filtration for a second round, still caused pore narrowing, confirming the presence of internal adsorption by the small-sized NOM fractions aside from size exclusion of the large-sized ones. However, they did not clarify which one or more surface interactions resulted in the internal adsorption. Therefore, a clear understanding of how each surface interaction contributes to different fouling types of ceramic membranes remains lacking, due to the difficulty in distinguishing the various surface interactions during fouling. Attempts to relate surface interactions of a ceramic membrane to its different types of fouling, such as internal adsorption, pore clogging and cake layer formation, are needed in future studies.

Effect of fouling on surface interactions and separation behaviour

Surface properties and interactions on a ceramic membrane incline to vary dynamically with a fouling progress. Fouling of a ceramic membrane typically consists of an early stage of rapid fouling, mainly due to clean membrane-foulant interactions, and a subsequently slow fouling stage, predominantly resulting from fouled membrane-foulant interactions (Arndt et al., 2016; Jermann et al., 2007; Nagasawa et al., 2020; Wang et al., 2013). In many studies, original surface properties of ceramic membranes seem not to reasonably account for or predict the whole fouling or separation process in relation to the ever-changing surface interactions during filtration. For instance, Hofs et al. (2011) and Lee and Cho (2004) reported that, when compared at similar pore sizes, TiO_2 and ZrO_2 membranes developed weaker electrostatic repulsion against NOM than polyamide TFC and PES/PVP membranes, but the ceramic membranes presented higher rejections of the NOM. Jin et al. (2010) and Yue et al. (2015) observed that a 300-nm pore-sized Al_2O_3 membrane instead exerted a higher rejection of low-MW organics (<1 kDa) than an 80-nm pore-sized Al_2O_3 membrane, during filtration with domestic wastewater. Therefore, apart from original surface properties of a ceramic membrane, its fouling characteristics (e.g. concentration polarisation, internal adsorption, pore clogging and cake build-up) can also play an important role in determining subsequent surface interactions and separation capabilities of the membrane (Fujioka et al., 2014; Zhao et al., 2018a). The formation of a conditioning film on/in ceramic membranes, as a result of foulant adsorption and/or cake layer build-up, is able to act as a secondary filtration layer at the later stage of filtration. Therefore, regardless of original surface properties of different types of ceramic membranes, the conditioning film formed by specific organic foulants may screen or modify the original surface properties of the membranes, thereby affecting the subsequent surface interactions and filtration

behaviour (Ng et al., 2020; Ying et al., 2014; Zaouri et al., 2017). As an example, several researchers observed minimal differences in tendency and magnitude of the fouling among ceramic membranes with different pore sizes/MWCOs (30–60 nm or 50–150 kDa) and among membranes with diverse starting materials (Al_2O_3, SiC, ZrO_2, PES and RC) (Arndt et al., 2016; Lee and Kim, 2014).

Surface interactions on/within the conditioning film (i.e. adsorptive and cake layers) of ceramic membranes are complicated, due to an ever-changing structure or composition of the adsorptive and cake layers during filtration. Very limited focus has been put on physicochemical and structural characteristics of the adsorptive and cake layers, which may play a significant role in filtration behaviour. Porosity of a cake layer on ceramic membranes has been counted as an important factor determining the rejection of organic substances through adsorption onto the porous cake layer (Yue et al., 2015; Zuriaga-Agustí et al., 2014). Additionally, as previously demonstrated (Zhang et al., 2016b; Zhang et al., 2013a), the inner and outer layers of the cake layer, formed during ceramic MF with AOM solutions, mainly comprised hydrophilic low-MW (~1 kDa) substances and hydrophobic high-MW (>20 kDa) biopolymers, respectively, wherein hydrophilic and hydrophobic interactions could sequentially take place in the inner and outer cake layers. The aforementioned fouling and separation behaviour during ceramic membrane filtration is illustrated in relation to the solute-membrane and solute-solute interactions, as shown in Figure 2.5.
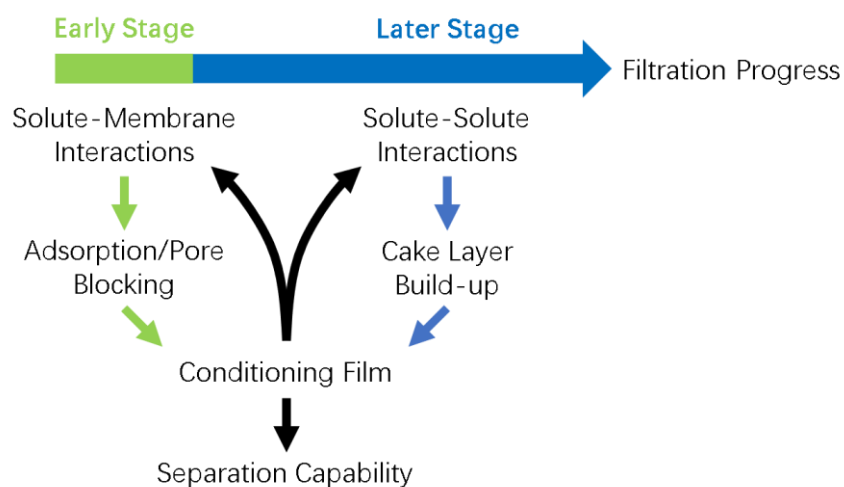
Figure 2.5 *An illustration of fouling and separation behaviour during ceramic membrane filtration in relation to solute-membrane and solute-solute interactions.*

2.3 Relating surface interactions and fouling/separation behaviour of ceramic membranes to oxidation processes

Compared to polymeric membranes, ceramic membranes present better chemical stability and longer operating lifetime, and thus have been considered more appropriate for integration with oxidation processes. There are mainly two types of oxidation/filtration hybrid processes: (i) pre-oxidation with catalysts and/or oxidants dispersed in the feed water prior to filtration, and (ii) *in-situ* oxidation with catalysts immobilized on/in the membrane and with oxidants dosed in the feed water during filtration (Rosman et al., 2018). This chapter is mainly focused on fouling/separation behaviour of ceramic membranes in oxidation/filtration hybrid processes, in relation to the effect of oxidation of the feed organics on surface interactions between the membranes and organic substances. Current oxidation technologies used in combination with ceramic membranes in water treatment, and their influence on fouling/separation behaviour of the membranes, are summarized in Table 2.2.

Table 2.2 *Oxidation technologies used in combination with ceramic membranes in water treatment (N.A.: not available)*

Oxidant	Dosage	Water type	Change in MW (kDa)	Change in polarity	Decrease of resistances (%)		Removal by oxidation (%)		DOC rejection by membranes (%)		Ref.
					R_r	R_{ir}	DOC	UV_{254}	Before oxidation	After oxidation	
O_3	1.5 mg O_3/mg DOC	AOM	≥20 ↓ 1–10 ↑	HPO→HPI	70.1	13.5	20.2	N.A.	43.4	18.1	(Wei et al., 2016)
O_3	2.0 mg O_3/mg DOC	NOM	0.5–10 ↓ ≤0.5 ↓	HPO→HPI	N.A.	N.A.	25	87.3	46	26	(Winter et al., 2016)
O_3	1.3 mg O_3/mg DOC	NOM	1–3 ↓ 0.2–0.5 ↑	HPO→HPI	N.A.	N.A.	22.9	N.A.	22.9	13.5	(Fan et al., 2015)
O_3	0.8 mg O_3/mg DOC	EfOM	67 ↓ 1.8 ↓	HPO→HPI	N.A.	N.A.	−4.8	47.1	N.A.	18.2	(Lehman and Liu, 2009)
O_3	0.75 mg O_3/mg DOC	MLSS	10–200 ↓ 1–10 ↓	N.A.	18.8	27.6	13.7	N.A.	N.A.	N.A.	(Tang et al., 2017)
O_3	0.75 mg O_3/mg DOC	SA	>150 ↓ 6–150 ↓ <6 ↑	N.A.	84.2	92.3	2.8	N.A.	27.1	16.7	(Song et al., 2017)
O_3	0.75 mg O_3/mg DOC	BSA	N.A.	N.A.	−830	−∞	20	N.A.	43.3	95.1	(Song et al., 2018)

O₃	0.6 mg O₃/mg DOC	NOM	1–10 ↓	HPO→HPI	47.1	20.3	N.A.	N.A.	9.9	8.7	(Cheng et al., 2017b)
O₃	1.33 mg O₃/mg DOC	EfOM	≥20 ↓ 0.35–20 ↓ <0.35 ↓	HPO→HPI	66.7	−3.6	33.6	61.8	16	14	(Liu et al., 2018a)
UV/H₂O₂	4 J/cm² 10 mg/L	NOM	0.5–10 ↓ ≤0.5 ↑	HPO→HPI	N.A.	N.A.	25	61.4	46.0	14.0	(Winter et al., 2016)
UV/H₂O₂	32 J/cm² 17 mg/L	AOM	>20 ↓ 0.35–20 ↓ <0.35 ↑	HPO→HPI	100	65	50	N.A.	52.0	12.0	(Zhang et al., 2015)
UV/PMS	0.7 J/cm² 0.2 mM	AOM	≥20 ↓ 1–20 ↑	HPO→HPI	40	0	14.6	27.7	11	<2	(Cheng et al., 2018)
UV/Fe(II)/PMS	0.7 J/cm² 0.1 mM 0.2 mM	AOM	≥20 ↓ 1–20 ↑	HPO→HPI	89	93	69.9	59.8	11	<3	(Cheng et al., 2018)
UV/TiO₂	0.3 g/L	HA	≥100 ↓ <100 ↑	HPO→HPI	62.8	59.7	70.5	14.6	N.A.	N.A.	(Yang et al., 2019)
Fe(II)/PMS	0.05 mM 0.05 mM	HA	N.A.	N.A.	84	97	93	96.2	N.A.	N.A.	(Cheng et al., 2017a)
Fe(II)/PMS	0.1 mM 0.1 mM	NOM	1–10 ↓	HPO→HPI	57.0	53.9	N.A.	N.A.	9.9	32.9	(Cheng et al., 2017b)
Fe(II)/PMS	0.1 mM 0.2 mM	AOM	≥20 ↓ 1–20 ↑	HPO→HPI	79	75	50.0	40.4	11	<2	(Cheng et al., 2018)

K₂FeO₄	0.2 mM	EfOM	≥20 ↓ <20 ↓	N.A.	N.A.	N.A.	25.5	46.1	5.6	6.0	(Liu et al., 2018b)
K₂FeO₄	0.15 mM	EfOM	≥20 ↓ 0.35–20 ↓ <0.35 ↓	HPO→HPI	60.3	82.1	38.7	42.4	16	13.0	(Liu et al., 2018a)
K₂FeO₄	0.15 mM	EfOM	≥20 ↓ 0.35–20 ↓ <0.35 ↓	HPO→HPI	38.3	−38.3	53.5	76.9	20	41.7	(Liu et al., 2019)
K₂FeO₄/ O₃	0.15 mM 1.33 mg O₃/mg DOC	EfOM	≥20 ↓ 0.35–20 ↓ <0.35 ↓	HPO→HPI	92.9	85.1	70.5	80.5	16	13.0	(Liu et al., 2018a)

2.3.1 Oxidation/ceramic membrane filtration hybrid processes

Oxidation scenarios applied in combination with ceramic membranes

With the purposes of enhancing contaminant removal and/or fouling mitigation during ceramic membrane filtration, pre-ozonation has mostly been used (Jiang et al., 2022; Karnik et al., 2005; Kim et al., 2008; Lehman and Liu, 2009; Xue et al., 2016). Other pre-oxidation protocols, involving chlorination (Sun et al., 2018), Fenton process (Chiu and James, 2006), PMS activation (Cheng et al., 2017a; Cheng et al., 2017b; Cheng et al., 2018; Wang et al., 2021), ferrate oxidation (Liu et al., 2018a; Liu et al., 2018b), photocatalysis (e.g. UV/H_2O_2 and UV/TiO_2) (Espíndola et al., 2019; Gray et al., 2020; Winter et al., 2016; Yang et al., 2019; Zhang et al., 2015), electrochemical oxidation (Du et al., 2019), and enzyme catalysed degradation (Chen and Columbia, 2011), have been studied. Many of them have been studied with polymeric membranes using smaller oxidant dosages and milder oxidation conditions, to avoid potential damages to the membrane structure. Ceramic membranes, having robust chemical stability, are able to withstand various oxidants and radicals. Although the basic oxidation pathways vary among these different pre-oxidation processes, their mechanisms regarding fouling mitigation of ceramic membranes are related to four aspects: (i) decreasing the organic loading in the feed water (Zhang et al., 2015), (ii) altering the molecular/colloidal sizes of the organic contaminants (Filloux et al., 2012; Lee et al., 2005; Nguyen and Roddick, 2010) and (iii) changing the solute-solute and solute-membrane interactive affinities (Van Geluwe et al., 2011; Wang et al., 2017; Zhu et al., 2010). In this section of the chapter, focus was put on the effect of pre-oxidation on fouling propensity, cleanability and separation capability of ceramic membranes, in relation to the changes in physicochemical properties of organic pollutants and in pollutant-membrane interactions.

Breakage and partial mineralization of organic substances

Fouling alleviation of ceramic membranes through oxidation of the feed organics cannot be solely attributed to the reduction of DOC remained in the feed water and/or retained on the membranes. In present literature, no statistically significant correlation has been observed between the extent of fouling alleviation and the reduction of DOC retained in the fouling layers, when using pre-oxidation prior to ceramic membrane filtration. Winter et al. (2016) reported that UV/H_2O_2 pre-oxidation of NOM reduced the DOC, retained by an 8-kDa ceramic membrane, more substantially (70.1%) than pre-ozonation (42.9 %), while the decrease in fouling resistances after UV/H_2O_2 oxidation (12.5%) was, in turn, much smaller than after pre-ozonation (75.6%). Several studies showed that, the reductions of DOC (19.8–29.5%) in the fouling layers, as a result of pre-ozonation (5 mg O_3 L^{-1}) of the feed organics (i.e. EfOM, MLSS and AOM), were smaller than those of filtration resistance

(23.3–43.7%) during ceramic UF with the ozonated feed waters (Liu et al., 2018a; Tang et al., 2017; Wei et al., 2016). Likewise, Yang et al. (2019) reported a smaller reduction of DOC (45%) in the fouling layer, as compared to a decrease in filtration resistance (62.5%) during ceramic UF of a UV/TiO$_2$ pre-oxidized HA solution. However, an opposite trend has also been documented that the DOC reduction (80.7%) in the fouling layer of a ceramic UF membrane, after UV/PMS pre-oxidation of an AOM solution, was much larger than the decrease in filtration resistance (35.0%) (Cheng et al., 2018). Therefore, the removal of specific organic fractions and/or the alteration in physicochemical properties of feed organics, are of greater importance than the reduction of DOC, when using oxidation as a pre-treatment step before ceramic membrane filtration.

2.3.2 Effect of oxidation on fouling/separation behaviour of ceramic membranes in relation to changes in surface interactions

Changes in molecular/colloidal sizes of feed organics and size exclusion

Fouling of ceramic membranes is mainly attributed to: (i) the formation of a cake layer by large-sized biopolymers and/or colloids on the membrane surface via size exclusion and (ii) internal adsorption or pore clogging by small-sized organics (Liu et al., 2018a; Liu et al., 2018b; Wei et al., 2016; Zhang et al., 2015). The occurrence or transition of the different fouling modes, during pre-oxidation incorporated ceramic membrane filtration, is related to the alterations of molecular and/or colloidal sizes of the foulants relative to the pore sizes of the membranes. Therefore, changes in the sizes of organic molecules and colloids during pre-oxidation of raw water, can affect the fouling and separation properties of ceramic membranes. Among literature, there has been no definite effect of feed water pre-oxidation on the changes in MW of the feed organics. Ozonation (Filloux et al., 2012; Song et al., 2017a; Wei et al., 2016), UV/H$_2$O$_2$ (Zhang et al., 2015), UV/TiO$_2$ (Yang et al., 2019), UV (or Fe(II))/PMS (Cheng et al., 2018), ferrate(VI) (He et al., 2021a) and enzymatic reactions (Chen and Columbia, 2011), have shown effective breakdown of high-MW organic fractions (e.g. EfOM, NOM, AOM, HA and SA) into low-MW ones. However, other investigators found that the amount of mixed liquor organics, EfOM and NOM decreased in their entire MW ranges as a result of pre-ozonation (Ibn Abdul Hamid et al., 2017; Lehman and Liu, 2009; Liu et al., 2018a; Tang et al., 2017) or UV/H$_2$O$_2$ pre-oxidation (Winter et al., 2016), without a significant change in the MW distributions. The inconclusive effect of these pre-oxidation processes on the MW variation of the feed organics, can be interpreted by the dependence of the oxidation efficiencies on both the nature of the raw waters and the oxidant dosages.

Size exclusion of loose ceramic (MF or UF) membranes weakens due to the breakage of high-MW organics into smaller fractions during pre-oxidation, thereby enabling more organics to pass through or be trapped within the membrane pores. As an example, Wei et al. (2016) observed that, during ceramic UF of an ozonated AOM solution, the DOC of the feed organics decreased maximumly by 20.2% with increasing the ozone dosage to 15 mg L^{-1}, but the DOC in the permeate increased by up to 15.8%. Hence, careful control of the extent of pre-oxidation is required to reach a reasonable compromise between the fouling mitigation and pollutant rejection of ceramic membranes. Additionally, as the cake layer on ceramic membranes can act as a secondary separation layer, pre-oxidation is thus able to decrease the size exclusion of the membranes by suppressing the cake build-up. Song et al. (2017a) and Chen and Columbia (2011) reported that the rejection rates of SA during ceramic MF or UF increased as a function of filtration time, because of enhanced size exclusion through the progressive formation of cake layers on the membranes, which was, however, weakened in the presence of pre-ozonation or alginate lyase based pre-oxidation. A number of researchers (Liu et al., 2018a; Tang et al., 2017; Winter et al., 2016; Yang et al., 2019) have demonstrated a reduction in cake formation on ceramic MF/UF membranes after pre-ozonation, UV/H_2O_2 or UV/TiO_2 pre-oxidation of raw water, as evidenced by DOC decreases (12.8–75.9%) in the cake layers or rapidly reaching limited cake growth. Moreover, a fraction of medium-MW (1–10 kDa) organic matter tends to be adsorbed or trapped within the internal pores of loose ceramic membranes, which have widely been verified to result in physically irreversible fouling regardless of the use of ozonation (Ibn Abdul Hamid et al., 2017; Im et al., 2019; Liu et al., 2018a; Song et al., 2017a; Wei et al., 2016), UV/H_2O_2 (Winter et al., 2016; Zhang et al., 2015), UV/TiO_2 (Yang et al., 2019) or UV/PMS (Cheng et al., 2018) as the pre-oxidation step. As such, the pore size of a ceramic membrane can, in theory, act as another factor determining the required degree of pre-oxidation. As an example, according to Winter et al. (2016), after NOM pre-oxidation with ozone or UV/H_2O_2, the DOC reductions (44.6–48.6% vs. 44.7–51.9%) of the fouling layers and the MW characteristics of the oxidized NOM were comparable for 1 kDa and 50 kDa ceramic membranes, whereas the resistance decrease of the 1 kDa membrane (10.4–18.5%) was much smaller than that of the 50 kDa membrane (88.3–93.7%).

Apart from MW alterations of soluble organic matter as a result of oxidative decomposition, the particulate/colloidal sizes of feed organics also vary during pre-oxidation. Pre-ozonation (Song et al., 2018; Yin et al., 2020; Yu et al., 2017) and iron-based advanced oxidation processes, such as Fe(II)/H_2O_2 (Chiu and James, 2006), ferrate(VI) (Liu et al., 2019) and Fe(II)/PMS (Cheng et al., 2017b; Cheng et al., 2018) pre-oxidation, have been reported to converse organic molecules into larger particles through micro-flocculation, aggregation or coagulation. There is, however, no consensus on

how the variation of particulate/colloidal sizes affects the performance of ceramic membranes. For instance, ferrate(VI) pre-treatment (0.15 mM) has proved to increase the mean sizes of the particles in secondary effluent from 150–250 to 240–360 nm, because of coagulation induced by the *in-situ* formed Fe(III), leading to a more porous fouling layer (with an increase in the porosity from <4% to 16–20%) during ceramic UF (Liu et al., 2018a; Liu et al., 2018b). However, Xue et al. (2016) reported that pre-ozonated ceramic membrane bioreactor, having smaller sludge flocs (~71.3 μm) than before pre-ozonation (~92.0 μm), in turn, developed lower fouling. Other two studies (Cheng et al., 2017a; Song et al., 2018) showed that the formation of micro-flocs or aggregates, during BSA pre-treatment by ozone or Fe(II)/PMS, aggravated the fouling of ceramic UF membranes.

Changes in hydrophobicity of feed organics and hydrophobic/hydrophilic interactions

Pre-oxidation of organic substances in raw water is capable of transforming the organics into less hydrophobic moieties, apart from directly mineralizing a proportion of the organics. A typical indication for the hydrophobicity/hydrophilicity transformation during oxidation is the decrease of SUVA (the ratio of UV_{254} (m^{-1}) to DOC (mg L^{-1})), representing hydrophobicity (or aromaticity) of organic matter (Weishaar et al., 2003). Diverse pre-oxidation processes, e.g. ozonation (Gong et al., 2008; Lehman and Liu, 2009; Winter et al., 2016), UV/H_2O_2 (Kim et al., 2009; Song et al., 2004; Winter et al., 2016), UV/TiO_2 (Huang et al., 2008; Song et al., 2017b; Yang et al., 2019), UV/PMS (Cheng et al., 2018), Fe(II)/PMS (Cheng et al., 2018; Fan et al., 2020) and ferrate(VI) (Song et al., 2016), have presented a decrease in SUVA from 1–5.5 to 0.5–2.5 L mg^{-1} m^{-1} for natural waters and wastewaters, corresponding to a conversion of the hydrophobic organics into hydrophilic and/or transphilic fractions or a preferential removal of the hydrophobic organics. As widely considered, a water type with SUVA > 4 L mg^{-1} m^{-1} contains mostly hydrophobic (aromatic) organic fractions, while waters with SUVA < 2–3 L mg^{-1} m^{-1} comprise mainly hydrophilic (aliphatic) fractions (Ates et al., 2007).

Although a variety of pre-oxidation technologies have proved to convert hydrophobic organic fractions into hydrophilic ones, fewer studies have related the hydrophobicity/hydrophilicity conversion of organic matter to the fouling of ceramic membranes. The increase in hydrophilicity of feed organics can have an effect on cake layer fouling of ceramic membranes, mainly through: (i) reaching limited cake growth early, (ii) forming a porous cake layer and (iii) improving the cleanability of the membranes. As documented by Yang et al. (2019), after UV/TiO_2 pre-oxidation of HA solutions, limited cake growth was reached more early during crossflow ceramic UF, and the formed cake layer was more readily reversed with backwash. They explained that the oxidized HA molecules with increased hydrophilicity became more susceptible to both the cross flow during

filtration and the backflow during backwash. Oxidized organic matter with increased hydrophilicity tends to bond with water molecules, thereby weakening the hydrophobic interactions between the organic matter and ceramic membranes and between the organic matter (Xue et al., 2016). For instance, Song et al. (2004) demonstrated that hydrophobic phenolic groups of NOM upon UV/H_2O_2 oxidation were converted to quinone groups, which were more prone to form hydrogen bonds with water molecules rather than binding to each other.

Many studies with regard to pre-oxidation coupled ceramic membrane filtration have demonstrated an ineffective removal (Cheng et al., 2018; Tang et al., 2017; Wei et al., 2016) or aggravation (Liu et al., 2018a; Zhang et al., 2015) of irreversible fouling (e.g. pore clogging) during filtration with oxidized feed waters, because of an increase in hydrophilic, low-MW organic fractions. Song et al. (2017a) and Im et al. (2019) reported an exception that the irreversible fouling was alleviated during ceramic UF with an alginate solution and wastewater effluent in the presence of pre-ozonation, presumably because some of the residual ozone penetrating into the membrane pores further cleaned the internal fouling. It remains, however, unclear how the ineffective removal of the irreversible fouling of the ceramic membranes with pre-oxidation was related to the more hydrophilic nature or the lower molecular weight of the oxidized feed organics. Zhang et al. (2015) observed that the more hydrophilic, medium-MW AOM after UV/H_2O_2 oxidation was more substantially retained (57.8%) by a ceramic MF membrane with causing higher irreversible fouling, than was the less hydrophilic, equally-sized AOM (15.2%) after coagulation. A study of Wei et al. (2016) provided evidence for that irreversible fouling of ceramic membranes is mainly related to hydrophilicity, rather than molecular weight, of feed organics. They demonstrated that the foulants, causing the irreversible fouling of the ceramic UF membrane, were predominantly present as the hydrophilic, medium-MW (1–10 kDa) fraction of AOM, whereas the hydrophobic fraction at the same MW was nearly not retained by the membrane. However, there are two studies reporting an opposite trend. Cheng et al. (2018) revealed that the less hydrophilic, medium-MW fraction of UV/PMS oxidized AOM led to higher irreversible fouling during ceramic UF than the more hydrophilic, equally-sized fraction of Fe(II)/PMS pre-treated AOM. Yang et al. (2019) found that, as compared to the case without pre-oxidation, an increased number of medium-MW HA fractions were retained within the pores of ceramic UF membranes after UV/TiO_2 pre-oxidation, however, the irreversible (internal) fouling was reduced as a result of the increased hydrophilicity of the medium-MW HA fractions. The difference in relative dominance between the changes in hydrophobicity/hydrophilicity and MW of these feed organics during pre-oxidation is a possible reason for the disagreement in the literature with regard to whether the more or the less hydrophilic

organics act as prevailing irreversible foulants. Therefore, understanding how medium MW in combination with hydrophilicity/hydrophobicity of oxidized organics behave as a combined mechanism for irreversible fouling of ceramic membranes, remains an interesting issue for further studies.

Changes in charge properties of feed organics and electrostatic interactions

Pre-oxidation is able to modify the charge properties of particles in feed water through oxidizing the organic coating on the surface of the particles, with the formation of relatively polar functionalities (e.g. aldehydes, ketones and carboxylic acids). Most studies reported an increase in negative charges of various feed organics, e.g. SA (Yu et al., 2017), BSA (Yin et al., 2020), NOM (Yu et al., 2018) and EfOM (Im et al., 2018; Liu et al., 2018a), upon ozonation, except for an opposite tendency observed during mixed liquor ozonation (Tang et al., 2017). The number of carboxylic groups of feed organics increases as a result of pre-ozonation, thereby enhancing their negatively charged nature (Yin et al., 2020; Zhu et al., 2010). Unlike pre-ozonation processes, feed organics, upon ferrate(VI) pre-oxidation, usually undergo a decrease in their negative charges, attributed to charge neutralization by the *in-situ* formed ferric oxyhydroxide (He et al., 2021a; He et al., 2021b). As previously demonstrated (Liu et al., 2019; Liu et al., 2018a; Liu et al., 2018b), ferrate(VI) pre-treatment weakened the electrostatic repulsion between suspended solids with reduced charges, resulting in increased mean particle sizes and thus an increase in porosity of the formed fouling layers on ceramic membranes. Ferric (oxyhydr)oxide particles (Fe_2O_3, $FeOOH$ and amorphous ferric), *in-situ* formed during the reduction of ferrate(VI), have a zeta potential of around 0 mV at pH = 7, and are able to adsorb ferrate oxidation products (e.g. carboxylic acid) via hydrogen bonding (Yang et al., 2018). The (oxyhydr)oxide particles with the adsorbed foulants are thus considered to remain an electrostatically repulsive interaction between the particles, further contributing to the porous structure of the fouling layer (He et al., 2023; Tang et al., 2022). The negatively charged functionalities (e.g. carboxylic groups) of feed organics tend to increase as a result of ferrate(VI) oxidation (Liu et al., 2018b; Tang et al., 2022) or other typical oxidation, such as UV/H_2O_2 (Ahmed et al., 2009; Backlund, 1992), UV/TiO_2 (Ruppert et al., 1994), with an indication of decreased pH of raw water along with oxidation. Nonetheless, it is not always true that foulants with more negative charges exert less fouling of negatively charged membranes, while having more fouling of positively charged membranes. As an example, Song et al. (2018) reported an occurrence of minimum fouling of a positively charged Al_2O_3 membrane after pre-ozonation of a BSA feed solution at 2 mg O_3 L^{-1}, wherein the negative charges of the BSA solution were highest and the membrane-BSA electrostatic attraction was strongest.

2.4 Conclusions and future prospects

This chapter reviewed current studies concerning surface interactions in relation to separation/fouling behaviour of ceramic membranes in water treatment in the absence and presence of oxidation, and proposed key knowledge gaps and future prospects. The results show that oxidation of organic matter in feed water can exert a positive or negative effect on separation capabilities and fouling mitigation of ceramic membranes, depending on the whole change of different surface interactions between the organic matter and the membranes.

Key knowledge gaps were identified, as listed below, based on the literature review and discussion.

(1)   Present knowledge on surface interactions in relation to fouling of ceramic membranes is mainly limited to MF and UF processes. A clear understanding of fouling behaviour and characteristics of ceramic NF membranes in water treatment is still lacking;

(2)   Available studies about utilizing oxidation methods for fouling control of ceramic membranes are predominantly focused on dosing oxidants in feed water, which suffers a risk of secondary pollution due to a potential passage of the oxidants and/or oxidation by-products into the permeate. Very little attention has been paid to using (catalytic) oxidation during cleaning of, in particular, ceramic NF membranes.

To address the aforementioned knowledge gaps, the following research directions are suggested:

(1)   Fouling behaviour and characteristics of ceramic NF membranes should be explored with both model foulants for a mechanism study and real water/wastewater matrices for applied research;

(2)   More efforts need to go into developing cost-effective coating methods for immobilizing a proper catalyst on/in a ceramic NF membrane. Oxidative cleaning of ceramic NF membranes, in terms of efficacy and mechanisms, should be studied in relation to specific fouling characteristics of the membranes.

List of abbreviations

PC	Polycarbonate
PES	Polyethersulfone

PVP	Polyvinyl pyrrolidone
PVDF	Polyvinylidene fluoride
PVC	Polyvinyl chloride
RC	Regenerated cellulose
TFC	Thin film composite
AFM	Atomic force microscopy
XDLVO	Extended Derjaguin-Landau-Verwey-Overbeek
MF	Microfiltration
UF	Ultrafiltration
NF	Nanofiltration
CTAB	Cetyl-trimethylammonium bromide
SDBS	Sodium dodecyl benzenesulfonate
SDS	Sodium dodecyl sulfate
DTAB	Dodecyl-trimethylammonium bromide
MW	Molecular weight
MWCO	Molecular weight cut-off
PEG	Polyethylene glycol
EPS	Extra-cellular polymeric substances
$KMnO_4$	Potassium permanganate
TiO_2	Titania

ZrO_2	Zirconia
Al_2O_3	Alumina
SiO_2	Silica
SiC	Silicon carbide
IONs	Iron oxide nanoparticles
$\alpha\text{-}Si_3N_4$	Silicon nitride
H_2O_2	Hydrogen peroxide
DOC	Dissolved organic carbon
UV_{254}	UV absorbance at 254 nm
SUVA	Specific UV absorbance at 254 nm
$^{\bullet}OH$	Hydroxyl radical
SMP	Soluble microbial product
AOM	Algal organic matter
MLSS	Mixed liquor suspended solid
EfOM	Effluent organic matter
NOM	Natural organic matter
OSPW	Oil sands process-affected water
PMS	Peroxymonosulfate
Fe(II)	Ferrous
HA	Humic acid

SA	Sodium alginate
BSA	Bovine serum albumin
R_r	Hydraulically reversible fouling resistance
R_{ir}	Hydraulically irreversible fouling resistance
R_t	Retention ability
HPO	Hydrophobic substance
HPI	Hydrophilic substance
TPI	Transphilic substance

References

Ahmed, B., Mohamed, H., Limem, E., Nasr, B., 2009. Degradation and mineralization of organic pollutants contained in actual pulp and paper mill wastewaters by a UV/H_2O_2 process. Industrial & Engineering Chemistry Research 48(7), 3370-3379.

Al-Abadleh, H.A., Grassian, V.H., 2003a. FT-IR study of water adsorption on aluminum oxide surfaces. Langmuir 19(2), 341-347.

Al-Abadleh, H.A., Grassian, V.H., 2003b. Oxide surfaces as environmental interfaces. Surface Science Reports 52(3), 63-161.

Alresheedi, M.T., Barbeau, B., Basu, O.D., 2019. Comparisons of NOM fouling and cleaning of ceramic and polymeric membranes during water treatment. Separation and Purification Technology 209, 452-460.

Árki, P., Hecker, C., Tomandl, G., Joseph, Y., 2019. Streaming potential properties of ceramic nanofiltration membranes – Importance of surface charge on the ion rejection. Separation and Purification Technology 212, 660-669.

Arndt, F., Ehlen, F., Schütz, S., Anlauf, H., Nirschl, H., 2016. Influence of operating parameters and membrane materials on fouling of ceramic hollow fibre membranes. Separation and Purification Technology 171, 289-296.

Asif, M.B., Li, C., Ren, B., Maqbool, T., Zhang, X., Zhang, Z., 2021. Elucidating the impacts of intermittent in-situ ozonation in a ceramic membrane bioreactor: Micropollutant removal, microbial community evolution and fouling mechanisms. Journal of Hazardous Materials 402, 123730.

Ates, N., Kitis, M., Yetis, U., 2007. Formation of chlorination by-products in waters with low SUVA–correlations with SUVA and differential UV spectroscopy. Water Research 41(18), 4139-4148.

Backlund, P., 1992. Degradation of aquatic humic material by ultraviolet light. Chemosphere 25(12), 1869-1878.

Bai, Z., Gao, S., Yu, H., Liu, X., Tian, J., 2022. Layered metal oxides loaded ceramic membrane activating peroxymonosulfate for mitigation of NOM membrane fouling. Water Research 222, 118928.

Barredo-Damas, S., Alcaina-Miranda, M.I., Iborra-Clar, M.I., Mendoza-Roca, J.A., 2012. Application of tubular ceramic ultrafiltration membranes for the treatment of integrated textile wastewaters. Chemical Engineering Journal 192, 211-218.

Chen, D., Columbia, M., 2011. Enzymatic control of alginate fouling of dead-end MF and UF ceramic membranes. Journal of Membrane Science 381(1), 118-125.

Chen, H., Jia, X., Wei, M., Wang, Y., 2017. Ceramic tubular nanofiltration membranes with tunable performances by atomic layer deposition and calcination. Journal of Membrane Science 528, 95-102.

Chen, M., Heijman, S.G.J., Luiten-Olieman, M.W.J., Rietveld, L.C., 2022. Oil-in-water emulsion separation: Fouling of alumina membranes with and without a silicon carbide deposition in constant flux filtration mode. Water Research 216, 118267.

Cheng, X., Liang, H., Ding, A., Tang, X., Liu, B., Zhu, X., Gan, Z., Wu, D., Li, G., 2017a. Ferrous iron/peroxymonosulfate oxidation as a pretreatment for ceramic ultrafiltration membrane: Control of natural organic matter fouling and degradation of atrazine. Water Research 113, 32-41.

Cheng, X., Liang, H., Ding, A., Zhu, X., Tang, X., Gan, Z., Xing, J., Wu, D., Li, G., 2017b. Application of Fe(II)/peroxymonosulfate for improving ultrafiltration membrane performance in surface water treatment: Comparison with coagulation and ozonation. Water Research 124, 298-307.

Cheng, X., Wu, D., Liang, H., Zhu, X., Tang, X., Gan, Z., Xing, J., Luo, X., Li, G., 2018. Effect of sulfate radical-based oxidation pretreatments for mitigating ceramic UF membrane fouling caused by algal extracellular organic matter. Water Research 145, 39-49.

Childress, A.E., Elimelech, M., 1996. Effect of solution chemistry on the surface charge of polymeric reverse osmosis and nanofiltration membranes. Journal of Membrane Science 119(2), 253-268.

Chiu, T.Y., James, A.E., 2006. Sustainable flux enhancement in non-circular ceramic membranes on wastewater using the Fenton process. Journal of Membrane Science 279(1), 347-353.

Chong, J.Y., Wang, R., 2019. From micro to nano: Polyamide thin film on microfiltration ceramic tubular membranes for nanofiltration. Journal of Membrane Science 587, 117161.

Dobrak, A., Verrecht, B., Van den Dungen, H., Buekenhoudt, A., Vankelecom, I.F.J., Van der Bruggen, B., 2010. Solvent flux behavior and rejection characteristics of hydrophilic and hydrophobic mesoporous and microporous TiO_2 and ZrO_2 membranes. Journal of Membrane Science 346(2), 344-352.

Doneva, T., Lafforgue, C., Chaufer, B., Rabiller, M., 2001. Influence of physicochemical conditions on amino acid adsorption on inorganic membranes. Desalination 133(2), 123-133.

Du, X., Zhang, K., Xie, B., Zhao, J., Cheng, X., Kai, L., Nie, J., Wang, Z., Li, G., Liang, H., 2019. Peroxymonosulfate-assisted electro-oxidation/coagulation coupled with ceramic membrane for manganese and phosphorus removal in surface water. Chemical Engineering Journal 365, 334-343.

Espíndola, J.C., Szymański, K., Cristóvão, R.O., Mendes, A., Vilar, V.J.P., Mozia, S., 2019. Performance of hybrid systems coupling advanced oxidation processes and ultrafiltration for oxytetracycline removal. Catalysis Today 328, 274-280.

Fan, J., Lin, T., Chen, W., Xu, H., Tao, H., 2020. Control of ultrafiltration membrane fouling during the recycling of sludge water based on Fe(II)-activated peroxymonosulfate pretreatment. Chemosphere 246, 125840.

Fan, X., Tao, Y., Wei, D., Zhang, X., Lei, Y., Noguchi, H., 2015. Removal of organic matter and disinfection by-products precursors in a hybrid process combining ozonation with ceramic membrane ultrafiltration. Frontiers of Environmental Science & Engineering 9(1), 112-120.

Fievet, P., Szymczyk, A., Labbez, C., Aoubiza, B., Simon, C., Foissy, A., Pagetti, J., 2001. Determining the zeta potential of porous membranes using electrolyte conductivity inside pores. Journal of Colloid and Interface Science 235(2), 383-390.

Filloux, E., Gallard, H., Croue, J.-P., 2012. Identification of effluent organic matter fractions responsible for low-pressure membrane fouling. Water Research 46(17), 5531-5540.

Fu, W., Wang, X., Zheng, J., Liu, M., Wang, Z., 2019. Antifouling performance and mechanisms in an electrochemical ceramic membrane reactor for wastewater treatment. Journal of Membrane Science 570-571, 355-361.

Fujioka, T., Khan, S.J., McDonald, J.A., Nghiem, L.D., 2014. Nanofiltration of trace organic chemicals: A comparison between ceramic and polymeric membranes. Separation and Purification Technology 136, 258-264.

Gao, N., Fan, W., Xu, Z.-K., 2020. Ceramic membrane with protein-resistant surface via dopamine/diglycolamine co-deposition. Separation and Purification Technology 234, 116135.

Geng, P., Chen, G., 2017. Antifouling ceramic membrane electrode modified by Magnéli Ti_4O_7 for electro-microfiltration of humic acid. Separation and Purification Technology 185, 61-71.

Gong, J., Liu, Y., Sun, X., 2008. O_3 and UV/O_3 oxidation of organic constituents of biotreated municipal wastewater. Water Research 42(4), 1238-1244.

Gray, H.E., Powell, T., Choi, S., Smith, D.S., Parker, W.J., 2020. Organic phosphorus removal using an integrated advanced oxidation-ultrafiltration process. Water Research 182, 115968.

Gray, S.R., Ritchie, C.B., Tran, T., Bolto, B.A., 2007. Effect of NOM characteristics and membrane type on microfiltration performance. Water Research 41(17), 3833-3841.

Gu, Q., Ng, T.C.A., Zhang, L., Lyu, Z., Zhang, Z., Ng, H.Y., Wang, J., 2020. Interfacial diffusion assisted chemical deposition (ID-CD) for confined surface modification of alumina microfiltration membranes toward high-flux and anti-fouling. Separation and Purification Technology 235, 116177.

Guo, Y., Song, Z., Xu, B., Li, Y., Qi, F., Croue, J.-P., Yuan, D., 2018. A novel catalytic ceramic membrane fabricated with $CuMn_2O_4$ particles for emerging UV absorbers degradation from aqueous and membrane fouling elimination. Journal of Hazardous Materials 344, 1229-1239.

Guo, Y., Xu, B., Qi, F., 2016. A novel ceramic membrane coated with MnO_2–Co_3O_4 nanoparticles catalytic ozonation for benzophenone-3 degradation in aqueous solution: Fabrication, characterization and performance. Chemical Engineering Journal 287, 381-389.

Hass, K.C., Schneider, W.F., Curioni, A., Andreoni, W., 1998. The chemistry of water on alumina surfaces: Reaction dynamics from first principles. Science 282(5387), 265-268.

He, H., Jing, W., Xing, W., Fan, Y., 2011. Improving protein resistance of α-Al_2O_3 membranes by modification with POEGMA brushes. Applied Surface Science 258(3), 1038-1044.

He, H., Liu, Y., Wang, L., Qiu, W., Li, D., Liu, Z., Ma, J., 2023. Improvements of ferrate(VI) pretreatment on membrane flux and membrane rejection using cheap NaClO reagent. Water Research 229, 119520.

He, H.-Y., Qiu, W., Liu, Y.-L., Xu, S.-Y., Ma, J., Wang, L., 2021a. Ferrate preoxidation alleviating membrane fouling through the formation of a hydrophilic prefiltration layer. ACS ES&T Engineering 1(11), 1576-1586.

He, H.-Y., Qiu, W., Liu, Y.-L., Yu, H.-R., Wang, L., Ma, J., 2021b. Effect of ferrate pre-oxidation on algae-laden water ultrafiltration: Attenuating membrane fouling and decreasing formation potential of disinfection byproducts. Water Research 190, 116690.

Herbig, R., Arki, P., Tomandl, G., Bräunig, R.E., 2003. Comparison of electrokinetic properties of ceramic powders and membranes. Separation and Purification Technology 32(1), 363-369.

Hofs, B., Ogier, J., Vries, D., Beerendonk, E.F., Cornelissen, E.R., 2011. Comparison of ceramic and polymeric membrane permeability and fouling using surface water. Separation and Purification Technology 79(3), 365-374.

Huang, X., Leal, M., Li, Q., 2008. Degradation of natural organic matter by TiO_2 photocatalytic oxidation and its effect on fouling of low-pressure membranes. Water Research 42(4), 1142-1150.

Ibn Abdul Hamid, K., Sanciolo, P., Gray, S., Duke, M., Muthukumaran, S., 2017. Impact of ozonation and biological activated carbon filtration on ceramic membrane fouling. Water Research 126, 308-318.

Im, D., Nakada, N., Fukuma, Y., Kato, Y., Tanaka, H., 2018. Performance of combined ozonation, coagulation and ceramic membrane process for water reclamation: Effects and mechanism of ozonation on virus coagulation. Separation and Purification Technology 192, 429-434.

Im, D., Nakada, N., Kato, Y., Aoki, M., Tanaka, H., 2019. Pretreatment of ceramic membrane microfiltration in wastewater reuse: A comparison between ozonation and coagulation. Journal of Environmental Management 251, 109555.

Jermann, D., Pronk, W., Meylan, S., Boller, M., 2007. Interplay of different NOM fouling mechanisms during ultrafiltration for drinking water production. Water Research 41(8), 1713-1722.

Jiang, T., Tian, T., Guan, Y.-F., Yu, H.-Q., 2022. Contrasting behaviors of pre-ozonation on ceramic membrane biofouling: Early stage vs late stage. Water Research 220, 118702.

Jin, L., Ong, S.L., Ng, H.Y., 2010. Comparison of fouling characteristics in different pore-sized submerged ceramic membrane bioreactors. Water Research 44(20), 5907-5918.

Kampf, C.J., Liu, F., Reinmuth-Selzle, K., Berkemeier, T., Meusel, H., Shiraiwa, M., Pöschl, U., 2015. Protein cross-linking and oligomerization through dityrosine formation upon exposure to ozone. Environmental Science & Technology 49(18), 10859-10866.

Karnik, B.S., Davies, S.H.R., Chen, K.C., Jaglowski, D.R., Baumann, M.J., Masten, S.J., 2005. Effects of ozonation on the permeate flux of nanocrystalline ceramic membranes. Water Research 39(4), 728-734.

Kasprzyk-Hordern, B., 2004. Chemistry of alumina, reactions in aqueous solution and its application in water treatment. Advances in Colloid and Interface Science 110(1), 19-48.

Kim, I., Yamashita, N., Tanaka, H., 2009. Performance of UV and UV/H_2O_2 processes for the removal of pharmaceuticals detected in secondary effluent of a sewage treatment plant in Japan. Journal of Hazardous Materials 166(2), 1134-1140.

Kim, J., Davies, S.H.R., Baumann, M.J., Tarabara, V.V., Masten, S.J., 2008. Effect of ozone dosage and hydrodynamic conditions on the permeate flux in a hybrid ozonation–ceramic ultrafiltration system treating natural waters. Journal of Membrane Science 311(1), 165-172.

Kim, J., Shan, W., Davies, S.H.R., Baumann, M.J., Masten, S.J., Tarabara, V.V., 2009. Interactions of aqueous NOM with nanoscale TiO_2: Implications for ceramic membrane filtration-ozonation hybrid process. Environmental Science & Technology 43(14), 5488-5494.

Kujawa, J., Al-Gharabli, S., Kujawski, W., Knozowska, K., 2017. Molecular grafting of fluorinated and nonfluorinated alkylsiloxanes on various ceramic membrane surfaces for the removal of volatile organic compounds applying vacuum membrane distillation. ACS Applied Materials & Interfaces 9(7), 6571-6590.

Larbot, A., Fabre, J.P., Guizard, C., Cot, L., 1988. Inorganic membranes obtained by sol-gel techniques. Journal of Membrane Science 39(3), 203-212.

Lee, S.-J., Dilaver, M., Park, P.-K., Kim, J.-H., 2013. Comparative analysis of fouling characteristics of ceramic and polymeric microfiltration membranes using filtration models. Journal of Membrane Science 432, 97-105.

Lee, S.-J., Kim, J.-H., 2014. Differential natural organic matter fouling of ceramic versus polymeric ultrafiltration membranes. Water Research 48, 43-51.

Lee, S., Cho, J., 2004. Comparison of ceramic and polymeric membranes for natural organic matter (NOM) removal. Desalination 160(3), 223-232.

Lee, S., Lee, K., Wan, W.M., Choi, Y., 2005. Comparison of membrane permeability and a fouling mechanism by pre-ozonation followed by membrane filtration and residual ozone in membrane cells. Desalination 178(1), 287-294.

Lee, S., Park, G., Amy, G., Hong, S.-K., Moon, S.-H., Lee, D.-H., Cho, J., 2002. Determination of membrane pore size distribution using the fractional rejection of nonionic and charged macromolecules. Journal of Membrane Science 201(1), 191-201.

Lee, W.J., Bao, Y., Hu, X., Lim, T.-T., 2019. Hybrid catalytic ozonation-membrane filtration process with CeOx and MnOx impregnated catalytic ceramic membranes for micropollutants degradation. Chemical Engineering Journal 378, 121670.

Lehman, S.G., Liu, L., 2009. Application of ceramic membranes with pre-ozonation for treatment of secondary wastewater effluent. Water Research 43(7), 2020-2028.

Li, C., Lu, Z., Ao, X., Sun, W., Huang, X., 2022. Degradation kinetics and removal efficiencies of pharmaceuticals by photocatalytic ceramic membranes using ultraviolet light-emitting diodes. Chemical Engineering Journal 427, 130828.

Li, L., Liu, Z., Zhang, Q., Meng, C., Zhang, T., Zhai, J., 2015. Underwater superoleophobic porous membrane based on hierarchical TiO_2 nanotubes: multifunctional integration of oil–water separation, flow-through photocatalysis and self-cleaning. Journal of Materials Chemistry A 3(3), 1279-1286.

Li, L., Wang, J.-W., Zhong, H., Hao, L.-Y., Abadikhah, H., Xu, X., Chen, C.-S., Agathopoulos, S., 2017. Novel α-Si_3N_4 planar nanowire superhydrophobic membrane prepared through in-situ nitridation of silicon for membrane distillation. Journal of Membrane Science 543, 98-105.

Li, Q., Elimelech, M., 2004. Organic fouling and chemical cleaning of nanofiltration membranes: Measurements and mechanisms. Environmental Science & Technology 38(17), 4683-4693.

Liu, J., He, K., Tang, S., Wang, T., Zhang, Z., 2019a. A comparative study of ferrous, ferric and ferrate pretreatment for ceramic membrane fouling alleviation in reclaimed water treatment. Separation and Purification Technology 217, 118-127.

Liu, J., Zhang, Z., Chen, Q., Zhang, X., 2018a. Synergistic effect of ferrate(VI)-ozone integrated pretreatment on the improvement of water quality and fouling alleviation of ceramic UF membrane in reclaimed water treatment. Journal of Membrane Science 567, 216-227.

Liu, J., Zhang, Z., Liu, Z., Zhang, X., 2018b. Integration of ferrate(VI) pretreatment and ceramic membrane reactor for membrane fouling mitigation in reclaimed water treatment. Journal of Membrane Science 552, 315-325.

Liu, Z., Zhu, X., Liang, P., Zhang, X., Kimura, K., Huang, X., 2019b. Distinction between polymeric and ceramic membrane in AnMBR treating municipal wastewater: In terms of irremovable fouling. Journal of Membrane Science 588, 117229.

Lu, D., Zhang, T., Gutierrez, L., Ma, J., Croué, J.-P., 2016. Influence of surface properties of filtration-layer metal oxide on ceramic membrane fouling during ultrafiltration of oil/water emulsion. Environmental Science & Technology 50(9), 4668-4674.

Lu, D., Zhang, T., Ma, J., 2015. Ceramic membrane fouling during ultrafiltration of oil/water emulsions: Roles played by stabilization surfactants of oil droplets. Environmental Science & Technology 49(7), 4235-4244.

Martínez, F., Martín, A., Prádanos, P., Calvo, J.I., Palacio, L., Hernández, A., 2000. Protein adsorption and deposition onto microfiltration membranes: The role of solute–solid interactions. Journal of Colloid and Interface Science 221(2), 254-261.

Moritz, T., Benfer, S., Arki, P., Tomandl, G., 2001a. Investigation of ceramic membrane materials by streaming potential measurements. Colloids and Surfaces A: Physicochemical and Engineering Aspects 195(1), 25-33.

Moritz, T., Benfer, S., Árki, P., Tomandl, G., 2001b. Influence of the surface charge on the permeate flux in the dead-end filtration with ceramic membranes. Separation and Purification Technology 25(1), 501-508.

Mullet, M., Fievet, P., Reggiani, J.C., Pagetti, J., 1997. Surface electrochemical properties of mixed oxide ceramic membranes: Zeta-potential and surface charge density. Journal of Membrane Science 123(2), 255-265.

Mullet, M., Fievet, P., Szymczyk, A., Foissy, A., Reggiani, J.C., Pagetti, J., 1999. A simple and accurate determination of the point of zero charge of ceramic membranes. Desalination 121(1), 41-48.

Murić, A., Petrinić, I., Christensen, M.L., 2014. Comparison of ceramic and polymeric ultrafiltration membranes for treating wastewater from metalworking industry. Chemical Engineering Journal 255, 403-410.

Mustafa, G., Wyns, K., Buekenhoudt, A., Meynen, V., 2016a. Antifouling grafting of ceramic membranes validated in a variety of challenging wastewaters. Water Research 104, 242-253.

Mustafa, G., Wyns, K., Buekenhoudt, A., Meynen, V., 2016b. New insights into the fouling mechanism of dissolved organic matter applying nanofiltration membranes with a variety of surface chemistries. Water Research 93, 195-204.

Mustafa, G., Wyns, K., Janssens, S., Buekenhoudt, A., Meynen, V., 2018. Evaluation of the fouling resistance of methyl grafted ceramic membranes for inorganic foulants and co-effects of organic foulants. Separation and Purification Technology 193, 29-37.

Mustafa, G., Wyns, K., Vandezande, P., Buekenhoudt, A., Meynen, V., 2014. Novel grafting method efficiently decreases irreversible fouling of ceramic nanofiltration membranes. Journal of Membrane Science 470, 369-377.

Nagasawa, H., Omura, T., Asai, T., Kanezashi, M., Tsuru, T., 2020. Filtration of surfactant-stabilized oil-in-water emulsions with porous ceramic membranes: Effects of membrane pore size and surface charge on fouling behavior. Journal of Membrane Science 610, 118210.

Nazzal, F.F., Wiesner, M.R., 1994. pH and ionic strength effects on the performance of ceramic membranes in water filtration. Journal of Membrane Science 93(1), 91-103.

Ng, T.C.A., Lyu, Z., Gu, Q., Zhang, L., Poh, W.J., Zhang, Z., Wang, J., Ng, H.Y., 2020. Effect of gradient profile in ceramic membranes on filtration characteristics: Implications for membrane development. Journal of Membrane Science 595, 117576.

Nguyen, S.T., Roddick, F.A., 2010. Effects of ozonation and biological activated carbon filtration on membrane fouling in ultrafiltration of an activated sludge effluent. Journal of Membrane Science 363(1), 271-277.

Nosaka, A.Y., Nishino, J., Fujiwara, T., Ikegami, T., Yagi, H., Akutsu, H., Nosaka, Y., 2006. Effects of thermal treatments on the recovery of adsorbed water and photocatalytic activities of TiO_2 photocatalytic systems. The Journal of Physical Chemistry B 110(16), 8380-8385.

Nyamutswa, L.T., Zhu, B., Collins, S.F., Navaratna, D., Duke, M.C., 2020. Light conducting photocatalytic membrane for chemical-free fouling control in water treatment. Journal of Membrane Science 604, 118018.

Park, H., Kim, Y., An, B., Choi, H., 2012. Characterization of natural organic matter treated by iron oxide nanoparticle incorporated ceramic membrane-ozonation process. Water Research 46(18), 5861-5870.

Park, N., Kwon, B., Kim, I.S., Cho, J., 2005. Biofouling potential of various NF membranes with respect to bacteria and their soluble microbial products (SMP): Characterizations, flux decline, and transport parameters. Journal of Membrane Science 258(1), 43-54.

Plakas, K.V., Mantza, A., Sklari, S.D., Zaspalis, V.T., Karabelas, A.J., 2019. Heterogeneous Fenton-like oxidation of pharmaceutical diclofenac by a catalytic iron-oxide ceramic microfiltration membrane. Chemical Engineering Journal 373, 700-708.

Puthai, W., Kanezashi, M., Nagasawa, H., Tsuru, T., 2017. Development and permeation properties of SiO_2-ZrO_2 nanofiltration membranes with a MWCO of <200. Journal of Membrane Science 535, 331-341.

Puthai, W., Kanezashi, M., Nagasawa, H., Wakamura, K., Ohnishi, H., Tsuru, T., 2016. Effect of firing temperature on the water permeability of SiO_2–ZrO_2 membranes for nanofiltration. Journal of Membrane Science 497, 348-356.

Qin, W., Guan, K., Lei, B., Liu, Y., Peng, C., Wu, J., 2015. One-step coating and characterization of α-Al_2O_3 microfiltration membrane. Journal of Membrane Science 490, 160-168.

Qu, F., Liang, H., Zhou, J., Nan, J., Shao, S., Zhang, J., Li, G., 2014. Ultrafiltration membrane fouling caused by extracellular organic matter (EOM) from Microcystis aeruginosa: Effects of membrane pore size and surface hydrophobicity. Journal of Membrane Science 449, 58-66.

Rosman, N., Salleh, W.N.W., Mohamed, M.A., Jaafar, J., Ismail, A.F., Harun, Z., 2018. Hybrid membrane filtration-advanced oxidation processes for removal of pharmaceutical residue. Journal of Colloid and Interface Science 532, 236-260.

Ruppert, G., Bauer, R., Heisler, G., 1994. UV-O_3, UV-H_2O_2, UV-TiO_2 and the photo-Fenton reaction – Comparison of advanced oxidation processes for wastewater treatment. Chemosphere 28(8), 1447-1454.

Sah, A., Castricum, H.L., Bliek, A., Blank, D.H.A., ten Elshof, J.E., 2004. Hydrophobic modification of γ-alumina membranes with organochlorosilanes. Journal of Membrane Science 243(1), 125-132.

Sbaï, M., Fievet, P., Szymczyk, A., Aoubiza, B., Vidonne, A., Foissy, A., 2003. Streaming potential, electroviscous effect, pore conductivity and membrane potential for the determination of the surface potential of a ceramic ultrafiltration membrane. Journal of Membrane Science 215(1), 1-9.

Shan, L., Fan, H., Guo, H., Ji, S., Zhang, G., 2016. Natural organic matter fouling behaviors on superwetting nanofiltration membranes. Water Research 93, 121-132.

Shang, R., Vuong, F., Hu, J., Li, S., Kemperman, A.J.B., Nijmeijer, K., Cornelissen, E.R., Heijman, S.G.J., Rietveld, L.C., 2015. Hydraulically irreversible fouling on ceramic MF/UF membranes: Comparison of fouling indices, foulant composition and irreversible pore narrowing. Separation and Purification Technology 147, 303-310.

Shirai, K., Sugimoto, T., Watanabe, K., Haruta, M., Kurata, H., Matsumoto, Y., 2016. Effect of water adsorption on carrier trapping dynamics at the surface of anatase TiO_2 nanoparticles. Nano Letters 16(2), 1323-1327.

Sneh, O., Cameron, M.A., George, S.M., 1996. Adsorption and desorption kinetics of H_2O on a fully hydroxylated SiO_2 surface. Surface Science 364(1), 61-78.

Son, J.-W., Sim, E.-H., Choi, N.-C., Kim, S.-B., Park, C.-Y., 2017. Comparative analysis for fouling characteristics of river water, secondary effluent, and humic acid solution in ceramic membrane ultrafiltration. Separation Science and Technology 52(13), 2199-2211.

Song, J., Zhang, Z., Tang, S., Tan, Y., Zhang, X., 2018. Does pre-ozonation or in-situ ozonation really mitigate the protein-based ceramic membrane fouling in the integrated process of ozonation coupled with ceramic membrane filtration? Journal of Membrane Science 548, 254-262.

Song, J., Zhang, Z., Zhang, X., 2017a. A comparative study of pre-ozonation and in-situ ozonation on mitigation of ceramic UF membrane fouling caused by alginate. Journal of Membrane Science 538, 50-57.

Song, L., Zhu, B., Gray, S., Duke, M., Muthukumaran, S., 2017b. Performance of hybrid photocatalytic-ceramic membrane system for the treatment of secondary effluent. Membranes 7(2), 20.

Song, W., Ravindran, V., Koel, B.E., Pirbazari, M., 2004. Nanofiltration of natural organic matter with H_2O_2/UV pretreatment: Fouling mitigation and membrane surface characterization. Journal of Membrane Science 241(1), 143-160.

Song, Y., Deng, Y., Jung, C., 2016. Mitigation and degradation of natural organic matters (NOMs) during ferrate(VI) application for drinking water treatment. Chemosphere 146, 145-153.

Song, Z., Fathizadeh, M., Huang, Y., Chu, K.H., Yoon, Y., Wang, L., Xu, W.L., Yu, M., 2016. TiO_2 nanofiltration membranes prepared by molecular layer deposition for water purification. Journal of Membrane Science 510, 72-78.

Sun, H., Liu, H., Han, J., Zhang, X., Cheng, F., Liu, Y., 2018. Chemical cleaning-associated generation of dissolved organic matter and halogenated byproducts in ceramic MBR: Ozone versus hypochlorite. Water Research 140, 243-250.

Sun, S., Yao, H., Fu, W., Hua, L., Zhang, G., Zhang, W., 2018. Reactive Photo-Fenton ceramic membranes: Synthesis, characterization and antifouling performance. Water Research 144, 690-698.

Szymanska, K., Zouboulis, A.I., Zamboulis, D., 2014. Hybrid ozonation–microfiltration system for the treatment of surface water using ceramic membrane. Journal of Membrane Science 468, 163-171.

Szymczyk, A., Pierre, A., Reggiani, J.C., Pagetti, J., 1997. Characterisation of the electrokinetic properties of plane inorganic membranes using streaming potential measurements. Journal of Membrane Science 134(1), 59-66.

Takeuchi, M., Martra, G., Coluccia, S., Anpo, M., 2005. Investigations of the structure of H_2O clusters adsorbed on TiO_2 surfaces by near-infrared absorption spectroscopy. The Journal of Physical Chemistry B 109(15), 7387-7391.

Tamura, H., Mita, K., Tanaka, A., Ito, M., 2001. Mechanism of hydroxylation of metal oxide surfaces. Journal of Colloid and Interface Science 243(1), 202-207.

Tang, C.Y., Kwon, Y.-N., Leckie, J.O., 2009. Effect of membrane chemistry and coating layer on physiochemical properties of thin film composite polyamide RO and NF membranes: I. FTIR and XPS characterization of polyamide and coating layer chemistry. Desalination 242(1), 149-167.

Tang, P., Liu, B., Xie, W., Wang, P., He, Q., Bao, J., Zhang, Y., Zhang, Z., Li, J., Ma, J., 2022. Synergistic mechanism of combined ferrate and ultrafiltration process for shale gas wastewater treatment. Journal of Membrane Science 641, 119921.

Tang, S., Zhang, Z., Zhang, X., 2017. New insight into the effect of mixed liquor properties changed by pre-ozonation on ceramic UF membrane fouling in wastewater treatment. Chemical Engineering Journal 314, 670-680.

Tuladhar, A., Dewan, S., Kubicki, J.D., Borguet, E., 2016. Spectroscopy and ultrafast vibrational dynamics of strongly hydrogen bonded OH species at the α-Al_2O_3(11$\bar{2}$0)/H_2O interface. The Journal of Physical Chemistry C 120(29), 16153-16161.

Tummons, E.N., Tarabara, V.V., Chew, Jia W., Fane, A.G., 2016. Behavior of oil droplets at the membrane surface during crossflow microfiltration of oil–water emulsions. Journal of Membrane Science 500, 211-224.

Van Geluwe, S., Braeken, L., Van der Bruggen, B., 2011. Ozone oxidation for the alleviation of membrane fouling by natural organic matter: A review. Water Research 45(12), 3551-3570.

Van Gestel, T., Vandecasteele, C., Buekenhoudt, A., Dotremont, C., Luyten, J., Leysen, R., Van der Bruggen, B., Maes, G., 2002. Salt retention in nanofiltration with multilayer ceramic TiO_2 membranes. Journal of Membrane Science 209(2), 379-389.

Van Oss, C.J., 2007. Development and applications of the interfacial tension between water and organic or biological surfaces. Colloids and Surfaces B: Biointerfaces 54(1), 2-9.

Wang, H., Park, M., Liang, H., Wu, S., Lopez, I.J., Ji, W., Li, G., Snyder, S.A., 2017. Reducing ultrafiltration membrane fouling during potable water reuse using pre-ozonation. Water Research 125, 42-51.

Wang, L., Miao, R., Wang, X., Lv, Y., Meng, X., Yang, Y., Huang, D., Feng, L., Liu, Z., Ju, K., 2013. Fouling behavior of typical organic foulants in polyvinylidene fluoride ultrafiltration membranes: Characterization from microforces. Environmental Science & Technology 47(8), 3708-3714.

Wang, S., Tian, J., Jia, L., Jia, J., Shan, S., Wang, Q., Cui, F., 2021. Removal of aqueous organic contaminants using submerged ceramic hollow fiber membrane coupled with peroxymonosulfate oxidation: Comparison of CuO catalyst dispersed in the feed water and immobilized on the membrane. Journal of Membrane Science 618, 118707.

Wang, X., Li, Y., Yu, H., Yang, F., Tang, C.Y., Quan, X., Dong, Y., 2020. High-flux robust ceramic membranes functionally decorated with nano-catalyst for emerging micro-pollutant removal from water. Journal of Membrane Science 611, 118281.

Wang, Z., Wan, Y., Xie, P., Zhou, A., Ding, J., Wang, J., Zhang, L., Wang, S., Zhang, T.C., 2019. Ultraviolet/persulfate (UV/PS) pretreatment of typical natural organic matter (NOM): Variation of characteristics and control of membrane fouling. Chemosphere 214, 136-147.

Wang, Z., Wei, Y.-M., Xu, Z.-L., Cao, Y., Dong, Z.-Q., Shi, X.-L., 2016. Preparation, characterization and solvent resistance of γ-Al_2O_3/α-Al_2O_3 inorganic hollow fiber nanofiltration membrane. Journal of Membrane Science 503, 69-80.

Wei, D., Tao, Y., Zhang, Z., Liu, L., Zhang, X., 2016. Effect of in-situ ozonation on ceramic UF membrane fouling mitigation in algal-rich water treatment. Journal of Membrane Science 498, 116-124.

Wei, D., Tao, Y., Zhang, Z., Zhang, X., 2016. Effect of pre-ozonation on mitigation of ceramic UF membrane fouling caused by algal extracellular organic matters. Chemical Engineering Journal 294, 157-166.

Weishaar, J.L., Aiken, G.R., Bergamaschi, B.A., Fram, M.S., Fujii, R., Mopper, K., 2003. Evaluation of specific ultraviolet absorbance as an indicator of the chemical composition and reactivity of dissolved organic carbon. Environmental Science & Technology 37(20), 4702-4708.

Winter, J., Uhl, W., Bérubé, P.R., 2016. Integrated oxidation membrane filtration process – NOM rejection and membrane fouling. Water Research 104, 418-424.

Wu, H., Xu, X., Shi, L., Yin, Y., Zhang, L.-C., Wu, Z., Duan, X., Wang, S., Sun, H., 2019. Manganese oxide integrated catalytic ceramic membrane for degradation of organic pollutants using sulfate radicals. Water Research 167, 115110.

Xu, M., Xu, C., Rakesh, K.P., Cui, Y., Yin, J., Chen, C., Wang, S., Chen, B., Zhu, L., 2020. Hydrophilic SiC hollow fiber membranes for low fouling separation of oil-in-water emulsions with high flux. RSC Advances 10(8), 4832-4839.

Xue, J., Zhang, Y., Liu, Y., Gamal El-Din, M., 2016. Effects of ozone pretreatment and operating conditions on membrane fouling behaviors of an anoxic-aerobic membrane bioreactor for oil sands process-affected water (OSPW) treatment. Water Research 105, 444-455.

Yang, T., Wang, L., Liu, Y., Jiang, J., Huang, Z., Pang, S.-Y., Cheng, H., Gao, D., Ma, J., 2018. Removal of organoarsenic with ferrate and ferrate resultant nanoparticles: Oxidation and adsorption. Environmental Science & Technology 52(22), 13325-13335.

Yang, T., Xiong, H., Liu, F., Yang, Q., Xu, B., Zhan, C., 2019. Effect of UV/TiO_2 pretreatment on fouling alleviation and mechanisms of fouling development in a cross-flow filtration process using a ceramic UF membrane. Chemical Engineering Journal 358, 1583-1593.

Yin, N., Zhong, Z., Xing, W., 2013. Ceramic membrane fouling and cleaning in ultrafiltration of desulfurization wastewater. Desalination 319, 92-98.

Yin, Z., Wen, T., Li, Y., Li, A., Long, C., 2020. Pre-ozonation for the mitigation of reverse osmosis (RO) membrane fouling by biopolymer: The roles of Ca^{2+} and Mg^{2+}. Water Research 171, 115437.

Ying, W., Siebdrath, N., Uhl, W., Gitis, V., Herzberg, M., 2014. New insights on early stages of RO membranes fouling during tertiary wastewater desalination. Journal of Membrane Science 466, 26-35.

Yopps, J.A., Fuerstenau, D.W., 1964. The zero point of charge of alpha-alumina. Journal of Colloid Science 19(1), 61-71.

Yu, W., Liu, T., Crawshaw, J., Liu, T., Graham, N., 2018. Ultrafiltration and nanofiltration membrane fouling by natural organic matter: Mechanisms and mitigation by pre-ozonation and pH. Water Research 139, 353-362.

Yu, W., Zhang, D., Graham, N.J.D., 2017. Membrane fouling by extracellular polymeric substances after ozone pre-treatment: Variation of nano-particles size. Water Research 120, 146-155.

Yue, X., Koh, Y.K.K., Ng, H.Y., 2015. Effects of dissolved organic matters (DOMs) on membrane fouling in anaerobic ceramic membrane bioreactors (AnCMBRs) treating domestic wastewater. Water Research 86, 96-107.

Zaouri, N., Gutierrez, L., Dramas, L., Garces, D., Croue, J.-P., 2017. Interfacial interactions between Skeletonema costatum extracellular organic matter and metal oxides: Implications for ceramic membrane filtration. Water Research 116, 194-202.

Zhang, J., Yu, H., Quan, X., Chen, S., Zhang, Y., 2016a. Ceramic membrane separation coupled with catalytic ozonation for tertiary treatment of dyestuff wastewater in a pilot-scale study. Chemical Engineering Journal 301, 19-26.

Zhang, L., Ng, T.C.A., Liu, X., Gu, Q., Pang, Y., Zhang, Z., Lyu, Z., He, Z., Ng, H.Y., Wang, J., 2020a. Hydrogenated TiO_2 membrane with photocatalytically enhanced anti-fouling for ultrafiltration of surface water. Applied Catalysis B: Environmental 264, 118528.

Zhang, Q., Fan, Y., Xu, N., 2009. Effect of the surface properties on filtration performance of Al_2O_3–TiO_2 composite membrane. Separation and Purification Technology 66(2), 306-312.

Zhang, Q., Jing, W., Fan, Y., Xu, N., 2008. An improved Parks equation for prediction of surface charge properties of composite ceramic membranes. Journal of Membrane Science 318(1), 100-106.

Zhang, S., Gutierrez, L., Qi, F., Croue, J.-P., 2020b. $SO_4^{\cdot-}$-based catalytic ceramic UF membrane for organics removal and flux restoration. Chemical Engineering Journal 398, 125600.

Zhang, S., Hedtke, T., Zhu, Q., Sun, M., Weon, S., Zhao, Y., Stavitski, E., Elimelech, M., Kim, J.-H., 2021. Membrane-confined iron oxychloride nanocatalysts for highly efficient heterogeneous fenton water treatment. Environmental Science & Technology 55(13), 9266-9275.

Zhang, X., Devanadera, M.C.E., Roddick, F.A., Fan, L., Dalida, M.L.P., 2016b. Impact of algal organic matter released from Microcystis aeruginosa and Chlorella sp. on the fouling of a ceramic microfiltration membrane. Water Research 103, 391-400.

Zhang, X., Fan, L., Roddick, F.A., 2013a. Understanding the fouling of a ceramic microfiltration membrane caused by algal organic matter released from Microcystis aeruginosa. Journal of Membrane Science 447, 362-368.

Zhang, X., Fan, L., Roddick, F.A., 2015. Effect of feedwater pre-treatment using UV/H_2O_2 for mitigating the fouling of a ceramic MF membrane caused by soluble algal organic matter. Journal of Membrane Science 493, 683-689.

Zhang, X., Guo, J., Wang, L., Hu, J., Zhu, J., 2013b. In situ ozonation to control ceramic membrane fouling in drinking water treatment. Desalination 328, 1-7.

Zhao, Q., Lu, D., Jiang, H., Zhao, Y., Sun, Y., Li, Z., Yang, M., Wang, P., Ma, J., 2019. Peroxymonosulfate-based cleaning technology for metal oxide-coated ceramic ultrafiltration membrane polluted by Alcian Blue 8GX dye: Radical and non-radical oxidation cleaning mechanism. Journal of Membrane Science 573, 210-217.

Zhao, Y.-y., Wang, X.-m., Yang, H.-w., Xie, Y.-f.F., 2018a. Effects of organic fouling and cleaning on the retention of pharmaceutically active compounds by ceramic nanofiltration membranes. Journal of Membrane Science 563, 734-742.

Zhao, Y., Lu, D., Cao, Y., Luo, S., Zhao, Q., Yang, M., Xu, C., Ma, J., 2018b. Interaction analysis between gravity-driven ceramic membrane and smaller organic matter: Implications for retention and fouling mechanism in ultralow pressure-driven filtration system. Environmental Science & Technology 52(23), 13718-13727.

Zhao, Y., Lu, D., Xu, C., Zhong, J., Chen, M., Xu, S., Cao, Y., Zhao, Q., Yang, M., Ma, J., 2020. Synergistic oxidation-filtration process analysis of catalytic $CuFe_2O_4$-tailored ceramic membrane filtration via peroxymonosulfate activation for humic acid treatment. Water Research 171, 115387.

Zhao, Y., Xing, W., Xu, N., Wong, F.-S., 2005. Effects of inorganic electrolytes on zeta potentials of ceramic microfiltration membranes. Separation and Purification Technology 42(2), 117-121.

Zheng, J., Wang, Z., Ma, J., Xu, S., Wu, Z., 2018. Development of an electrochemical ceramic membrane filtration system for efficient contaminant removal from waters. Environmental Science & Technology 52(7), 4117-4126.

Zhou, J.-e., Chang, Q., Wang, Y., Wang, J., Meng, G., 2010. Separation of stable oil–water emulsion by the hydrophilic nano-sized ZrO_2 modified Al_2O_3 microfiltration membrane. Separation and Purification Technology 75(3), 243-248.

Zhu, H., Wen, X., Huang, X., 2010. Membrane organic fouling and the effect of pre-ozonation in microfiltration of secondary effluent organic matter. Journal of Membrane Science 352(1), 213-221.

Zhu, L., Chen, M., Dong, Y., Tang, C.Y., Huang, A., Li, L., 2016. A low-cost mullite-titania composite ceramic hollow fiber microfiltration membrane for highly efficient separation of oil-in-water emulsion. Water Research 90, 277-285.

Zuriaga-Agustí, E., Alventosa-deLara, E., Barredo-Damas, S., Alcaina-Miranda, M.I., Iborra-Clar, M.I., Mendoza-Roca, J.A., 2014. Performance of ceramic ultrafiltration membranes and fouling behavior of a dye-polysaccharide binary system. Water Research 54, 199-210.

Chapter 3

INTEGRATION OF OXALIC ACID CHELATION AND FENTON PROCESS FOR SYNERGISTIC RELAXATION-OXIDATION OF PERSISTENT GEL-LIKE FOULING OF CERAMIC NANOFILTRATION MEMBRANES
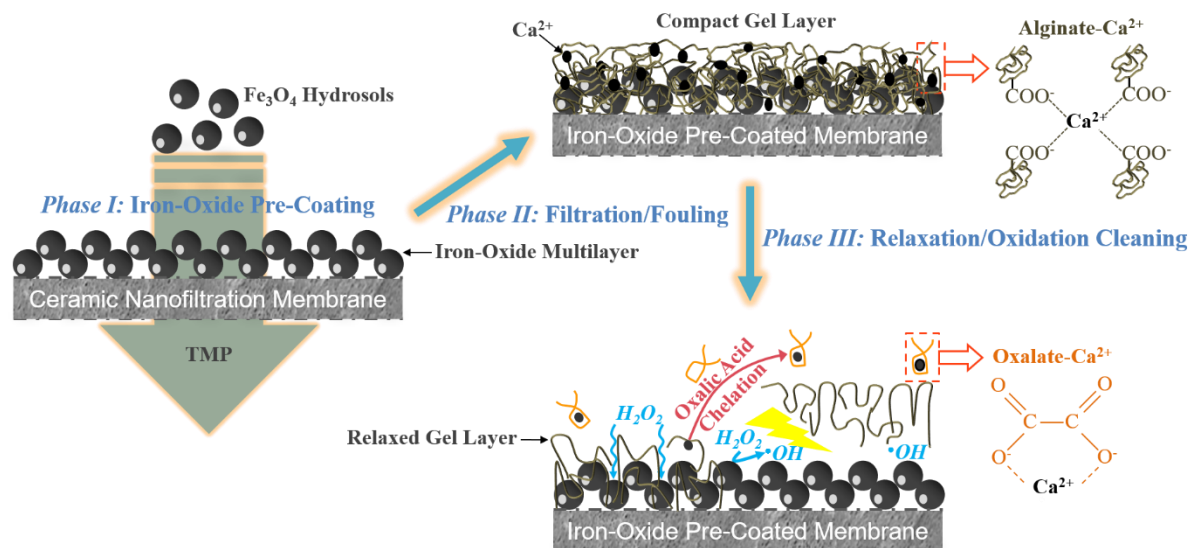
This chapter has been published as:

Abstract

Ceramic nanofiltration (NF) is a newly-developed technology for water recycling, but is still limited to pilot-scale applications. Lacking efficient and eco-friendly strategies for cleaning ceramic NF membrane impedes its scaling-up in industries. Forward flush, backwash and acidic/caustic cleaning are not efficient enough. In this chapter, a novel oxalic acid-aided Fenton process was proposed for synergistic relaxation/oxidation of persistent Ca^{2+}-mediated gel-like fouling of ceramic NF membrane. A reactive catalyst layer was online pre-coated on top of the membrane via a pressure-driven cross-flow pre-filtration of Fe_3O_4 hydrosols. The gel-like fouling was simulated by alginate in the presence of Ca^{2+} ions. Results show that the Fe_3O_4 loading could be readily tuned from 0.16 to 1.34 g m^{-2} by altering the permeate flux during the pre-coating. The membrane permeance loss due to the pre-coating was minimal (<10%). The combination of oxalic acid chelation and Fenton-based oxidation resulted in high flux recovery (85.07%) for the iron-oxide pre-coated membrane, whereas the single treatment by hydrogen peroxide (H_2O_2) or oxalic acid was inefficient. This synergistic effect was attributed to relaxation of the Ca^{2+}-mediated gel layer via oxalic acid/Ca^{2+} chelation, which presumably facilitated H_2O_2 diffusion at the Fe_3O_4/foulant interface. The iron-oxide pre-coated membrane maintained stable initial normalized fluxes (83.33–90.15%) through the oxalic acid/H_2O_2 cleaning over five cycles, with no need of refreshing the iron-oxide pre-coat. Additionally, the leaching of iron from the iron-oxide pre-coat by oxalic acid was suppressed by the oxalic acid/H_2O_2 combination, owing to a reactive shielding by competitive sorption of H_2O_2 onto the Fe_3O_4 surface. Overall, the synergistic relaxation/oxidation method, demonstrated in this chapter provides new insights into improving reactivity of Fenton-based processes on hybrid catalytic ceramic membranes for water treatment or fouling control.

3.1 Introduction

Ceramic nanofiltration (NF) has emerged as an attractive new technology for non-potable water recycling from municipal sewage and secondary wastewater effluent, given its good robustness and separation capability upon various organic molecules (>450 Da) and small colloids (Fujioka et al., 2014; Kramer et al., 2015). Formation of a low permeable gel layer on the surface of ceramic NF membranes during filtration, plays a significant role in the membrane fouling, which affects the water-yielding capacity and energy consumption in water treatment (Wang and Waite, 2008; Zhao et al., 2018). Typically, polysaccharides (i.e. alginate) are considered to be a major contributor to the gel layer formation, attributing to the strong bridging between carboxylic groups of the polysaccharide molecules and divalent or multivalent metal ions (i.e. Ca^{2+} and Fe^{3+}) (Xin et al., 2016;

Xin et al., 2015; Zhang et al., 2017). Regardless of the hydrophilic surface (contact angle: 20–30°) of ceramic NF membranes, forward flush is ineffective for the gel-type fouling due to its strong adherence to the membrane (Mustafa et al., 2014; Zhao et al., 2018). Backwash cannot be applied to ceramic NF membranes because of physical damage to the end-sealing under high transmembrane pressures (TMP), in addition, the backwash velocity is limited at pressures below 10 bar (Fujioka et al., 2018). Therefore, off-line chemical cleaning of the membranes with alkaline, acid, or hypochlorite is frequently needed, disrupting the continuous filtration and influencing the membrane integrity (van den Brink et al., 2009; Wadekar and Vidic, 2018). In addition, chemical cleaning agents, such as NaOH and citric acid, are incapable of fully eliminating the foulants even if the flux was entirely recovered, leading to a progressive flux decrease with successive filtration cycles (Zhao et al., 2018).

Membrane modification with Fenton catalysts enables foulant removal on the membrane surface via on-site generation of reactive oxygen species (i.e. $^{\bullet}OH$), after addition of hydrogen peroxide (H_2O_2) (Mauter et al., 2018). The co-existence of catalysts, H_2O_2 and foulants on a catalyst-modified membrane surface could create conditions that are favourable for fouling layer decay, because of the short diffusive transport distance in Fenton oxidation processes at the catalyst/foulant interface (Yang et al., 2016). The Fenton oxidation processes on the membrane surface aim to attack the anchoring sites at the catalytic membrane/foulant interface, which would result in fouling layer detachment. De Angelis and de Cortalezzi (2016) reported that Fenton reactions on an iron-oxide modified ceramic membrane achieved a flux recovery of 80% with bovine serum albumin degradation percentage of 40%, indicating an underlying detachment or relaxation of the fouling layer by Fenton oxidation. According to Sun et al. (2018), UV/H_2O_2 photo-Fenton oxidation on a α-FeOOH-coated ceramic membrane was able to limit the increase of TMP to a plateau level, during continuous filtration of humic acid solutions. Above mentioned studies, however, only have paid attention to the viability of using membrane-surface-localized Fenton reactions for fouling control, but in water treatment by ceramic membranes, a persistent fouling layer (i.e. gel-like foulants) on the membrane surface may affect the reactivity of Fenton processes, which is still unresolved and poorly understood (De Angelis and de Cortalezzi, 2016; Sun et al., 2018).

Accumulation of foulants on catalytic membranes shortens the mass transfer distance of $^{\bullet}OH$ for foulant decay, which, in principle, is favourable for catalysed oxidation on the membrane surface (Zhang et al., 2016). However, the fouling layer itself, as an undesirable steric barrier, could limit the diffusive transport of H_2O_2 onto the catalytic sites and hamper the oxidation of foulants. In particular, the gel layer composed of biopolymers (i.e. polysaccharides) on the membrane surface could act as a

mass transfer hindrance (Zhou et al., 2017). With the aid of Ca^{2+} ions, ubiquitous in natural water bodies, the cross-linked networks of the gel layer would be further intensified and compressed under pressure-driven filtration, due to intermolecular bridging between foulant molecules or charge screening by Ca^{2+} (Li et al., 2009; Zhang et al., 2017). As such, the Ca^{2+}-mediated gel-like fouling layer, with low permeance, affects the application of Fenton-coupled ceramic membranes for water treatment or fouling control in practice (Chen et al., 2016; Wang and Waite, 2008). Therefore, H_2O_2 mass transfer on catalyst-immobilized membranes should be improved to enhance Fenton oxidation for fouling control.

Ligand exchange reactions, governed by chelating agents, are capable of extracting Ca^{2+} from the Ca^{2+}-mediated gel layer, rendering a relaxed conformation of the gel layer through resuming intra- or inter-molecular or foulant-membrane electrostatic repulsion or destructing intermolecular bridging (Li and Elimelech, 2004). As such, loosening fouling layer structures could also be expected as a factor contributing to flux recovery, in addition to removing the fouling layer from membrane surfaces. Nonetheless, Song et al. (2004) has reported that chelating agent cleaning might be ineffective for Ca^{2+}-unbound foulant molecules, which are generally protonated under acidic conditions. As reported by Athanasekou et al. (2009), ceramic NF membranes, with alginate deposited on their surfaces, would undergo an evident permeance drop (~50%) upon exposure to divalent metal cations, due to pore narrowing/blocking induced by complexation between the divalent metal cations and alginate's carboxylic groups. It can thus be speculated that some residual foulants on membranes, after Ca^{2+} extraction through chelation cleaning, could release their binding sites (i.e. carboxylic groups) for free metal cations (i.e. Ca^{2+}) in aqueous phase, which might reorganize cross-linked gel networks on the membranes and lead to a flux decline upon exposure to Ca^{2+}. Additionally, some foulants, tightly embedded in the concavities or pore-openings of membrane surfaces, were not amendable to chelation cleaning (Lu et al., 2016b; Song et al., 2004).

In this chapter, a novel synergistic method of using chelating-agent relaxation and Fenton-based oxidation was proposed, for cleaning persistent gel-like fouling of ceramic NF membranes. Fe_3O_4 hydrosol nanoparticles were adopted as active Fenton catalysts to form an iron-oxide pre-coat on the membrane surface prior to fouling, due to their capability of triggering Fenton-based oxidation and facile synthesis processes. Sodium alginate, which is known to form gel aggregates through a so-called egg-box model in the presence of calcium ions, was chosen as a representative gel-like foulant to develop a gel layer on the membranes (van den Brink et al., 2009; Zhang et al., 2017). As suggested by pre-coated membranes prepared by particle materials (i.e. iron oxide and powdered activated

carbon) reported elsewhere, the gel foulants are supposed to be deposited on top of the iron-oxide multilayer and within its porous channels (Kim et al., 2017; Soesanto et al., 2019). Oxalic acid was used to assist the Fenton-oxidative cleaning of the iron-oxide pre-coated membranes, in light of its functions of complexing with Ca^{2+}-mediated gel layer and good resistance to $^\bullet$OH-radical oxidation (Rodríguez et al., 2009).

3.2 Materials and methods

3.2.1 Chemicals and membranes

Ferric chloride hexahydrate ($FeCl_3 \cdot 6H_2O$, ≥99.0%), ferrous chloride ($FeCl_2$, ≥98.0%), sodium alginate (≥99.0%) and oxalic acid ($C_2H_2O_4$, ≥99.0%) were purchased from Sigma-Aldrich. H_2O_2 (30%), calcium chloride dihydrate ($CaCl_2 \cdot 2H_2O$, ≥99.0%), H_2O_2 test kits (limit of detection (LOD): 0.03−6 mg L^{-1}) and iron test kits (LOD: 0.10−5 mg L^{-1}) were purchased from Merck (Germany). All chemicals were used as received. Commercially available TiO_2 NF membranes (Inopor GmbH, Germany) with nominal molecular weight cut-off of 450 Da and mean pore size of 0.9 nm were used in this chapter (Table S1). The membranes have a single channel and a tubular configuration with dimensions of 10 mm in outer diameter, 7 mm in channel diameter and 100 mm in length. The effective filtration area of each membrane is 0.00163 m^2. The membranes were sealed with epoxy glue on the membranes edges to avoid feed water passing through the edges prior to use. The membranes were operated in an inside-out mode during filtration.

3.2.2 Synthesis of iron oxide hydrosol nanoparticles

Wet-state Fe_3O_4 hydrosol catalysts were synthesized with the sol-gel method (Kang et al., 1996). In brief, 4.00 g $FeCl_2$ and 17.07 g $FeCl_3 \cdot 5H_2O$ were successively dissolved into 0.1 L of a 0.60 M HCl solution. The acidified solution of ferrous/ferric ions (Fe(II)/Fe(III)) was then dropwise added into 2.0 L of a 0.15 M NaOH solution with continuously stirring at a speed of 200 rpm, until the solution reached a pH of 2.5. The obtained black Fe_3O_4 hydrosols appeared well suspended and dispersed, which were favourable for iron-oxide pre-coating through pressure-driven pre-filtration processes. The Fe_3O_4 hydrosols were stored in a fridge at 4 °C prior to use.

3.2.3 Integrative pre-coating/filtration/cleaning system
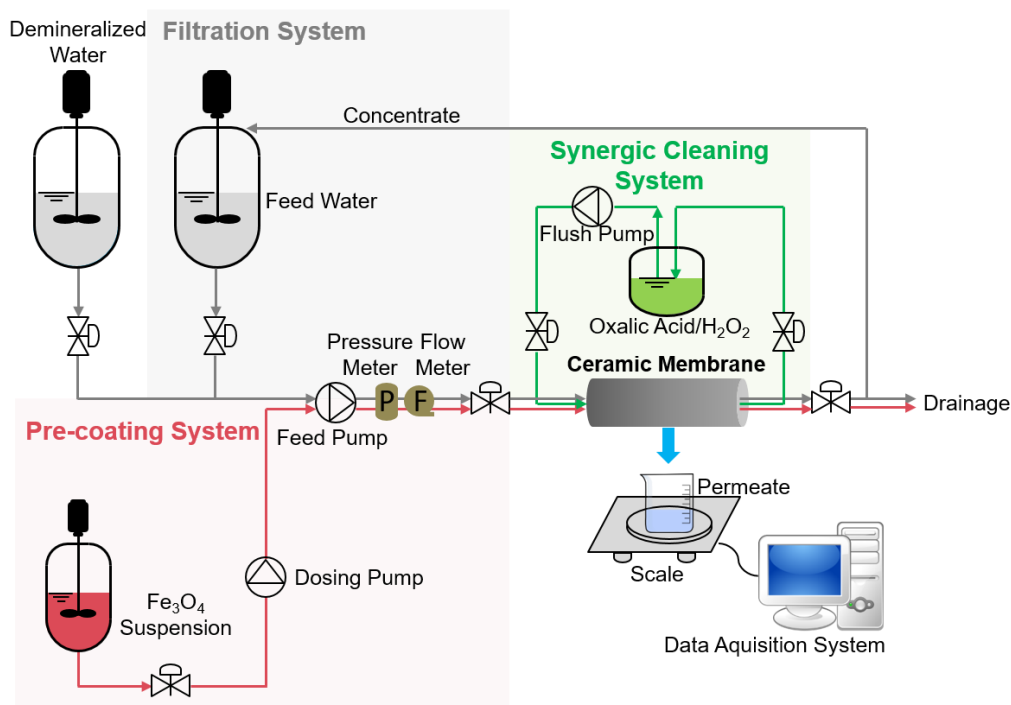
Figure 3.1 *Schematic of integrative pre-coating/filtration/cleaning system of ceramic nanofiltration membrane.*

Catalyst pre-coating, fouling and cleaning of ceramic NF membranes were operated in an integrative apparatus (Figure 3.1). Fe_3O_4 hydrosols were used for the catalyst pre-coating through a cross-flow filtration to in situ form a uniform iron-oxide pre-coat on the membrane surface. The Fe_3O_4 suspension (47.0 mM) was spiked into a demineralized water feed stream and the pre-coating filtration was operated at TMP of 2.0–10.0 bar and at a cross-flow velocity of 0.65 m s^{-1} for 30 min. Laminar cross-flow inside the membrane channel was adopted to promote Fe_3O_4 deposition onto the membrane surface. The Fe_3O_4 loading on the membranes, ahead of fouling/cleaning experiments, was determined by fully dissolving the iron oxide pre-coat with oxalic acid solutions and measuring the dissolved iron. For a ceramic NF membrane with a specific permeance, the Fe_3O_4 loading can be readily reproduced by tuning permeate volume during Fe_3O_4 pre-filtration under a certain TMP. Therefore, the Fe_3O_4 loading amount, measured before batch experiments, can be regarded as the initial iron loading. The deposition and packing of Fe_3O_4 nanoparticles largely relied on the permeate flux and cross flow velocity (Anantharaman et al., 2020), which determined the mass transported to the membrane surface (nominal Fe_3O_4 loading) and the mass swept away from the membrane (Fe_3O_4 loss), respectively. The nominal loading mass and coating efficiency of Fe_3O_4 nanoparticles could be calculated as described in Text S3.1.

Fouling processes were conducted after the iron oxide pre-coating of ceramic NF membranes, using a synthetic foulant sodium alginate. NaCl (5.0 mM) and $CaCl_2$ (3.0 mM) were added into sodium alginate solutions (0.8 g L^{-1}) to simulate the solution chemistry of natural waters. $NaHCO_3$ (1.0 mM) was added to maintain pH 7.0 (Text S3.2). Filtration was carried out in a bench-scale cross-flow mode (Figure 3.1). Prior to fouling tests, the pristine and iron-coated membranes were pre-compacted with demineralized water under 3.0 bar until a stable flux was reached. The membranes were then stabilized with demineralized water for 10 min to determine the stable initial permeate flux (J_0). During the fouling experiments, the retentate was recycled to the feed tank (50 L), while the permeate was collected continuously for measuring the permeate flux. The filtration experiments were executed at a constant TMP of 3.0 bar with initial fluxes of >50 L m^{-2} h^{-1} during fouling, which should be a regular flux for ceramic NF and sufficient for the formation of gel fouling with concentrated alginate solutions (Kramer et al., 2019). A cross-flow velocity of 1.0 m s^{-1} were adopted during the fouling experiments (for 60 min). The Reynolds number of 6116 was used during the filtration to create turbulent conditions. In the filtration tests with the iron-oxide pre-coated membranes, the content of total iron in the permeate side was lower than the detection limit of 0.1 mg L^{-1}, which is below the permissible limit of iron in drinking water (0.3 mg L^{-1}, WHO standard) (Haldar et al., 2020).

Membrane cleaning was performed by circulating a mixed solution of oxalic acid/H_2O_2 in the feed channel as illustrated in Figure 3.1. The cleaning performance was evaluated by tracking the permeate flux over multiple filtration cycles. An oxalic acid/H_2O_2 solution with 30.0 mM H_2O_2, 11.1 mM oxalic acid and pH = 2.5 were adopted, corresponding to the optimum value for Fenton cleaning based on previously executed optimization tests (data not shown). Herein, as suggested by Mailen et al. (1981), degradation of oxalic acid by H_2O_2 could be assumed negligible due to the slow reaction rate ($k < 2.8 \times 10^{-6}$ M^{-1} s^{-1}) at 20 °C. Membrane cleaning in our experiments was conducted at a low cross-flow velocity (0.02 m s^{-1}), in order to reduce the hydraulic scouring on the iron-oxide pre-coat. Each fouling/cleaning cycle consisted of four sequential steps: a) permeate flux test using demineralized water, b) filtration of the synthetic foulant solution, c) membrane cleaning with the oxalic acid and/or H_2O_2 solution, and d) permeate flux test using demineralized water. Cleaning with only oxalic acid or H_2O_2, or with a combination of oxalic acid and H_2O_2 were conducted in parallel for the pristine and Fe_3O_4-coated membranes, respectively, in order to separately explore the individual roles of oxalic acid and H_2O_2 in the synergistic oxalic acid-assisted Fenton cleaning. Afterwards, the cleaned membranes were soaked into a $CaCl_2$ solution (3.0 mM, pH = 7.0), then the flux decline upon Ca^{2+} exposure (for 12 h) was investigated to evaluate the foulant removal from the membrane surface,

since re-compaction of remaining foulants could occur and form again a compact layer due to Ca^{2+} complexation. Flux recovery ratios after membrane cleaning were calculated using Equation (3.1).

$$F_r = \frac{J_c - J_f}{J_w - J_f} \times 100\%$$
(3.1)

where J_c (L m^{-2} h^{-1}) is the flux of demineralized water after cleaning, J_w (L m^{-2} h^{-1}) represents the initial flux of demineralized water prior to fouling tests, and J_f (L m^{-2} h^{-1}) is designated to the water flux after membrane fouling. The filtration/cleaning experiments were performed in duplicate, and the variations in terms of membrane permeance before/during fouling or after cleaning were within a 5% difference.

Multicycle fouling/cleaning experiments were also conducted at bench scale, with a fouling duration of 60 min and cleaning time of 15 min in each cycle. The unified membrane fouling index (*UMFI*) was used to quantitatively assess the total fouling and chemically irreversible fouling of the iron-oxide pre-coat with the oxalic acid-coupled Fenton cleaning. A detailed description of the *UMFI* has been provided elsewhere (Huang et al., 2009). The *UMFI* was defined as a slope in the linear equation given in Equation (3.2).

$$\frac{1}{J_s'} = 1 + (UMFI) \times V_s$$
(3.2)

where J_s' is the normalized specific permeate flux, and V_s (L m^{-2}) represents the unit permeate volume. A higher *UMFI* (m^2 L^{-1}) value implies a faster decrease of J_s'. Herein, the total fouling refers to the membrane fouling before hydraulic or chemical cleaning, and the chemically irreversible fouling denotes the residual fouling after chemical cleaning (oxalic acid/H_2O_2 cleaning). The total fouling index (*TFI*) was further calculated by a linear regression of fouling data of each filtration cycle. The chemically irreversible fouling index (*CIFI*) was finally determined by collecting the starting points of each filtration cycle by linear regression. The two-point approach, using the starting points of the first and final cycles, was also adopted for comparison (Huang et al., 2009).

Real surface water was also fed to the iron-oxide pre-coated ceramic NF membrane to test the applicability of the oxalic acid-aided Fenton-based cleaning strategy in practice. Canal water was collected at the Delftse Schie (Delft, the Netherlands) and pre-filtrated with a fine sieve of 1 mm mesh width before NF. Key water quality parameters of the canal water are summarised in Table S3.2. It should be noted that the fouling with alginate solutions is an accelerated fouling with a much higher load (0.8 g L^{-1}) than that of the pilot experiment in canal water treatment (11.9 mg L^{-1}, Table S3.2).

As suggested by one of our previous studies, using this model solutions, a pilot fouling experiment of five days could be simulated in two hours, due to the faster fouling by the concentrated alginate solutions (Kramer et al., 2015).

3.2.4 Characterization of iron oxide nanoparticles and membranes and analysis of water quality

Morphologies of Fe_3O_4 nanoparticles and top/cross-sectional views of iron-coated membranes were observed by transmission electron microscope (TEM, JEM-2100 HR, JEOL, Japan) and scanning electron microscopy (SEM, Hitachi S-3400 II, Japan) equipped with energy dispersive spectroscopy (EDS). X-ray diffraction (XRD) was performed with an XRD diffractometer (D8-Advance, Bruker, USA) with Cu Kα radiation at 45 kV and 40 mA. Specific surface area was determined by N_2 adsorption-desorption tests at 77 K (ASAP-2010C, Micromeritics Instrument, USA). The standard Brunauer-Emmett-Teller model was used to calculate the surface area (S_{BET}) of the dried particles. Average particle size of Fe_3O_4 nanoparticles was estimated based on the S_{BET} value presuming a spherical morphology of the Fe_3O_4 (Text S3.3). Dissolved organic carbon (DOC) was determined by a total organic carbon analyser (TOC-VCPH, Shimadzu, Japan). The ions in the canal water samples were measured by ion chromatography (883 Basic IC plus, Metrohm Instrument, the Netherlands). UV_{254} was determined by UV/vis spectrometer (GENESYS 10S UV-Vis, Thermo Scientific, USA) with a quartz cell (1 cm). Fe Leaching of iron oxide pre-coat was measured in a photometer (Spectroquant NOVA 60, Merck KGaA, Germany) using iron test kits. H_2O_2 concentration was measured by hydrogen peroxide test kits. During each test, the samples were filtered through 0.45 μm filters to retain possible impurities.

3.2.5 Iron leaching of iron-oxide pre-coated membranes

Stability and Fenton-based (homogeneous or heterogeneous) reactions are greatly dependent on the Fe leaching of iron-oxide pre-coat. To understand the iron leaching, the dissolution of iron from the iron-oxide pre-coat was explored during the membrane cleaning with sole oxalic acid (or H_2O_2) and oxalic acid/H_2O_2 combination. The iron-oxide pre-coated membranes were subjected to Ca^{2+}-alginate fouling with varying durations (i.e. 1 and 3 h) to simulate actual conditions of iron leaching during membrane cleaning. The iron leaching tests were performed at 20 °C and pH 2.5. Aliquots of 8.0 mL were withdrawn at selected time intervals and filtered for analysing the Fe concentration to determine the iron dissolution rate of the iron-oxide pre-coat. During batch cleaning, the dissolved (or fallen) iron was detected, which could be used for determining the loss amount of Fe_3O_4 from the

membrane in cleaning processes. For determining the iron loss during the H_2O_2 batch cleaning, oxalic acid was introduced into H_2O_2 solutions after the batch cleaning so as to entirely dissolve the fallen Fe_3O_4 solids, which assured that all the lost iron could be measured as Fe(II) or Fe(III) ions. In order to study the possible competition between H_2O_2 and oxalic acid towards the active sites on the Fe_3O_4 catalytic layer, adsorption of oxalic acid was conducted in the absence and presence of H_2O_2. To exclude the interference of ceramic membrane, the solid particles, dried from Fe_3O_4 hydrosols, were used for the adsorption experiments. The Fe_3O_4 particles (1.0 g L^{-1}) were mixed and stirred with oxalic acid (0.55 and 11.0 mM) at pH = 2.5 in the absence and presence of H_2O_2 (30.0 mM). The loading of oxalic acid on the Fe_3O_4 powders was determined based on mass balance.

3.3 Results and discussion

3.3.1 Characterization of iron-oxide pre-coated membranes
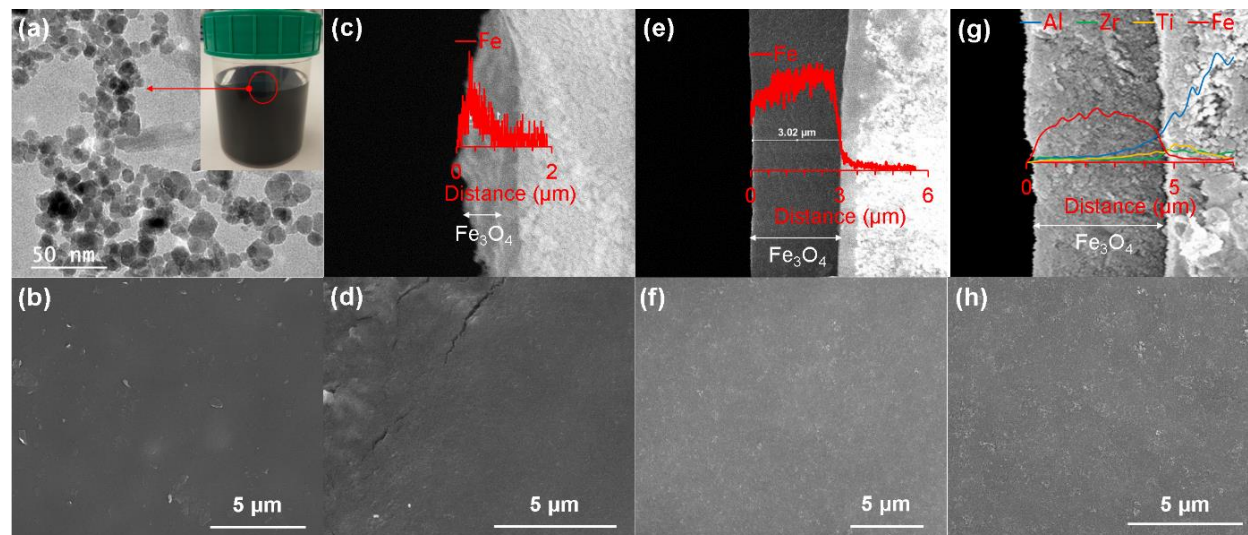
Figure 3.2 *Characterization of Fe_3O_4 hydrosols and ceramic nanofiltration membranes: (a) TEM image of Fe_3O_4 hydrosol nanoparticles. (b) Top-view SEM image of pristine membrane. Cross-section SEM images with inset EDS profiles and top-view SEM images of iron-oxide pre-coated membranes prepared at (c, d) 2.0 bar, (e, f) 6.0 bar and (g, h) 10.0 bar.*

Figure 3.2a shows that the Fe_3O_4 hydrosol nanoparticles were suspended and well-dispersed in aqueous solutions, supplying good characteristics for Fe_3O_4 pre-coating. Spherical configurations were observed for most Fe_3O_4 nanoparticles with diameters <20 nm, a minor fraction of the nanoparticles exhibited a distinctive acicular-like structure that might be typical for goethite nanorods (Figure 3.2a) (Tang et al., 2006). The average particle size of the Fe_3O_4 nanoparticles was

12.72 nm (Table S3.3) larger than the nominal pore size (0.9 nm on average, provided by the manufacturer, Table S3.1) of the membranes, indicating that the Fe_3O_4 nanoparticles could be successfully deposited onto the membrane surface without penetrating into the membrane pores. As depicted in Figure 3.2c, e and g, the membranes pre-filtered with Fe_3O_4 nanoparticles at higher TMP (6.0 and 10.0 bar) presented thicker (3.0 and 4.7 μm, respectively) and more uniform iron-oxide layers than that formed at 2.0 bar (1.1 μm in thickness, nonuniform), probably attributing to a larger permeate volume and greater compaction effect under the higher pressures. Additionally, the Fe_3O_4 layers (1.1–4.7 μm) appeared to be much thicker than that of the TiO_2 active layer (~50 nm, supplied by the manufacturer), suggesting that the abundant nanostructured and interconnected channels, stacked by the Fe_3O_4 nanoparticles on the membrane surface, could also act as a pre-filtration media before filtration over the active layer. As such, the Fe_3O_4 layer could be used as a protective film to alleviate the fouling of the membranes in water treatment (Lu et al., 2016a). According to the top-view SEM image (Figure 3.2b), the pristine membrane displayed a dense smooth active layer surface with no apparent defects on the top surface. The iron-oxide pre-coated membranes, however, had relatively rough surfaces (Figure 3.2d, f and h). The iron-oxide layers prepared at 6.0 and 10.0 bar exhibited more homogeneous surfaces than that formed at 2.0 bar.

3.3.2 Iron oxide loading and its impact on permeance of ceramic NF membranes
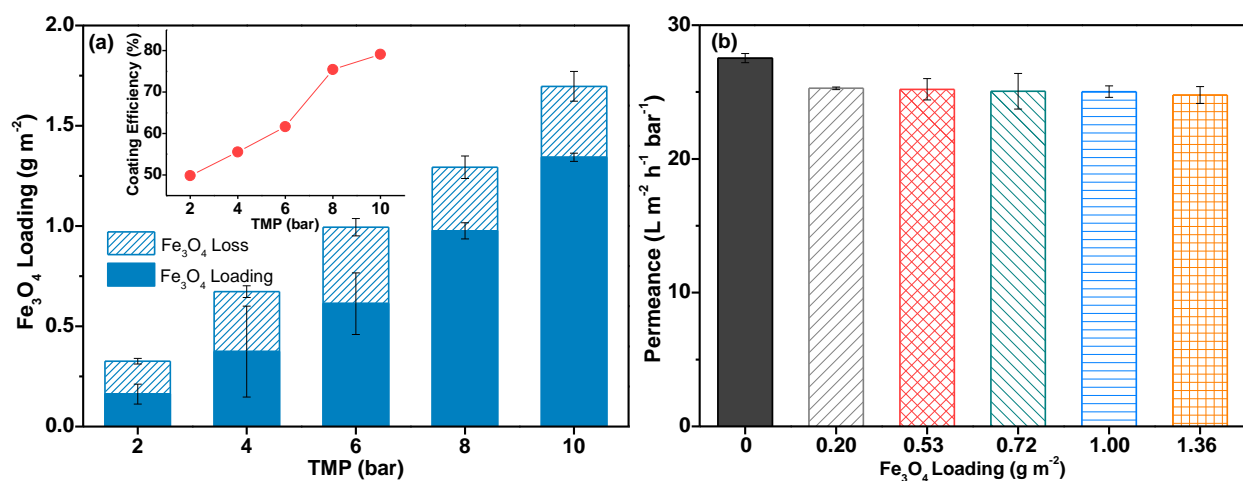
Figure 3.3 *(a) Fe_3O_4 loading during pre-coating filtration at different transmembrane pressures (TMP). Inset: Fe_3O_4 coating efficiency vs. applied TMP. (b) Effect of Fe_3O_4 loading on the permeance of iron-oxide pre-coated membranes. Error bars represent standard deviation of the values in duplicate.*

As shown in Figure 3.3a, the actual loading of Fe_3O_4 (0.16–1.34 g m^{-2}) appeared to be somewhat smaller than estimates (0.33–1.70 g m^{-2}) through Fe_3O_4 retention during the cross-flow filtration,

determined by the permeate volume and Fe_3O_4 concentration (13.02±0.62 mg L^{-1}) in the feed (Text S3.1). This was probably because the permeate flow inclined to deposit the Fe_3O_4 nanoparticles onto the membrane surface to form a cake layer, while the shearing force of cross-flow tended to flush away the accumulated particles, to some extent lowering the actual Fe_3O_4 loading on the membranes (Song and Elimelech, 1995). Herein, measurement of Fe_3O_4 loss was also considered when determining the actual loading amount of Fe_3O_4 nanoparticles (Text S3.1), in order to optimize TMP for improving coating efficiency. The actual loading of Fe_3O_4 was positively related to the TMP, suggesting that a higher permeate flux was more favourable for Fe_3O_4 deposition on the membrane surface. Under each filtration TMP, it was inevitable to lose a part of Fe_3O_4 particles due to the shearing force of cross-flow filtration, but the proportion of the Fe_3O_4 mass loss was decreased from 50.20% to 20.86% with increasing the TMP from 2.0 to 10.0 bar. Thus, the coating efficiency was successfully improved from 49.80% to 79.14% by a higher operating TMP, as indicated by the inset of Figure 3.3a.

As depicted in Figure 3.3b, in comparison with the pristine membrane, the Fe_3O_4 loading of 0.20 g m^{-2} decreased the membrane permeance by only 8.18%. Subsequently, the permeance reached a plateau even when the Fe_3O_4 loading was further increased to 1.36 g m^{-2} (adopted in our experiments), which led to a permeance decline of 9.98%. The low influence of the iron-oxide loadings (or thickness) on the demineralized water permeance of the membrane could be interpreted by the much higher porosities (>0.9, Text S3.4) of the iron-oxide layers than that of the supporting membrane (0.3–0.4, provided by the manufacturer). In contrast to the stable permeance of ceramic NF membranes (~25 L m^{-2} h^{-1} bar^{-1}) loaded with different amounts of Fe_3O_4 (0.20–1.36 g m^{-2}), pre-coating of microfiltration (MF) and ultrafiltration (UF) membranes, as earlier reported, produced a sharp decline in membrane permeance (by ~90%) after coating with nanoparticles (i.e. multi-walled carbon nanotubes and magnesium hydroxides), due to a rapid pore blockage of the membranes (Ajmani et al., 2012; Zhao et al., 2005). The Fe_3O_4 coating layer on the ceramic NF membranes was expected to be sufficiently porous with gaps between the particles larger than the membrane pore size due to the much larger size of the Fe_3O_4 particles (12.72 nm) than that of the nominal membrane pores (0.9 nm), which correspondingly provided interconnected channels for maintaining a steady water permeation. This advantage of ceramic NF membranes made it feasible to tune catalyst loading on the membranes without considerable loss of membrane permeance, in order to supply adequate active sites for catalysed reactions on the membrane surface.

3.3.3 Fenton oxidative cleaning of iron-oxide pre-coated membranes without using oxalic acid
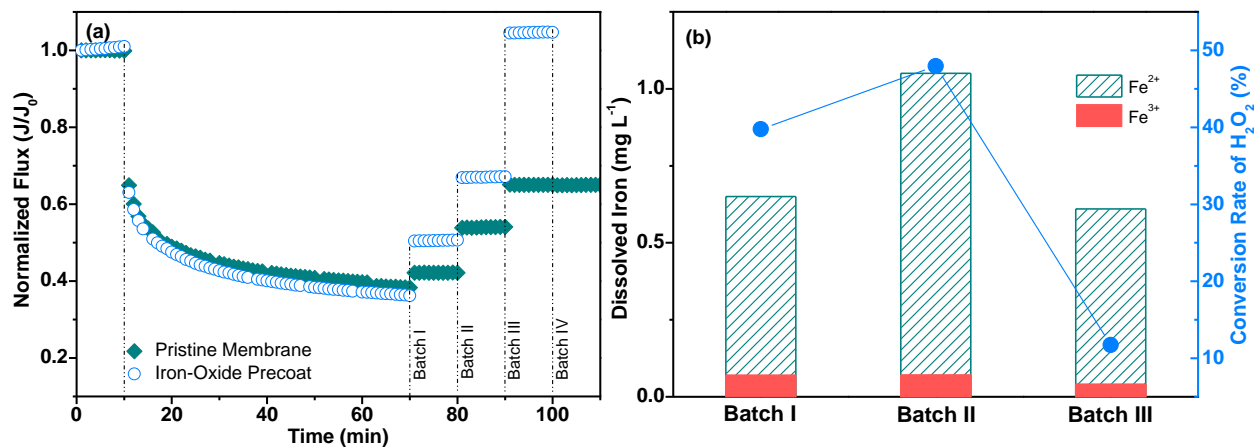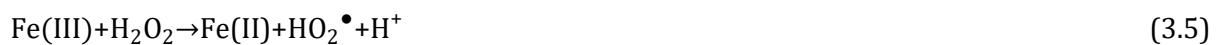

Figure 3.4 *(a) Batch cleaning of pristine and iron-oxide pre-coated membranes with single H_2O_2 ([H_2O_2]$_0$ = 30.0 mM, pH = 2.5). (b) Iron leaching and H_2O_2 conversion during H_2O_2 cleaning of iron-oxide pre-coated membrane.*

As observed in Figure 3.4a, the permeate flux of both the pristine and iron-oxide pre-coated membranes underwent an abrupt drop during the initial stage of fouling with Ca^{2+}-alginate solutions, probably due to partial pore narrowing/plugging by alginate branches (Wang et al., 2013). Afterwards, a slower decrease of the permeate flux was observed, until the end of filtration, likely attributing to gradual formation of a cake layer (Zuriaga-Agustí et al., 2014). The evident flux decline during the fouling processes indicated that the fluxes applied in the experiments should be beyond the critical flux (Field et al., 1995). Subsequently, the fouled iron-oxide pre-coated and pristine membranes were, respectively, subjected to three and four batches (20 h for each batch) of H_2O_2 cleaning (30.0 mM, pH = 2.5). The demineralized water flux of the pristine membrane was slowly restored during three consecutive cleaning batches until a flux recovery of 43.29%, presumably owing to direct oxidation by H_2O_2 of low oxidation power (reduction potential ($E°H_2O_2/H_2O$) = 1.763 V) (Katsounaros et al., 2012). After the third cleaning batch, the flux reached a plateau, manifesting that the remaining alginate residues on the membrane surface were resistant to the direct oxidation by H_2O_2. However, the flux recovery of the iron-oxide pre-coated membrane in each cleaning batch was much higher than that of the membrane without pre-coat, likely ascribed to the high oxidation power of $^\bullet OH$ ($E°^\bullet OH$, H^+/H_2O = 2.730±0.017 V) generated by Fe_3O_4-initiated Fenton reactions (Gligorovski et al., 2015). After the third cleaning batch, the flux appeared even slightly higher than

its initial level, which was likely caused by partial loss of Fe_3O_4 layer from the membrane surface because of the long cleaning process with H_2O_2 solutions.

To verify the contribution of Fenton-based processes to membrane cleaning, iron leaching and H_2O_2 conversion were simultaneously monitored. As depicted in Figure 3.4b, during each batch cleaning of the iron-oxide pre-coated membrane, Fe(II) ions (0.6–1.0 mg L^{-1}) were detected as the dominant iron species leached from the Fe_3O_4 layer, and a decrease of H_2O_2 concentration (by 12–48%) was also observed. Typically, the dissolved Fe(II) would instantaneously react with H_2O_2 through homogenous Fenton reactions to generate $^\bullet$OH radicals (Equation (3.3), $k = 63$ M^{-1} s^{-1}) (Brillas et al., 2009). However, due to the overdose of H_2O_2 relative to the dissolved Fe(II) ([H_2O_2]:[Fe(II)] = 30/0.01 mM/mM), the produced free $^\bullet$OH in the aqueous phase inclined to be scavenged by the excessive H_2O_2 (Equation (3.4), $k = 2.7\times10^7$ M^{-1} s^{-1}), instead of degrading membrane foulants (Chen et al., 2011). By comparing the reaction rates of Equation (3.5) and (3.6), the Fe(II), prevailing in the bulk solution, should originate from the HO$_2^\bullet$-governed reduction of Fe(III) (Equation (3.6), $k = 2\times10^3$ M^{-1} s^{-1}) rather than from the Fe(III) reduction by H_2O_2 (Equation (3.5), $k = 2.7\times10^{-3}$ M^{-1} s^{-1}) (Chen et al., 2011; Duesterberg et al., 2008). These results suggested that homogeneous Fenton reactions of H_2O_2 with Fe(II) (or Fe(III)) did not play an important role in $^\bullet$OH generation for the oxidative cleaning.

$$Fe(II)+H_2O_2+H^+\rightarrow Fe(III)+^\bullet OH+H_2O \tag{3.3}$$

$$H_2O_2+^\bullet OH\rightarrow H_2O+HO_2^\bullet \tag{3.4}$$

$$Fe(III)+H_2O_2\rightarrow Fe(II)+HO_2^\bullet+H^+ \tag{3.5}$$

$$Fe(III)+HO_2^\bullet\rightarrow Fe(II)+O_2+H^+ \tag{3.6}$$

Therefore, in the H_2O_2 cleaning, the foulant decay presumably proceeded through heterogeneous Fenton processes, catalysed by the Fe_3O_4 surface. Regarding this, Lin and Gurol (1998) proposed the reaction routes of H_2O_2 decomposition on iron oxide surfaces (Equations (3.7)–(3.11)):

$$\equiv Fe(II)\text{-}OH+H_2O_2\rightarrow\equiv Fe(III)\text{-}OH+^\bullet OH \tag{3.7}$$

$$\equiv Fe(III)\text{-}OH+H_2O_2\rightarrow(H_2O_2)_{ads} \tag{3.8}$$

$$(H_2O_2)_{ads}\rightarrow\equiv Fe(II)+H_2O+HO_2^\bullet \tag{3.9}$$

$$HO_2^{\bullet} \leftrightarrow H^+ + O_2^{\bullet-} \ (pKa=4.8) \tag{3.10}$$

$$\equiv Fe(III)\text{-}OH + HO_2^{\bullet} \rightarrow \equiv Fe(II) + H_2O/OH^- + O_2 \tag{3.11}$$

Herein, the heterogeneous Fenton reactions took place at the Fe_3O_4-foulant interface, where the iron-oxide catalysts, foulants and H_2O_2 co-existed. The H_2O_2 surface reactions and $^{\bullet}OH$ formation at the Fe_3O_4-foulant interface were then favourable for the oxidative detachment of the fouling layer from the membrane surface (Huling et al., 2007). Prior to the surface reactions, H_2O_2 should be diffusively transported from the bulk solution to the Fe_3O_4-foulant interface, where it was supposed to react with the Fe_3O_4 layer. Therefore, it could be anticipated that the limited H_2O_2 penetration into the Fe_3O_4-foulant interface inclined to prolong the time that was needed for cleaning the iron-oxide pre-coated membrane, attributing to the H_2O_2 diffusion barrier caused by the compact fouling layer (Ang et al., 2011).

3.3.4 Oxalic acid-aided Fenton cleaning of iron-oxide pre-coated membranes
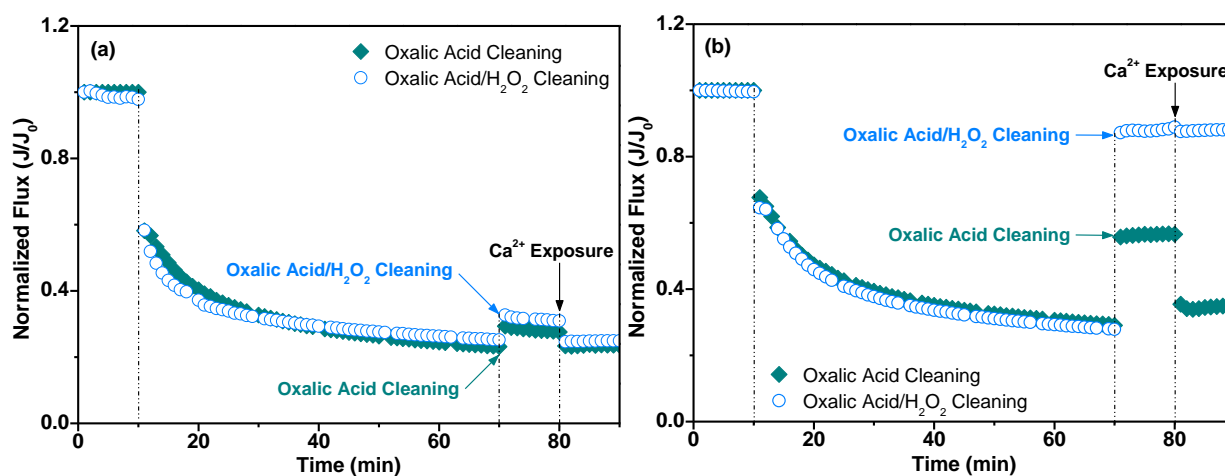
Figure 3.5 *Cleaning of (a) pristine and (b) iron-oxide pre-coated membranes with single oxalic acid and oxalic acid/H_2O_2 combination ([oxalic acid]$_0$ = 11.1 mM, [H_2O_2]$_0$ =30.0 mM, pH = 2.5). The Ca^{2+} exposure tests were conducted at [Ca^{2+}]$_0$ = 3.0 mM and pH = 7.0.*

As depicted in Figure 3.5a, the permeate fluxes of pristine membranes were poorly restored (by 5.81% or 7.96%, respectively) by sole oxalic acid (11.1 mM) or binary oxalic acid/H_2O_2 (11.1 mM, 30.0 mM) cleaning. Without a Fe_3O_4 catalytic layer, the slight flux recoveries were likely attributed to fouling layer relaxation by oxalic acid or weak oxidation by H_2O_2. Owing to the higher stability constant of Ca^{2+}-oxalate (logβ = 3.0−3.4) than that of Ca^{2+}-alginate (logβ = 2.2), oxalic acid should be capable of

extracting the Ca^{2+} out of the cross-linked Ca^{2+}-alginate matrix and loosening its compact configuration (Kaisheva and Kaishev, 2015; Smith and Martell, 1987). Meanwhile, the water fluxes of the oxalic acid (or oxalic acid/H_2O_2) treated pristine membranes nearly decreased to their before-cleaning levels after Ca^{2+} exposure (3.0 mM). This result signified that in the non-oxidative cleaning system, some foulants, loosened by oxalic acid, still persisted on the membrane surface or in the membrane pores, and tended to be re-organised into a cross-linked conformation through complexing with Ca^{2+} (Mustafa et al., 2016). As observed in Figure 3.5b, oxalic acid cleaning resulted in a higher flux recovery (38.73%) for the iron-oxide pre-coated membrane, presumably because the oxalic acid could dissolve some Fe_3O_4 (leached Fe_T: 43.31%, 4.46 mg L^{-1}, Table 3.1), and then partially detached the Ca^{2+}-alginate layer. The flux also encountered a decline (by 78.07%) after Ca^{2+} exposure, further confirming that the remaining gel layer was re-compacted upon exposure to Ca^{2+}. Notably, the flux was recovered by 85.07% when combining H_2O_2 and oxalic acid for cleaning the iron-oxide pre-coated membrane and no flux decrease was observed upon Ca^{2+} exposure. This result suggested that the gel-like fouling layer was sufficiently removed from the iron-oxide pre-coat by the synergistic cleaning of oxalic acid relaxation and Fenton oxidation. Herein, the surface $^\bullet OH$ radicals were expected to preferentially attack the alginate molecules without evident scavenging by oxalic acid, due to the much lower reaction rate of $^\bullet OH$/oxalic acid ($k^\bullet OH$/oxalic acid = 1.4×10^6 M^{-1} s^{-1}) than that of $^\bullet OH$/alginate ($k^\bullet OH$/alginate = 9.2×10^7 M^{-1} s^{-1}) (Lester et al., 2013; Xue et al., 2009). In comparison with the Fenton cleaning without using oxalic acid (Section 3.3.3), the synergistic oxalic acid/H_2O_2 cleaning of the iron-oxide pre-coated membrane consumed much less H_2O_2 (9.6%, Table 3.1) and shorter cleaning time (1 h), which was presumably attributable to an accelerated diffusion of H_2O_2 to the Fe_3O_4/foulant interface due to gel layer relaxation by oxalic acid.

Table 3.1 *Cleaning performance of precoated and pristine membranes (ND: not detected)*

Membranes	Cleaning agents	Dissolved Fe^{2+} (mg L^{-1})	Dissolved Fe^{3+} (mg L^{-1})	H_2O_2 conversion (%)	Flux recovery (%)
Iron-oxide precoat	Oxalic acid/H_2O_2	ND	0.66	9.6	85.07
Iron-oxide precoat	H_2O_2	ND	ND	0	7.80
Iron-oxide precoat	Oxalic acid	0.25	4.21	-	38.73
Pristine membrane	Oxalic acid/H_2O_2	-	-	0	7.96
Pristine membrane	H_2O_2	-	-	0	6.31
Pristine membrane	Oxalic acid	-	-	-	5.81
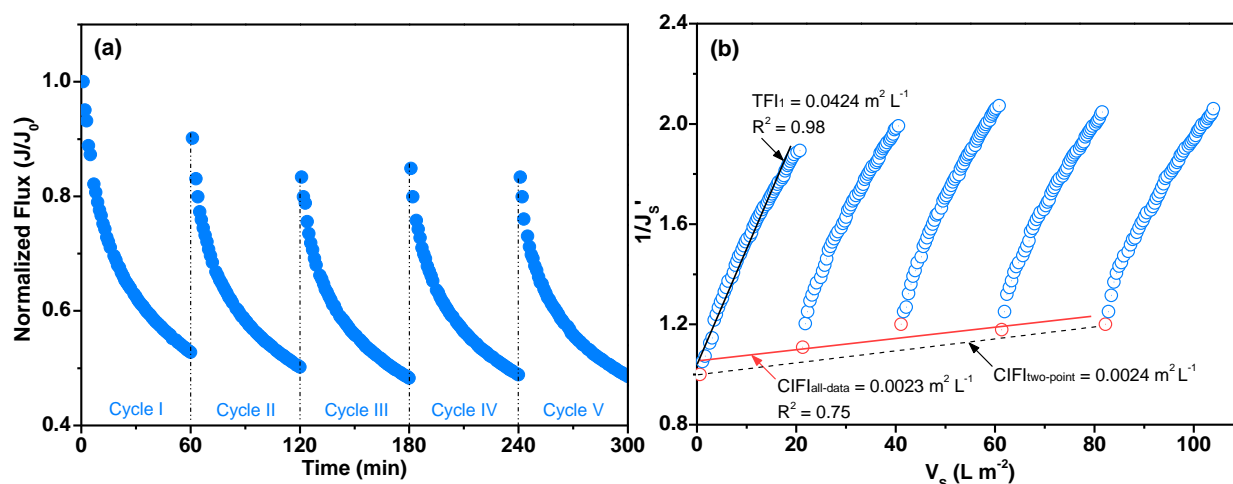
Figure 3.6 *(a) Multicycle filtration/cleaning of iron-oxide pre-coated membrane by oxalic acid/H_2O_2 combination ([oxalic acid]$_0$ = 11.1 mM, [H_2O_2]$_0$ = 30.0 mM, pH = 2.5). (b) Evaluation of total fouling indices (TFI) and chemically irreversible fouling indices (CIFI). The iron-oxide pre-coat was not refreshed between the cycles.*

Practicality of the synergistic oxalic acid/H_2O_2 cleaning was evaluated via multicycle filtration/cleaning with the iron-oxide pre-coated membrane (Figure 3.6a). Each cycle included filtration of Ca^{2+}-alginate solution (0.8 g L^{-1}) for 1 h, followed by oxalic acid/H_2O_2 (11.1 mM/30.0 mM) cleaning for 15 min. The iron-oxide pre-coat was not refreshed between the cycles. Within the first three cycles of oxalic acid/H_2O_2 cleaning, over 90% of the initial flux was maintained, and then the initial flux decreased to ~83%. After the third cleaning, the initial normalized flux of the membrane reached a plateau level of 83–85%. These results implied that most of the gel-like foulants could be reversed from the iron-oxide pre-coated membrane by the synergistic oxalic acid/H_2O_2 cleaning, while some irreversible fouling might occur at the early stage (i.e. the first three cycles) of the multicycle filtration/cleaning (Athanasekou et al., 2009). The slightly higher initial normalized flux (84.9%) after the third cleaning, than that after the second cleaning (83.3%), was possibly resulted from a partial falling-off of the Fe_3O_4 layer from the membrane, which might release some blocked pores for water permeation. Kramer et al. (2020) reported that hydraulic backwash could recover the permeance of gel-fouled ceramic NF membranes maximally by 43% but damaged the membrane integrity, and forward flush slightly restored the permeance (<10%). This indicated that the synergistic cleaning method of this chapter might be a promising substitute for conventional hydraulic backwash and forward flush for cleaning ceramic NF membranes. As depicted in Figure S3.1, approximately 26.5% of the Fe_3O_4 nanoparticles were leached after five cleaning cycles, probably due to the hydraulic scouring and chemical leaching during the oxalic acid/H_2O_2 circulation.

As suggested by Pan et al. (2015), the remaining iron-oxide layer (~2.1 μm in thickness, Figure 3.7a) after five filtration/cleaning cycles was likely ascribed to the drag forces caused by radial flow, frictional forces and molecular forces between the particles. Furthermore, the iron layer still presented a homogeneous and dense coating on the membrane surface (Figure 3.7b), which could provide sufficient active sites for Fenton-based reactions. Additionally, as shown in Figure 3.7c, the XRD patterns of the iron-oxide pre-coated membrane corresponded to the cubic spinel structure of Fe_3O_4, signifying an abundance of active Fe_3O_4 species on the membrane surface (Kim et al., 2012). After multicycle filtration/cleaning, the characteristic peaks of the Fe_3O_4 nanoparticles were almost unchanged except for a presence of reflection peaks of γ-Fe_2O_3 (maghemite), indicating a partial conversion of the Fe_3O_4 to the γ-Fe_2O_3 phase after oxidation reactions (Kim et al., 2012). The XRD profiles showed an evident α-Al_2O_3 crystalline phase of the Al_2O_3 supporting layer, but no apparent characteristic peaks of TiO_2 and ZrO_2 were observed, which indicated an amorphous structure of the TiO_2 active layer and ZrO_2 inter-layer (Anisah et al., 2018).
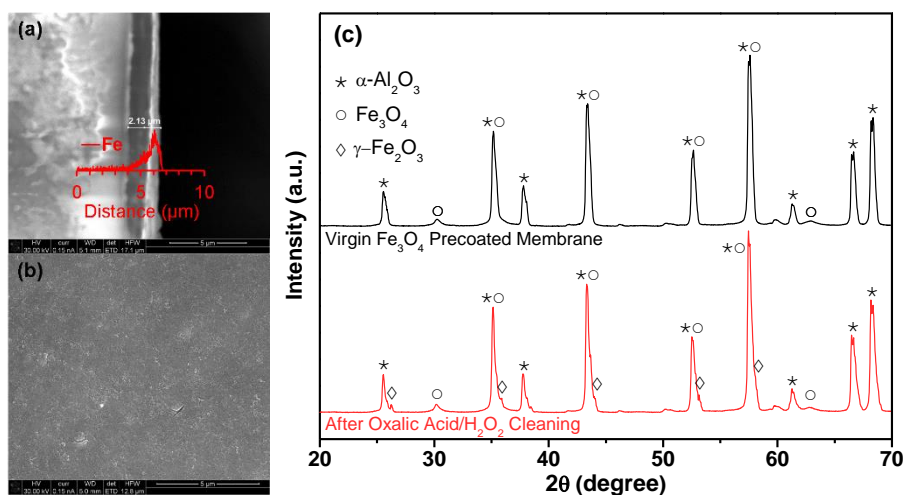
Figure 3.7 *(a) Cross-section SEM image with inset EDS profile and (b) top-view SEM image of pre-coated membrane after five cycles of fouling and oxalic acid/H_2O_2 cleaning. (c) XRD patterns of pre-coated membrane before and after five cycles of fouling and oxalic acid/H_2O_2 cleaning.*

To predict the long-term performance of using oxalic acid-assisted Fenton oxidation for cleaning iron-oxide pre-coated membrane, the fouling reversibility, developed in the multicycle filtration/cleaning, was quantitatively studied through a statistical analysis of the unified membrane fouling index (*UMFI*) values. As observed in Figure 3.6b, the regression-line slopes of the cyclic fouling curves from Equation (3.2) (Huang et al., 2009) corresponded to total fouling index (*TFI*) values of five filtration cycles, varying in a range of 3.51×10^{-2} to 4.24×10^{-2} m^2 L^{-1} (averaging

3.94×10^{-2} m² L⁻¹, $R^2 \geq 0.98$). These values were much higher than the *TFI* value (1.13×10^{-3} m² L⁻¹) in ceramic UF membrane fouling by Ca²⁺-alginate as reported by Alresheedi et al. (2019), suggesting a faster fouling tendency of the ceramic NF membrane by gel-like foulants compared to the ceramic UF membrane. The chemically irreversible fouling index (*CIFI*$_{all\text{-}data}$) value was 2.3×10^{-3} m² L⁻¹, as represented by the slope of the regression-line connecting the starting points of the five fouling curves ($R^2 = 0.75$), which was comparable to the *CIFI*$_{two\text{-}point}$ (2.4×10^{-3} m² L⁻¹) determined by the two-point approach (Huang et al., 2009). The chemically irreversible fouling ratio (*CIFI/TFI* = 5.8%) in the oxalic acid/H₂O₂ cleaning (15 min) was much lower than those (20% and 38%, respectively) in NaOH (10 mM) and NaClO (14 mM) cleaning with even longer duration (4 h), indicating a higher efficiency and reversibility of using oxalic acid-aided Fenton oxidation for cleaning gel-like fouling, compared to the conventional NaOH and NaClO cleaning (Alresheedi et al., 2019).

3.3.5 Iron leaching of iron-oxide pre-coated membranes
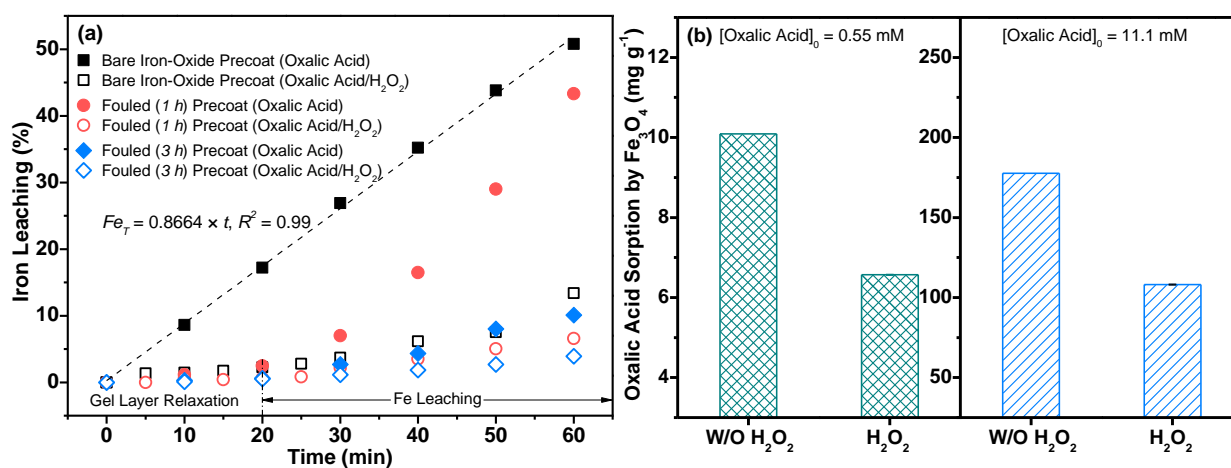
Figure 3.8 *(a) Iron leaching of bare and fouled iron-oxide pre-coat by oxalic acid and oxalic acid/H₂O₂ cleaning ([oxalic acid]₀ = 11.1 mM, [H₂O₂]₀ = 30.0 mM, pH = 2.5). (b) Oxalic acid sorption by Fe₃O₄ powders with and without (W/O) addition of H₂O₂ ([Fe₃O₄]₀ = 1.0 g L⁻¹, [H₂O₂]₀ = 30.0 mM, pH = 2.5).*

The combined use of iron-oxide pre-coat and oxalic acid favoured iron leaching, as observed in Figure 3.8. This could be potentially attributed to three underlying mechanisms, such as protonation, non-reductive complexation and reductive dissolution (Cwiertny et al., 2009). Herein, the protonation and reductive dissolution were excluded to be the possible causes for the iron dissolution, due to the negligible pH variation (pH = 2.5–2.6, Figure S3.2) during Fe₃O₄/oxalic acid (or Fe₃O₄/oxalic acid-H₂O₂) interactions and minimal Fe(II) generation after the oxalic acid or oxalic acid/H₂O₂ treatment (Fe(II) ≤ 0.25 mg L⁻¹, Table 3.1). Non-reductive complexation of Fe₃O₄/oxalic acid was thus supposed

to act as the dominant pathway for the iron leaching from the iron-oxide pre-coat surface (Xu et al., 2019). The comparison of the iron leaching from the iron-oxide pre-coat by oxalic acid (11.0 mM) and oxalic acid/H_2O_2 (11.0/30.0 mM) in the presence and absence of Ca^{2+}-alginate fouling layer is illustrated in Fig. 8a. The iron leaching of the bare iron-oxide pre-coat by oxalic acid could be described as a linear function of time ($Fe_T = 0.8664 \cdot t$, $R^2 = 0.99$). This result suggested that the Fe leaching of the iron-oxide pre-coat by oxalic acid was possibly governed by slow ionization of the oxalic acid ($pK_{a1} = 1.25$, $pK_{a2} = 4.27$), which constantly supplied dissociated oxalic acid for iron dissolution (Darken, 1941). Additionally, the maximal Fe leaching (13.4%) of the iron-oxide pre-coat by oxalic acid/H_2O_2 combination appeared much lower than that caused by oxalic acid (50.8%) within an identical time scale (60 min), which indicated a potential inhibition of iron dissolution by H_2O_2 addition into oxalic acid solutions (Rodríguez et al., 2011).

As suggested by Xue et al. (2009), the dissolution of Fe_3O_4 via complexation is a surface-controlled reaction occurring in two steps, adsorption of ligand on oxide surfaces through ligand exchange and iron dissolution by weakening Fe-O bonds of Fe_3O_4. To elucidate the inhibiting effect of H_2O_2 on the oxalic acid-induced iron leaching of the iron-oxide pre-coat, the surface adsorption of oxalic acid on Fe_3O_4 colloids was investigated with batch adsorption tests in the presence and absence of H_2O_2. As depicted in Figure 3.8b, the adsorption of oxalic acid ([oxalic acid]$_0$ = 0.55 mM) by the Fe_3O_4 colloids was markedly decreased by 34.9% by H_2O_2 addition into the Fe_3O_4/oxalic acid matrix, even a greater inhibition (by 39.1%) by H_2O_2 on the oxalic acid adsorption could be observed for the oxalic acid of higher initial concentration (11.1 mM). Moreover, since the free oxalic acid remaining in the solution was increased after the H_2O_2 addition (Figure S3.3), most of the oxalic acid was thus supposed not to be degraded by Fenton-based oxidation but remained in the aqueous phase or on the Fe_3O_4 surface (Rodríguez et al., 2009). Therefore, the decreased iron-leaching of the iron-oxide pre-coat in the oxalic acid/H_2O_2 matrix was presumably not attributable to potential degradation of oxalic acid in the presence of H_2O_2, but to an underlying adsorptive competition between H_2O_2 and oxalic acid on the Fe_3O_4 surface, which was also found by Rodríguez et al. (2011).

Compared with the bare iron-oxide pre-coat, the Ca^{2+}-alginate fouled (for 1 h) membane underwent firstly a minimal Fe dissolution (Fe_T leaching: 2.47%) by oxalic acid at the early stage (20 min), but developed an exponential increase at the later stage (Fe_T leaching: 43.31%) (Figure 3.8a). The nonlinear two-stage profile of leached Fe_T vs. time suggested that the iron leaching rate of the fouled iron-oxide pre-coat was not entirely surface-reaction limited, but also relied on transport-controlled steps, such as oxalic acid diffusion through the gel layer (Huling et al., 2007). As such, it could be

inferred that the Ca^{2+}-alginate gel layer as a steric barrier supressed the iron leaching at an early stage, but inclined to be loosened by oxalic acid following continuous oxalic acid/Ca^{2+}-alginate complexation, which in turn promoted the diffusion of oxalic acid onto the Fe_3O_4 surface (Liu et al., 2018). Hence, during the 15-min oxalic acid/H_2O_2 cleaning in the multicycle filtration/cleaning (Section 3.3.4), the compact gel-like cake layer, formed on the iron-oxide pre-coat, made that the hydraulic scouring could not directly act on the iron-oxide pre-coat surface, which protected the iron layer from being flushed away by cross flow to some extent. Likewise, the introduction of H_2O_2 restricted the Fe leaching by oxalic acid (by 84.8%), likely due to a promoted diffusion and competitive adsorption of H_2O_2 onto the iron-oxide pre-coat surface. This result well accounted for the desirable stability and reproducibility of the iron-oxide pre-coat during multicycle runs of oxalic acid-aided Fenton cleaning, as discussed in Section 3.3.4. A two-stage leaching of iron, but to a less extent (Fe_T leaching: 10.1% by oxalic acid, 3.9% by oxalic acid/H_2O_2), could also be observed with a more severely fouled (for 3 h) iron-oxide pre-coat. The findings of the oxalic acid/H_2O_2 cleaning (Section 3.3.4, Figure 3.5) and the iron leaching experiments (Figure 3.8) demonstrated an underlying synergistic effect between oxalic acid and H_2O_2, regarding the gel layer relaxation/oxidation and Fe-leaching suppression, for effective de-fouling of iron-oxide pre-coated ceramic NF membranes, which can be illustrated by Scheme 3.1.
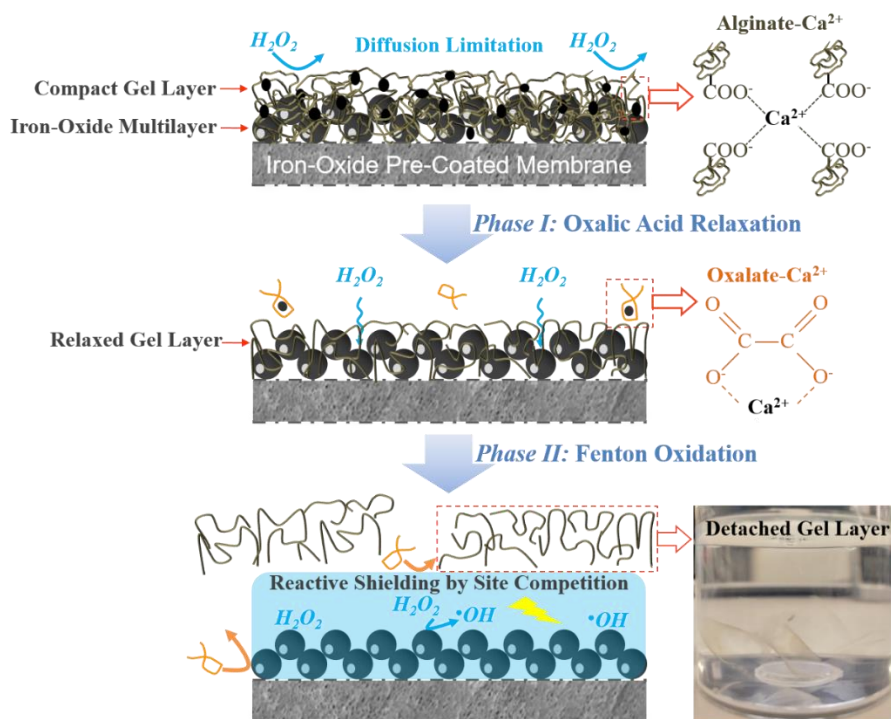
Scheme 3.1 *Synergistic effect of oxalic acid relaxation and Fenton oxidation of pre-coated membranes.*

3.3.6 Implications for the direct treatment of surface water

Filtration of canal water for 5 d was performed using a Fe_3O_4 pre-coated ceramic NF membrane, with 15-min oxalic acid/H_2O_2 cleaning every 24 h. The relative production downtime during membrane cleaning was 0.62 min h^{-1}, much lower than the value (2.6 min h^{-1}) of NaClO cleaning for ceramic NF membranes reported by Kramer et al. (2015). The iron-oxide pre-coat (pre-coated for 30 min) was reused over the five cycles (5 d) of canal water filtration, which would presumably exert an insignificant impact on the continuous operations of the pre-coated membranes in practice. As depicted in Figure S3.4a, a fast drop of permeance (~38.7%) was also observed in the NF processes of the canal water, when switching the pure water filtration to the canal water filtration, which was similar to the phenomenon found in the NF with alginate (Figure 3.4a). The membrane permeance with canal water decreased by 48.7% in the first cycle, indicating the high fouling potential of the canal water towards the membrane. The initial canal-water permeance for the following cycles were recovered to ~90% after oxalic acid/H_2O_2 cleaning, implying high cleaning efficiencies during the long-term filtration with canal water. During the five cycles, the oxalic acid/H_2O_2 solution was reused, which reduced the consumption of chemicals and production of oxalic acid wastewater. As mentioned by earlier studies, oxalic acid could be well degraded in aerobic conditions with microbial treatment technologies (i.e. activated sludge), a normal aerobic wastewater treatment plant could thus deal with the produced oxalic acid wastewater (Nakamura et al., 2004). Furthermore, Table S3.2 presents that the iron-oxide pre-coated membrane rejected ~90% of DOC and UV$_{254}$, suggesting its high rejection of organic matter probably owing to steric exclusion by the ceramic NF membrane. By contrast, the rejection rates of anions and cations appeared to be much lower, which were 43−78% and 27−42%, respectively. Notably, after the five cycles (5 d) of filtration/cleaning, there still was a certain amount of iron-oxide pre-coat (~0.9 μm in thickness, Figure S3.4b) remaining on the membrane surface, indicating a potential applicability of using iron-oxide pre-coated NF membranes for long-term water treatment.

3.3.7 Research needs and challenges

The cleaning strategy, proposed in this chapter, provides a pathway of using pressure-driven pre-filtration of Fe_3O_4 nanoparticles to obtain a catalytic ceramic NF system for fouling control in water treatment. However, the long-term usage of Fe_3O_4-pre-coated ceramic NF membrane in industries may be limited by the stability and reactivity of catalyst pre-coat. Further studies on using stable and active catalysts for improving the pre-coated catalytic ceramic membrane are thus needed. Additionally, as can be speculated from this chapter, the synergistic relaxation-oxidation method,

currently tested as a proof of principle, may apply to other types of Ca^{2+}-mediated fouling (i.e. humic acids) due to their similar mechanisms in the formation of a gel layer on membrane surfaces via Ca^{2+} bridging (Li and Elimelech, 2004). We thus believe that understanding the roles of oxalic acid and Fenton-based oxidation in the typical Ca^{2+}-mediated alginate fouling, may provide insights into handling other Ca^{2+}-derived fouling with an integration of chelation/oxidation. However, the integrative method should be further piloted in practice and explored for more complex real water matrices, also to understand how other compounds could interfere.

3.4 Conclusions

In this chapter, a synergistic method of coupling oxalic acid chelation and Fe_3O_4-activated Fenton oxidation process was proposed for cleaning persistent gel-like fouling of ceramic NF membrane. The conclusions can be drawn as follows:

(1) Cross-flow pre-filtration of Fe_3O_4 nanoparticles was able to pre-coat a uniform reproducible iron-oxide layer on top of the ceramic NF membrane. The pre-coat thickness was controlled by the trans-membrane pressure (2.0–10.0 bar), only causing a minimal decrease of membrane permeance (<10%).

(2) Synergistic effect between oxalic acid relaxation and Fenton-based oxidation processes played a key role in the removal of gel layer, which was presumably attributed to enhanced diffusive transport of H_2O_2 at the iron-oxide pre-coat/foulant interface.

(3) Oxalic acid-aided Fenton cleaning for 15 min achieved stable initial normalized fluxes (83.33–90.15%) of the iron-oxide pre-coated membrane during five filtration/cleaning cycles, with no need of refreshing the iron-oxide pre-coat between the cycles. The leaching of iron from the iron-oxide pre-coat was suppressed in the oxalic acid/H_2O_2 matrix, which was likely due to a reactive shielding by competitive reactions of H_2O_2 on the Fe_3O_4 surface.

Supplementary data

Text S3.1 Calculation of Fe_3O_4 coating efficiency of ceramic nanofiltration membrane

The actual coating mass (M_a, g m^{-2}) of Fe_3O_4 nanoparticles on the membrane surface can be calculated by introducing a coating efficiency index (α) related to the nominal coating mass (M_n, g m^{-2}), according to Equation (S3.1).

$$M_a = \alpha \cdot M_n = \frac{\alpha \cdot C_{Fe} \cdot V}{A_m} = \alpha \cdot C_{Fe} \cdot \int_0^t J \, dt \tag{S3.1}$$

where α is the ratio of the Fe_3O_4 mass deposited on the membrane surface to those transported to the membrane, C_{Fe} (g L^{-1}) is the bulk concentration of Fe_3O_4 nanoparticles in the filtration module, V (L) is the permeate volume, J (L m^{-2} h^{-1}) is the permeate flux during the Fe_3O_4 filtration, A_m (m^2) is the effective filtration area of the membranes, t (h) is the filtration time. As such, the Fe_3O_4 mass flushed by the shear force of the cross-flow (M_l, g m^{-2}) can be calculated as indicated by Equation (S3.2).

$$M_l = M_n - M_a \tag{S3.2}$$

Text S3.2 Preparation procedure of Ca^{2+}-alginate fouling solution

In total 30.0 L of synthetic sewage water was used for each filtration experiment. The sodium alginate (0.8 g L^{-1}) solution was first dissolved and stirred in a water tank of 30 L demineralized water. NaCl (5.0 mM) was added to provide ion strength of the fouling solution. Gel-like fouling solution was triggered by mixing $CaCl_2 \cdot 2H_2O$ (3.0 mM) into the alginate solution with continuous stirring. $NaHCO_3$ was added to the synthetic fouling solution to provide buffering properties. NaOH (1.0 M) and HCl (1.0 M) were used to adjust the pH to 7.0.

Text S3.3 Calculation of average size of Fe_3O_4 particles dried from Fe_3O_4 hydrosols

Assuming nonporous spherical particles and a theoretical density (5.17 g cm^{-3}) of the Fe_3O_4 solid particles dried from Fe_3O_4 hydrosols, an average particle diameter of Fe_3O_4 particles could be calculated based on its BET specific surface area (91.20 m^2 g^{-1}, Table S1) with Equation (S3.3) (Kirillov, 2009):

$$D = \frac{6 \times 10^{-6}}{A_S \cdot d} \tag{S3.3}$$

where A_S (m^2 g^{-1}) is the specific surface area, D (m) represents the diameter of nanoparticles, and d (g m^{-3}) is designated to the density of nanoparticles.

Text S3.4 Calculation of porosities of iron-oxide pre-coating layers

As the loading mass and thickness of iron-oxide pre-coating layers have been measured in this chapter, the porosities of the iron-oxide layers with different iron loadings can thus be estimated based on Equation (S3.4), as previously reported by Altmann and Ripperger (1997):

$$H = \frac{M}{\rho_s \cdot (1 - \varepsilon)} \qquad (S3.4)$$

where H (m) is the thickness of the pre-coating layers, M (g m^{-2}) is the loading mass of iron oxides, ρ_s is the density of Fe$_3$O$_4$ nanoparticles (5.17 g cm^{-3}). ε is the porosity of the iron-oxide layers.

Table S3.1 Parameters of ceramic nanofiltration membranes

Parameters	Value
Outer diameter (mm)	10
Channel diameter (mm)	7
Membrane area (m^2)	0.00163
Mean pore size (nm)	0.9

Table S3.2 Water quality parameters and rejection of compounds of canal water by Fe$_3$O$_4$ pre-coated ceramic NF membrane

Parameters	Raw canal water	Rejection (%)
DOC (mg L^{-1})	11.95	89.89
UV$_{254}$ (cm^{-1})	0.37	90.88
Conductivity (mS cm^{-1})	2.43	38.02
Ca^{2+} (mg L^{-1})	77.64	41.77
Mg^{2+} (mg L^{-1})	17.71	34.34
Na$^+$ (mg L^{-1})	76.16	28.75
K$^+$ (mg L^{-1})	12.28	27.89
PO$_4^{3-}$ (mg L^{-1})	6.66	77.91
SO$_4^{2-}$ (mg L^{-1})	48.14	43.73
Cl$^-$ (mg L^{-1})	121.10	50.32
Br$^-$ (mg L^{-1})	1.84	47.39
NO$_3^-$ (mg L^{-1})	2.50	48.32

Table S3.3 Parameters of Fe$_3$O$_4$ nanoparticles

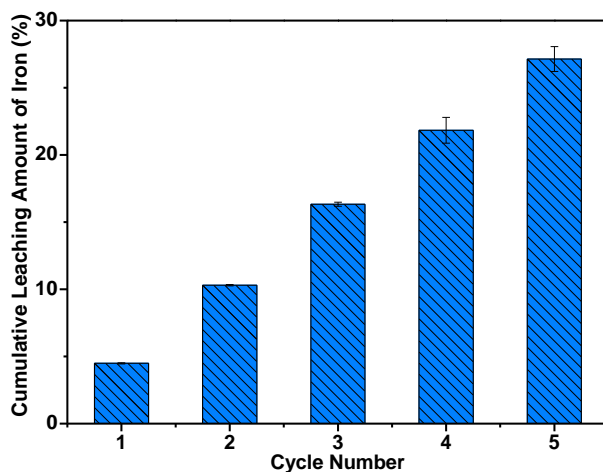| Iron oxides	BET surface area (m^2 g^{-1})	Particle diameter (nm)
Fe$_3$O$_4$	91.20	12.72

Figure S3.1 *Cumulative iron leaching of pre-coat layer during multicycle oxalic acid/H_2O_2 cleaning.*
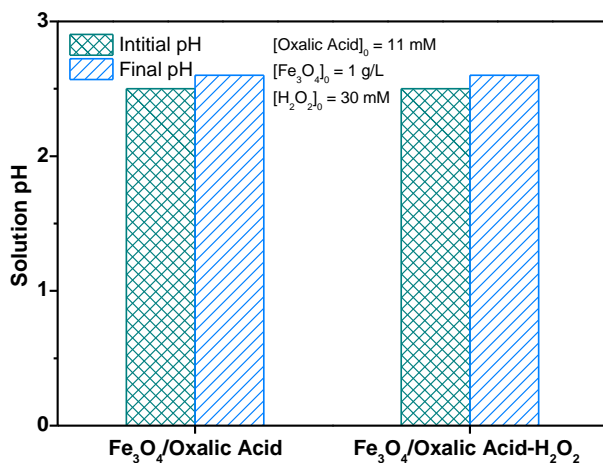

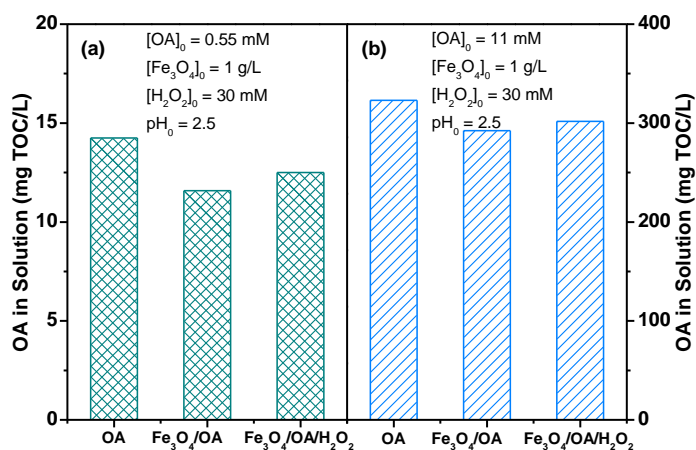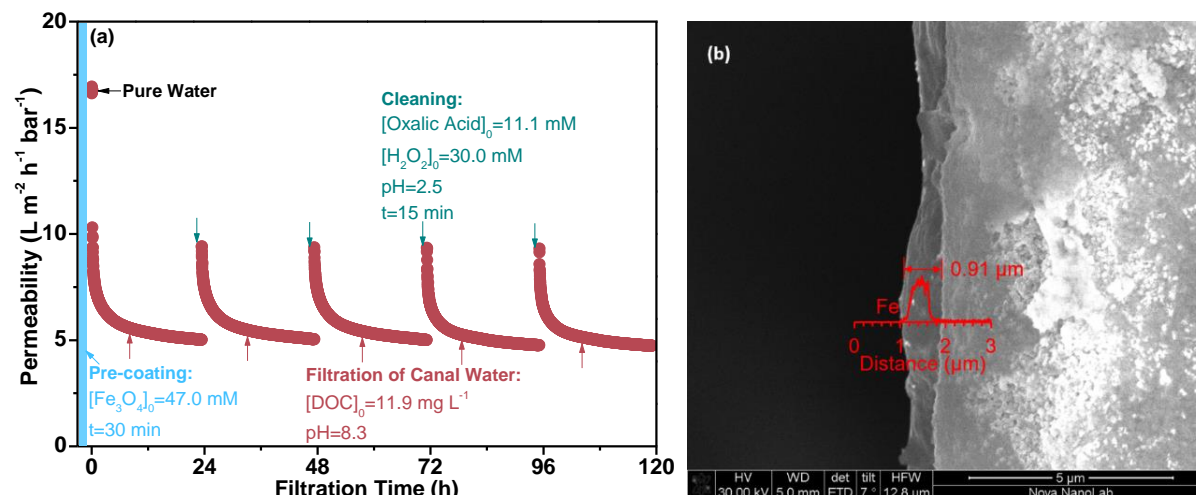**Figure S3.2** *pH evolution during iron leaching tests of Fe_3O_4 in oxalic acid and oxalic acid/H_2O_2 solution.*

Figure S3.3 *Oxalic acid (OA) evolution in Fe_3O_4/oxalic acid or Fe_3O_4/oxalic acid-H_2O_2 systems.*

Figure S3.4 *(a) Permeance evolution over time of Fe_3O_4 pre-coated ceramic NF membrane during the filtration of canal water at constant pressure of 3.0 bar, with oxalic acid/H_2O_2 cleaning every 24 h. The iron-oxide pre-coat was not refreshed between the cycles. (b) Cross-section SEM image with inset EDS profile of iron-oxide pre-coated membrane after five cycles (5 d) of canal water filtration and oxalic acid/H_2O_2 cleaning.*

References

Ajmani, G.S., Goodwin, D., Marsh, K., Fairbrother, D.H., Schwab, K.J., Jacangelo, J.G., Huang, H., 2012. Modification of low pressure membranes with carbon nanotube layers for fouling control. Water Research 46(17), 5645-5654.

Alresheedi, M.T., Basu, O.D., Barbeau, B., 2019. Chemical cleaning of ceramic ultrafiltration membranes – Ozone versus conventional cleaning chemicals. Chemosphere 226, 668-677.

Altmann, J., Ripperger, S., 1997. Particle deposition and layer formation at the crossflow microfiltration. Journal of Membrane Science 124(1), 119-128.

Anantharaman, A., Chun, Y., Hua, T., Chew, J.W., Wang, R., 2020. Pre-deposited dynamic membrane filtration – A review. Water Research 173, 115558.

Ang, W.S., Tiraferri, A., Chen, K.L., Elimelech, M., 2011. Fouling and cleaning of RO membranes fouled by mixtures of organic foulants simulating wastewater effluent. Journal of Membrane Science 376(1), 196-206.

Anisah, S., Puthai, W., Kanezashi, M., Nagasawa, H., Tsuru, T., 2018. Preparation, characterization, and evaluation of TiO_2-ZrO_2 nanofiltration membranes fired at different temperatures. Journal of Membrane Science 564, 691-699.

Athanasekou, C.P., Papageorgiou, S.K., Kaselouri, V., Katsaros, F.K., Kakizis, N.K., Sapalidis, A.A., Kanellopoulos, N.K., 2009. Development of hybrid alginate/ceramic membranes for Cd^{2+} removal. Microporous and Mesoporous Materials 120(1), 154-164.

Brillas, E., Sirés, I., Oturan, M.A., 2009. Electro-Fenton process and related electrochemical technologies based on Fenton's reaction chemistry. Chemical Reviews 109(12), 6570-6631.

Chen, J., Zhang, M., Li, F., Qian, L., Lin, H., Yang, L., Wu, X., Zhou, X., He, Y., Liao, B.-Q., 2016. Membrane fouling in a membrane bioreactor: High filtration resistance of gel layer and its underlying mechanism. Water Research 102, 82-89.

Chen, L., Ma, J., Li, X., Zhang, J., Fang, J., Guan, Y., Xie, P., 2011. Strong enhancement on Fenton oxidation by addition of hydroxylamine to accelerate the ferric and ferrous iron cycles. Environmental Science & Technology 45(9), 3925-3930.

Cwiertny, D.M., Hunter, G.J., Pettibone, J.M., Scherer, M.M., Grassian, V.H., 2009. Surface chemistry and dissolution of α-FeOOH nanorods and microrods: Environmental implications of size-dependent interactions with oxalate. The Journal of Physical Chemistry C 113(6), 2175-2186.

Darken, L.S., 1941. The ionization constants of oxalic acid at 25° from conductance measurements. Journal of the American Chemical Society 63(4), 1007-1011.

De Angelis, L., de Cortalezzi, M.M.F., 2016. Improved membrane flux recovery by Fenton-type reactions. Journal of Membrane Science 500, 255-264.

Duesterberg, C.K., Mylon, S.E., Waite, T.D., 2008. pH effects on iron-catalyzed oxidation using Fenton's reagent. Environmental Science & Technology 42(22), 8522-8527.

Field, R.W., Wu, D., Howell, J.A., Gupta, B.B., 1995. Critical flux concept for microfiltration fouling. Journal of Membrane Science 100(3), 259-272.

Fujioka, T., Hoang, A.T., Okuda, T., Takeuchi, H., Tanaka, H., Nghiem, L.D., 2018. Water reclamation using a ceramic nanofiltration membrane and surface flushing with ozonated water. International Journal of Environmental Research and Public Health 15(4), 799.

Fujioka, T., Khan, S.J., McDonald, J.A., Nghiem, L.D., 2014. Nanofiltration of trace organic chemicals: A comparison between ceramic and polymeric membranes. Separation and Purification Technology 136, 258-264.

Gligorovski, S., Strekowski, R., Barbati, S., Vione, D., 2015. Environmental implications of hydroxyl radicals (•OH). Chemical Reviews 115(24), 13051-13092.

Haldar, D., Duarah, P., Purkait, M.K., 2020. MOFs for the treatment of arsenic, fluoride and iron contaminated drinking water: A review. Chemosphere 251, 126388.

Huang, H., Young, T., Jacangelo, J.G., 2009. Novel approach for the analysis of bench-scale, low pressure membrane fouling in water treatment. Journal of Membrane Science 334(1), 1-8.

Huling, S.G., Jones, P.K., Lee, T.R., 2007. Iron optimization for Fenton-driven oxidation of MTBE-spent granular activated carbon. Environmental Science & Technology 41(11), 4090-4096.

Kaisheva, N.S., Kaishev, A.S., 2015. Potentiometric titration for determining the composition and stability of metal(II) alginates and pectinates in aqueous solutions. Russian Journal of Physical Chemistry A 89(7), 1216-1222.

Kang, Y.S., Risbud, S., Rabolt, J.F., Stroeve, P., 1996. Synthesis and characterization of nanometer-size Fe_3O_4 and γ-Fe_2O_3 particles. Chemistry of Materials 8(9), 2209-2211.

Katsounaros, I., Schneider, W.B., Meier, J.C., Benedikt, U., Biedermann, P.U., Auer, A.A., Mayrhofer, K.J.J., 2012. Hydrogen peroxide electrochemistry on platinum: Towards understanding the oxygen reduction reaction mechanism. Physical Chemistry Chemical Physics 14(20), 7384-7391.

Kim, B.-C., Nam, J.-W., Kang, K.-H., 2017. Dynamic membrane filtration using powdered iron oxide for SWRO pre-treatment during red tide event. Journal of Membrane Science 524, 604-611.

Kim, W., Suh, C.-Y., Cho, S.-W., Roh, K.-M., Kwon, H., Song, K., Shon, I.-J., 2012. A new method for the identification and quantification of magnetite–maghemite mixture using conventional X-ray diffraction technique. Talanta 94, 348-352.

Kirillov, S.A., 2009. Surface area and pore volume of a system of particles as a function of their size and packing. Microporous and Mesoporous Materials 122(1), 234-239.

Kramer, F.C., Shang, R., Heijman, S.G.J., Scherrenberg, S.M., van Lier, J.B., Rietveld, L.C., 2015. Direct water reclamation from sewage using ceramic tight ultra- and nanofiltration. Separation and Purification Technology 147, 329-336.

Kramer, F.C., Shang, R., Rietveld, L.C., Heijman, S.J.G., 2019. Influence of pH, multivalent counter ions, and membrane fouling on phosphate retention during ceramic nanofiltration. Separation and Purification Technology 227, 115675.

Kramer, F.C., Shang, R., Rietveld, L.C., Heijman, S.J.G., 2020. Fouling control in ceramic nanofiltration membranes during municipal sewage treatment. Separation and Purification Technology 237, 116373.

Lester, Y., Avisar, D., Mamane, H., 2013. Ozone degradation of Cyclophosphamide – Effect of alkalinity and key effluent organic matter constituents. Ozone: Science & Engineering 35(2), 125-133.

Li, Q., Elimelech, M., 2004. Organic fouling and chemical cleaning of nanofiltration membranes: Measurements and mechanisms. Environmental Science & Technology 38(17), 4683-4693.

Li, S., Heijman, S.G.J., Verberk, J.Q.J.C., Verliefde, A.R.D., Kemperman, A.J.B., van Dijk, J.C., Amy, G., 2009. Impact of backwash water composition on ultrafiltration fouling control. Journal of Membrane Science 344(1), 17-25.

Lin, S.-S., Gurol, M.D., 1998. Catalytic decomposition of hydrogen peroxide on iron oxide: Kinetics, mechanism, and implications. Environmental Science & Technology 32(10), 1417-1423.

Liu, C., Leng, W., Vikesland, P.J., 2018. Controlled evaluation of the impacts of surface coatings on silver nanoparticle dissolution rates. Environmental Science & Technology 52(5), 2726-2734.

Lu, D., Cheng, W., Zhang, T., Lu, X., Liu, Q., Jiang, J., Ma, J., 2016a. Hydrophilic Fe_2O_3 dynamic membrane mitigating fouling of support ceramic membrane in ultrafiltration of oil/water emulsion. Separation and Purification Technology 165, 1-9.

Lu, D., Zhang, T., Gutierrez, L., Ma, J., Croué, J.-P., 2016b. Influence of surface properties of filtration-layer metal oxide on ceramic membrane fouling during ultrafiltration of oil/water emulsion. Environmental Science & Technology 50(9), 4668-4674.

Mailen, J.C., Tallent, O.K., Arwood, P.C., 1981. Destruction of oxalate by reaction with hydrogen peroxide, p. 30, United States.

Mauter, M.S., Zucker, I., Perreault, F., Werber, J.R., Kim, J.-H., Elimelech, M., 2018. The role of nanotechnology in tackling global water challenges. Nature Sustainability 1(4), 166-175.

Mustafa, G., Wyns, K., Buekenhoudt, A., Meynen, V., 2016. New insights into the fouling mechanism of dissolved organic matter applying nanofiltration membranes with a variety of surface chemistries. Water Research 93, 195-204.

Mustafa, G., Wyns, K., Vandezande, P., Buekenhoudt, A., Meynen, V., 2014. Novel grafting method efficiently decreases irreversible fouling of ceramic nanofiltration membranes. Journal of Membrane Science 470, 369-377.

Nakamura, Y., Daidai, M., Kobayashi, F., 2004. Ozonolysis mechanism of lignin model compounds and microbial treatment of organic acids produced. Water Science and Technology 50(3), 167-172.

Pan, Y., Wang, W., Wang, W., Wang, T., 2015. Prediction of particle deposition and layer growth in the preparation of a dynamic membrane with cross-flow microfiltration. RSC Advances 5(108), 89015-89024.

Rodríguez, E., Fernández, G., Ledesma, B., Álvarez, P., Beltrán, F.J., 2009. Photocatalytic degradation of organics in water in the presence of iron oxides: Influence of carboxylic acids. Applied Catalysis B: Environmental 92(3), 240-249.

Rodríguez, E.M., Fernández, G., Álvarez, P.M., Hernández, R., Beltrán, F.J., 2011. Photocatalytic degradation of organics in water in the presence of iron oxides: Effects of pH and light source. Applied Catalysis B: Environmental 102(3), 572-583.

Smith, R.M., Martell, A.E., 1987. Critical stability constants, enthalpies and entropies for the formation of metal complexes of aminopolycarboxylic acids and carboxylic acids. Science of The Total Environment 64(1), 125-147.

Soesanto, J.F., Hwang, K.-J., Cheng, C.-W., Tsai, H.-Y., Huang, A., Chen, C.-H., Cheng, T.-W., Tung, K.-L., 2019. Fenton oxidation-based cleaning technology for powdered activated carbon-precoated dynamic membranes used in microfiltration seawater pretreatment systems. Journal of Membrane Science 591, 117298.

Song, L., Elimelech, M., 1995. Theory of concentration polarization in crossflow filtration. Journal of the Chemical Society, Faraday Transactions 91(19), 3389-3398.

Song, W., Ravindran, V., Koel, B.E., Pirbazari, M., 2004. Nanofiltration of natural organic matter with H_2O_2/UV pretreatment: Fouling mitigation and membrane surface characterization. Journal of Membrane Science 241(1), 143-160.

Sun, S., Yao, H., Fu, W., Hua, L., Zhang, G., Zhang, W., 2018. Reactive Photo-Fenton ceramic membranes: Synthesis, characterization and antifouling performance. Water Research 144, 690-698.

Tang, B., Wang, G., Zhuo, L., Ge, J., Cui, L., 2006. Facile route to α-FeOOH and α-Fe$_2$O$_3$ nanorods and magnetic property of α-Fe$_2$O$_3$ nanorods. Inorganic Chemistry 45(13), 5196-5200.

van den Brink, P., Zwijnenburg, A., Smith, G., Temmink, H., van Loosdrecht, M., 2009. Effect of free calcium concentration and ionic strength on alginate fouling in cross-flow membrane filtration. Journal of Membrane Science 345(1), 207-216.

Wadekar, S.S., Vidic, R.D., 2018. Comparison of ceramic and polymeric nanofiltration membranes for treatment of abandoned coal mine drainage. Desalination 440, 135-145.

Wang, L., Miao, R., Wang, X., Lv, Y., Meng, X., Yang, Y., Huang, D., Feng, L., Liu, Z., Ju, K., 2013. Fouling behavior of typical organic foulants in polyvinylidene fluoride ultrafiltration membranes: Characterization from microforces. Environmental Science & Technology 47(8), 3708-3714.

Wang, X.-M., Waite, T.D., 2008. Gel layer formation and hollow fiber membrane filterability of polysaccharide dispersions. Journal of Membrane Science 322(1), 204-213.

Xin, Y., Bligh, M.W., Kinsela, A.S., Waite, T.D., 2016. Effect of iron on membrane fouling by alginate in the absence and presence of calcium. Journal of Membrane Science 497, 289-299.

Xin, Y., Bligh, M.W., Kinsela, A.S., Wang, Y., David Waite, T., 2015. Calcium-mediated polysaccharide gel formation and breakage: Impact on membrane foulant hydraulic properties. Journal of Membrane Science 475, 395-405.

Xu, T., Zhu, R., Shang, H., Xia, Y., Liu, X., Zhang, L., 2019. Photochemical behavior of ferrihydrite-oxalate system: Interfacial reaction mechanism and charge transfer process. Water Research 159, 10-19.

Xue, X., Hanna, K., Despas, C., Wu, F., Deng, N., 2009. Effect of chelating agent on the oxidation rate of PCP in the magnetite/H_2O_2 system at neutral pH. Journal of Molecular Catalysis A: Chemical 311(1), 29-35.

Yang, X.-j., Xu, X.-m., Xu, X.-c., Xu, J., Wang, H.-l., Semiat, R., Han, Y.-f., 2016. Modeling and kinetics study of Bisphenol A (BPA) degradation over an FeOCl/SiO_2 Fenton-like catalyst. Catalysis Today 276, 85-96.

Zhang, J., Jiao, X.-L., Xia, Y.-G., Liu, F.-F., Pang, Y.-P., Zhao, X.-F., Chen, D.-R., 2016. Enhanced catalytic activity in liquid-exfoliated FeOCl nanosheets as a Fenton-like catalyst. Chemistry – A European Journal 22(27), 9321-9329.

Zhang, M., Lin, H., Shen, L., Liao, B.-Q., Wu, X., Li, R., 2017. Effect of calcium ions on fouling properties of alginate solution and its mechanisms. Journal of Membrane Science 525, 320-329.

Zhao, Y.-y., Wang, X.-m., Yang, H.-w., Xie, Y.-f.F., 2018. Effects of organic fouling and cleaning on the retention of pharmaceutically active compounds by ceramic nanofiltration membranes. Journal of Membrane Science 563, 734-742.

Zhao, Y., Tan, Y., Wong, F.-S., Fane, A.G., Xu, N., 2005. Formation of dynamic membranes for oily water separation by crossflow filtration. Separation and Purification Technology 44(3), 212-220.

Zhou, Z., He, X., Zhou, M., Meng, F., 2017. Chemically induced alterations in the characteristics of fouling-causing bio-macromolecules – Implications for the chemical cleaning of fouled membranes. Water Research 108, 115-123.

Zuriaga-Agustí, E., Alventosa-deLara, E., Barredo-Damas, S., Alcaina-Miranda, M.I., Iborra-Clar, M.I., Mendoza-Roca, J.A., 2014. Performance of ceramic ultrafiltration membranes and fouling behavior of a dye-polysaccharide binary system. Water Research 54, 199-210.

Chapter 4

ADSORPTION AND CAKE LAYER FOULING IN RELATION TO FENTON CLEANING OF CERAMIC NANOFILTRATION MEMBRANES
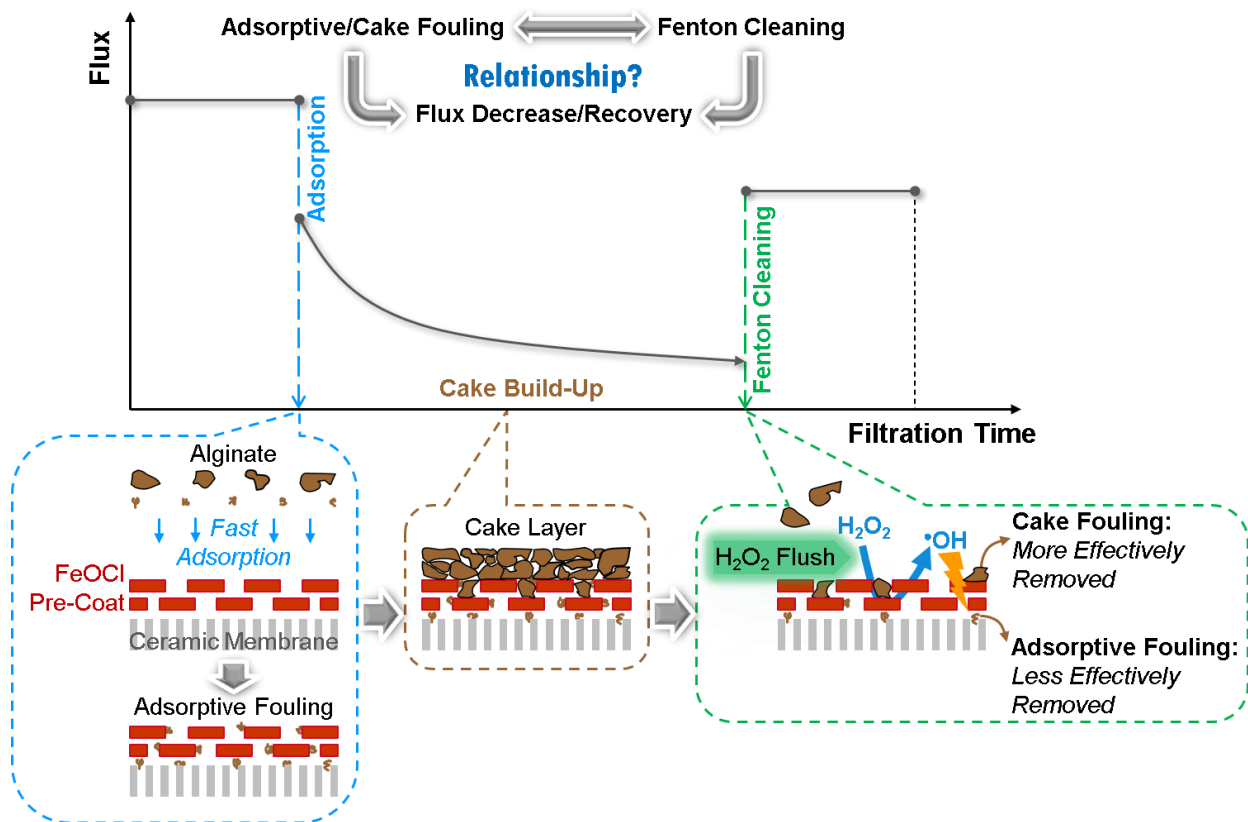
This chapter is based on:

Lin, B., Rietveld, L.C., Yao, L., and Heijman, S.G.J. Adsorption and cake layer fouling in relation to Fenton cleaning of ceramic nanofiltration membranes, under review in *Journal of Membrane Science*.

Abstract

Catalytic ceramic nanofiltration (NF) is a promising technology for advanced water treatment, given its high separation selectivity and reactive surfaces for oxidative removal of fouling. However, a clear understanding of the relation between fouling types and oxidative cleaning efficacy is important for establishing stable filtration/cleaning operations. In this chapter, Fenton cleaning, using a hydrogen peroxide solution and an iron oxychloride catalyst pre-coat layer on top of ceramic NF membranes, was studied with respect to biopolymer fouling, simulated by sodium alginate in the presence of calcium. Adsorption (in the absence of a permeate flow) and constant-pressure filtration (with a permeate flow) experiments were performed to distinguish between decreases in permeance as a result of either adsorptive or cake fouling. Results showed that the flux evolution could be divided into an initial sharp flux decline, due to adsorption of the foulants, and a subsequent gradual flux decrease, resulting from cake build-up on the membrane. The two-stage flux decrease was enhanced during the constant-pressure filtration experiments, because they start at a high flux with a high fouling rate, while the flux gradually decreases as fouling proceeds. During multiple adsorption/cake filtration/Fenton cleaning cycles, the cake fouling was sufficiently removed by Fenton cleaning in contrast to the adsorptive fouling. However, the total permeate production during ceramic NF was not influenced by the remaining adsorptive fouling (after cleaning), since the adsorptive fouling always only occurs at the beginning of each cycle. The findings provided new insights into the criteria for evaluating and optimizing the efficacy of oxidative (Fenton) cleaning during ceramic NF in water treatment.

4.1 Introduction

Ceramic nanofiltration (NF) has emerged as a promising technology for advanced water treatment, owing to its high selectivity over a broad variety of contaminants (e.g. multivalent ions, pathogens and organic molecules/colloids) and durability against harsh operating environments (Caltran et al., 2020). However, membrane fouling is a critical obstacle for up-scaling and implementation of ceramic NF membranes in industry, e.g. for wastewater reclamation and direct treatment of surface water (Fujioka et al., 2018; Kramer et al., 2015). In particular, fouling, developed by accumulation of organic biopolymers (e.g. polysaccharides), with formation of a compact cake layer on the membrane, hampers physical and chemical cleaning regimes. A forward flush is not effective enough to remove the sticky cake layer (Mustafa et al., 2016; Zhao et al., 2018), while a hydraulic backwash at high backwash pressures and long-term uses of sodium hypochlorite damage the end sealing of tubular

ceramic NF membranes, resulting in an increase in the membrane defects (Kramer et al., 2020; Kramer et al., 2019).

Catalytic ceramic membranes, functionalizing the membrane surface with oxidative reactivity, provide a potential oxidation route for fouling removal. Over the past decade, several advanced oxidation processes, including Fenton reactions (De Angelis and de Cortalezzi, 2016; Sun et al., 2018c), catalytic ozonation (Park et al., 2012; Zhu et al., 2013), peroxymonosulfate activation (Bao et al., 2019; Wang et al., 2020b), have tentatively been incorporated in catalyst-tailored ceramic membranes to produce reactive oxygen species (e.g. $^\bullet OH$, $O_2^{\bullet-}$ and $SO_4^{\bullet-}$ radicals) on the membrane surface and/or within the inner pores, potentially removing fouling. De Angelis and de Cortalezzi (2016) observed that the flux recovery of iron-oxide coated ceramic membranes (fouled with humic acids) by Fenton cleaning, was much higher (97%) than those by forward flush (41%) or acidic/caustic cleaning (39–42%). Zhang et al. (2020) demonstrated that the flux of MnO_2-Co_3O_4 coated ceramic membranes was recovered by 97% with peroxymonosulfate-based oxidative cleaning, while it was only restored by 70–75% using backwash or acidic/caustic cleaning. However, present knowledge about catalytic ceramic membranes, regarding their fouling characteristics and oxidative cleaning effectiveness, is mainly limited to ceramic microfiltration and ultrafiltration processes, and not to ceramic nanofiltration.

Fouling of ceramic NF by soluble and colloidal biopolymers (e.g. polysaccharide) has been considered a multifaceted process, involving adsorption, pore constriction/blockage and cake development (Mustafa et al., 2014; Zhao et al., 2018). Fujioka et al. (2018) reported that the increase in transmembrane pressure (TMP) during ceramic NF of a wastewater was reduced by about 60% via ozonated water flush, but it remained unclear how the ozonation cleaning corresponded to, or was influenced by, different fouling pathways. As an indication of multiple fouling pathways, a two-stage flux decrease pattern, comprising a rapid decline in permeation flux at the early stage of filtration and a gradual flux decline afterwards, has previously been recognized for ceramic NF membranes, during constant pressure experiments, presumably resulting from strong foulant-membrane interactions (e.g. polar and electrostatic interactions) or a high starting flux (Mustafa et al., 2016; Zhao et al., 2018). Besides, a recent study presented a steep flux decline (30–40%), occurring upon switching the feed from pure water to an alginate solution during ceramic NF (Lin et al., 2021). Nonetheless, the exact reason for the rapid flux decline and how it affects cleaning performance is still unanswered. Kramer et al. (2020) observed a flux recovery of 75% by Fenton cleaning over an

iron-oxide coated ceramic NF membrane fouled by alginate, however, the sharp flux decline relative to the initial clean water flux was not taken into account.

Therefore, the objective of this chapter was to study the fouling characteristics of a catalytic ceramic NF membrane and the relation between various types of fouling and the efficacy of Fenton cleaning. Iron oxychloride (FeOCl), a reactive heterogeneous Fenton catalyst, was pre-coated on top of a commercial ceramic (TiO_2) NF membrane, for catalysing the *in-situ* decomposition of hydrogen peroxide (H_2O_2) into hydroxyl radicals (${}^\bullet OH$) on the membrane surface (Sun et al., 2018a; Sun et al., 2018b; Yang et al., 2013). Sodium alginate, in the presence of calcium ions, was employed as a typical surrogate for polysaccharide foulants, identified as the major fouling substance of membranes in domestic wastewater (Guo et al., 2020; Meng et al., 2022; Wang et al., 2021). Flux restoration percentages, determined in terms of both pure water flux and foulant solution flux, were used as an indication for oxidative cleaning efficacy and evaluated in relation to the various fouling types of the FeOCl pre-coated membrane in a constant-pressure filtration mode.

4.2 Materials and methods

4.2.1 Reagents and materials

Ferric chloride hexahydrate ($FeCl_3 \cdot 6H_2O$, ≥99.0%) and sodium alginate (≥99.0%) were purchased from Sigma-Aldrich. Calcium chloride dihydrate ($CaCl_2 \cdot 2H_2O$, ≥99.0%) and H_2O_2 (30%) were purchased from Merck KGaA (Germany). All chemicals were used as received. Ceramic NF membranes (Inopor GmbH, Germany) with a mean pore size of 0.9 nm (Inopor data) were used in this chapter. The membranes have a tubular single-channel configuration (outer diameter: 10 mm, inner diameter: 7 mm, length: 100 mm) with active layers made of TiO_2. Both ends of the tubular membranes were sealed with silica glass. The membranes were operated in an inside-out filtration mode.

4.2.2 Preparation of FeOCl catalyst and FeOCl pre-coated membrane

The FeOCl catalyst was synthesized through a thermal annealing method (Sun et al., 2018a). $FeCl_3 \cdot 6H_2O$ powder (10.0 g), as the precursor, was heated in a sealed crucible at a heating rate of 20 °C min^{-1} to 220 °C and remained for 1 h in a muffle furnace. The reaction equation is presented in Equation (4.1).

$$FeCl_3 \cdot H_2O \rightarrow FeOCl + 2HCl + 5H_2O \qquad (4.1)$$

The FeOCl suspension was prepared by dispersing 4.0 g of the as-prepared FeOCl catalysts in 1.0 L of demineralised water with 10-min sonication. A cross-flow pre-filtration, with the FeOCl suspension, spiked into the main feed stream (demineralized water), was then conducted to pre-coat a catalyst layer on the membrane surface (Figure S4.1, Supplementary Data). Herein, a laminar crossflow of 0.2 m s^{-1} (Reynolds number (*Re*) = 1510) and a high TMP (20.0 bar) were adopted to boost the formation and compaction of a uniform catalyst layer on the membrane surface.

4.2.3 Single- and multi-cycle fouling/cleaning experiments

Filtration experiments of pristine and FeOCl pre-coated membranes were performed in a constant-pressure mode with a bench-scale cross-flow filtration apparatus (OSMO Inspector 2, Convergence Industry, the Netherlands). A high organic loading (0.8 g L^{-1}) of sodium alginate was adopted to develop accelerated fouling during a period of only 2 h, which simulates a five-day fouling period, obtained during pilot tests with ceramic NF of sewage (Kramer et al., 2015). NaCl (5.0 mM) and CaCl$_2$ (3.0 mM) were added as background salts to stimulate the formation of colloidal foulants, while NaHCO$_3$ (1.0 mM) was added as a buffer to maintain the solution at pH = 7.0. The filtration/cleaning protocol of the membranes comprised four sequential phases (Figure 4.1a): (i) initial pure water flux (J_{w1}), (ii) flux decline (from J_{f1} to J_{f2}) during filtration with alginate solutions, (iii) membrane cleaning, and (iv) pure water flux (J_{w2}). The filtration and cleaning experiments were performed in duplicate. The concentrate was recirculated into the feed flow, while the permeate was consecutively collected for measuring the permeate flux over time, using a scale and a data acquisition system. The temperature-corrected permeance was calculated according to Text S4.1 (Supplementary Data). Fouling characteristics and cleaning efficacy of the membranes were evaluated by calculating the initial fouling ratio (R_i), cake fouling ratio (R_c) and flux recovery ratio (F_r) with Equations (4.2)–(4.4), respectively.

$$R_i = \frac{J_{w1} - J_{f1}}{J_{w1}} \times 100\% \tag{4.2}$$

$$R_c = \frac{J_{f1} - J_{f2}}{J_{w1}} \times 100\% \tag{4.3}$$

$$F_r = \frac{J_{w2} - J_{f2}}{J_{w1} - J_{f2}} \times 100\% \tag{4.4}$$

Single cycle fouling

In order to explore the impact of different fouling characteristics of the membranes on the efficacy of Fenton cleaning, varying hydrodynamic conditions, i.e. TMP = 2.0, 3.0 and 4.0 bar and cross-flow velocity (CFV) = 0.3 and 0.9 m s^{-1} were used in the single-cycle fouling experiments (1 h). Membrane cleaning experiments were executed by H_2O_2 circulation (30.0 or 60.0 mM, pH = 3.3) at a laminar crossflow (CFV = 0.2 m s^{-1}, *Re* = 1116) for 1 h (Figure S4.1, Supplementary Data) to reduce hydraulic scouring over the pre-coat layer on the membrane. To compare with the efficacy of Fenton cleaning of the pre-coated membrane, a forward flush was conducted on the pristine membrane by circulating demineralized water inside the membrane channel at CFV = 2.2 m s^{-1} (*Re* = 15097) for 20 min without applying a TMP. To study the membrane fouling characteristics in the presence and absence of a FeOCl pre-coat, the same pristine membrane was used, first for the fouling test without pre-coating and then for the pre-coating/fouling test. Chemical cleaning by a sodium hypochlorite solution (0.2%) was performed between the two tests until reaching the initial permeance of the pristine membrane. To identify the cake fouling, variation of the filtered volume was described by the classical cake filtration law as presented in Equation (4.5) (Ognier et al., 2002; Yao et al., 2018):

$$\frac{t}{V} = \frac{K_c}{2} V + \frac{1}{J_0} \tag{4.5}$$

where K_c (s m^{-2}) is the cake filtration constant, V (m³) the filtered volume, J_0 the initial flux during filtration with the alginate solution, t the filtration time.

Multiple cycle fouling

The efficacy of Fenton cleaning of the FeOCl pre-coated membrane was further assessed over multiple cycles, using relatively thick and thin cake layer fouling, respectively, without renewing the pre-coat layer between the cycles to elucidate fouling/cleaning behaviour of the pre-coated membrane in repeated uses. The multicycle fouling experiments were done with a turbulent flow (Re = 6039) inside the membrane channel at CFV = 0.9 m s^{-1}. The thick cake fouling was obtained during filtration with the alginate solution for 1 h at an initial pure water flux of 47.1 L m^{-2} h^{-1}. The thick cake fouling was cleaned by means of H_2O_2 flush ($[H_2O_2]_0$ = 60.0 mM, pH = 3.3), followed by forward flush with demineralized water, over three repeated cycles. The thin cake fouling was obtained during filtration with the alginate solution for 30 min (shorter than that for the thick cake fouling) at an initial pure water flux of 39.5 L m^{-2} h^{-1}, and cleaned by H_2O_2 flush ($[H_2O_2]_0$ = 30.0 mM, pH = 3.3), over five cycles. In order to study the relation between various fouling types (i.e. adsorptive fouling and cake growth) and Fenton cleaning, an adsorption step (5 min, as described in Section 4.2.4) was incorporated in the thick cake fouling test, prior to each cycle of filtration, using the same alginate

solution. To further verify the effect of adsorptive fouling on Fenton cleaning, adsorption/cleaning was executed throughout five cycles, involving pure water filtration, adsorption with the alginate solution (30 min, the same as that for the thin cake fouling experiment) and Fenton cleaning ($[H_2O_2]_0$ = 30.0 mM, pH = 3.3) at each cycle, also without refreshing the pre-coat layer.
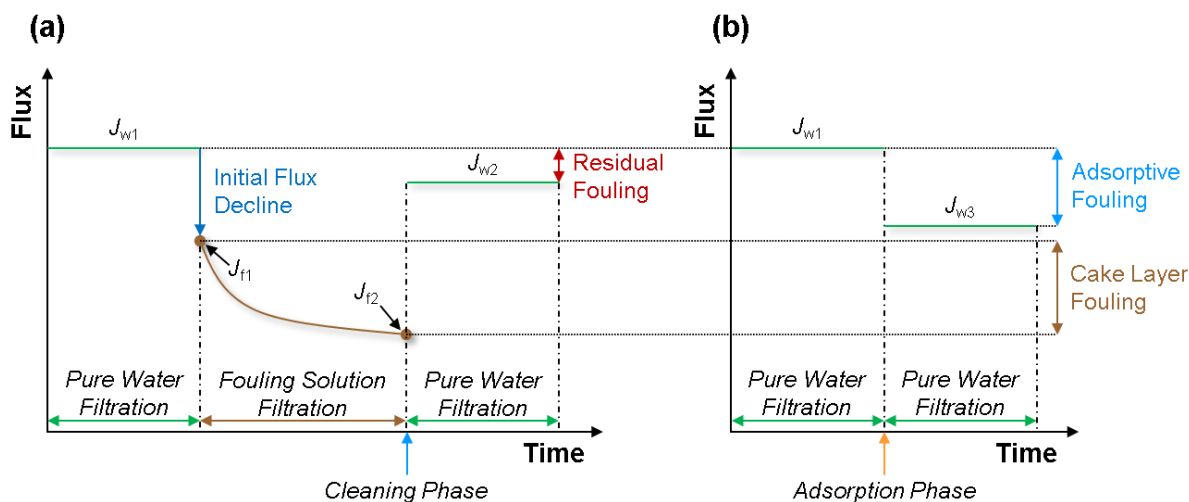
Figure 4.1 Conceptual illustration of flux evolution during (a) fouling and (b) adsorption experiments.

4.2.4 Adsorption experiments of ceramic NF membranes

Adsorption of alginate foulants onto pristine and FeOCl pre-coated membranes was conducted in the same filtration apparatus and under the same crossflow conditions as were the fouling/cleaning experiments, only without a permeate flow (TMP = 0 bar) through the membranes. The adsorption experiments were to identify adsorptive fouling of the membranes and to distinguish its role in permeance decrease from that of cake fouling. As conceptually illustrated in Figure 4.1b, the membranes were first subjected to filtration (TMP = 2.0 or 3.0 bar, CFV = 0.9 m s^{-1}) with demineralized water to determine initial pure water fluxes (denoted as J_{w1}). The initial pure water fluxes were used as a baseline to normalize the flux evolution before and after the adsorption steps. Prior to the start of adsorption, the demineralized water in the filtration setup was discharged and fully replaced with the alginate solution. Subsequently, the alginate solution was circulated within the membrane channels at CFV = 0.9 m s^{-1} for 1, 5 or 30 min, without allowing any permeate flow in the filtration system. Finally, demineralized water was filtered through the fouled membranes to measure pure water fluxes (denoted as J_{w3}) after adsorption. The adsorptive fouling ratios (R_a) were calculated, using Equation (4.6), to assess the effect of foulant adsorption on initial flux declines.

$$R_a = \frac{J_{w1} - J_{w3}}{J_{w1}} \times 100\% \tag{4.6}$$

4.2.5 Characterization and analysis

Polyethylene glycols (PEGs) (Sigma-Aldrich, Germany) of five molecular weights (200, 300, 400, 600 and 1000 Da) were used as tracer compounds to determine the real molecular weight cut-off (MWCO) of the membrane, defined as the molecular weight of a tracer molecule that is retained with an efficiency of 90% by the membrane, as earlier reported by Shang et al. (2017). The PEG samples, collected in the feed and permeate solutions, were analysed by high-performance size exclusion chromatography (Prominence, Shimadzu, Japan), equipped with a refractive index detector (RID-20A, Shimadzu, Japan) and a gel permeation column (5 mm 30 Å, PSS GmbH, Germany). The particle size distribution of Ca-alginate colloids was measured with a blue laser diffraction particle size analyser (S3500, Microtrac Retsch GmbH, Germany). The top-view and cross-sectional images of the pristine and FeOCl pre-coated membranes were taken, using a scanning electron microscope (SEM) (S-3400N, Hitachi High-Technologies, Japan) installed with energy dispersive spectroscopy.

4.3 Results and discussion

4.3.1 Characterization of membranes and foulants

A smooth and dense top surface was observed for the pristine membrane, without showing any visible defects on the membrane surface (Figure 4.2a). The curve of PEG rejection as a function of PEG molecular weight (Figure 4.2b) corresponds to a pore size of MWCO = 688 Da of the pristine membrane. Other studies have also reported larger measured MWCO values than the nominal MWCO (450 Da, Inopor data) of similar membranes (Caltran et al., 2020; Mustafa et al., 2016). Figure 4.2c displays the top surface of the FeOCl pre-coated membrane, which appeared to be much rougher than that of the pristine membrane. The FeOCl particles were present as long-strip sheets with, approximately, 4−6 μm in length, 1 μm in width and 0.2−0.3 μm in thickness, comparable to the dimensions of lab-prepared FeOCl reported elsewhere (Chen et al., 2021; Sun et al., 2018a). The porous pre-coat layer, formed by stacking of the FeOCl particles on the membrane surface, had pore sizes of 0.1−0.5 μm, as estimated from Figure 4.2c. As a result of the much larger pore sizes of the pre-coat layer than those (0.9 nm, Inopor data) of the active membrane layer, the pre-coat layer led to a minor reduction in pure water permeance of the membrane (<4%, Table S4.1, Supplementary Data). In other studies where particles (e.g. zirconium and iron oxides) were pre-coated on low-pressure membranes, however, a considerable decrease (>70%) in pure water permeance occurred

due to pore blockage, since the particle sizes and the pore sizes were similar (Kim et al., 2017; Wang et al., 2020a). As indicated by the cross-sectional SEM view and the corresponding Fe/Cl distribution on the pre-coated membrane (Figure 4.2d), the pre-coat layer, having a thickness of around 4.6 μm, was uniformly coated on the membrane surface.
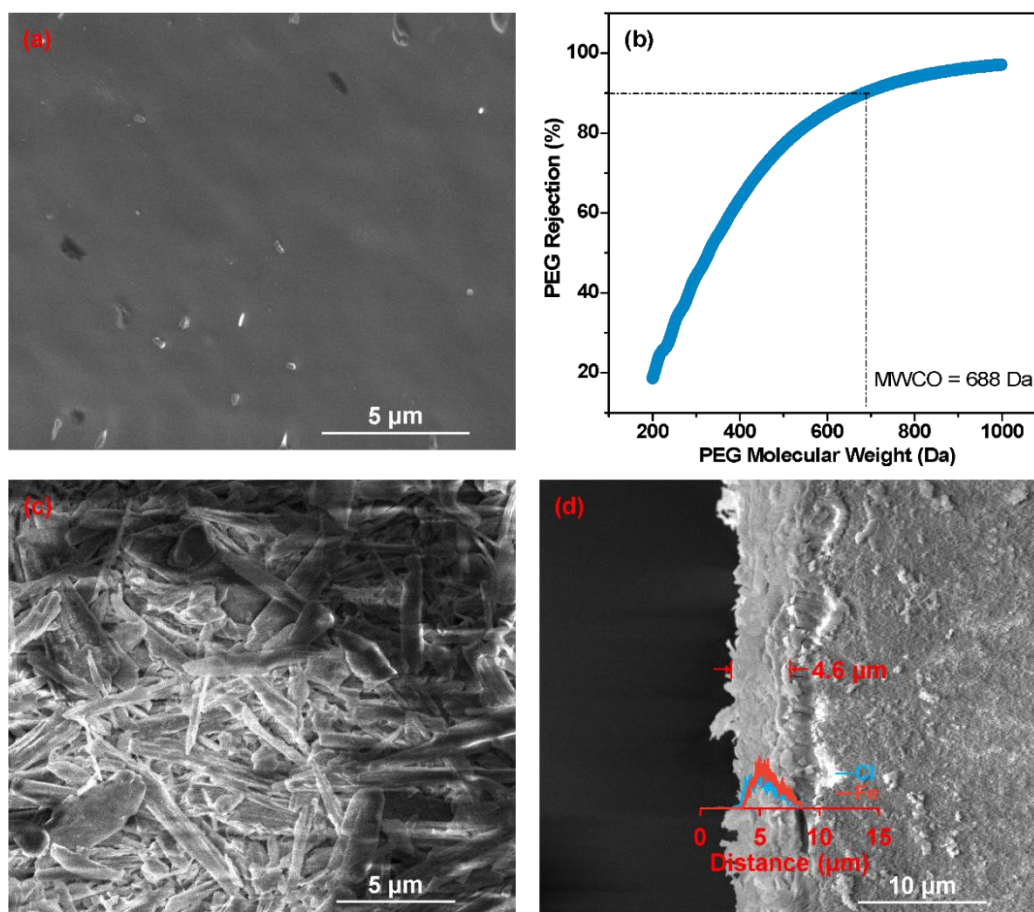
***Figure 4.2*** *(a) Top-view scanning electron microscope (SEM) image of pristine ceramic NF membrane. (b) Polyethylene glycol (PEG) rejection curve of the membrane. The dashed line shows the PEG molecular weight with a rejection rate of 90%. (c) Top-view and (d) cross-sectional SEM images with energy dispersive spectroscopy line scanning of Fe and Cl elements on the cross-section of FeOCl pre-coated membrane.*

The colloids in the alginate solution had a particle size distribution of 10–1000 μm (Figure S4.2, Supplementary Data), and were thus much larger than the pore sizes of the pre-coat layer. This implies that the Ca-alginate colloids, upon contact (or filtering) with the pre-coated membrane, would mostly deposit (or be intercepted) on the FeOCl pre-coat via steric exclusion, instead of directly contacting the active membrane layer (Yao et al., 2009). However, apart from the large-sized

alginate colloids, as suggested by Katsoufidou et al. (2007) and Kim and Dempsey (2013), free alginate molecules are also expected to be present in the solution, having a molecular weight distribution from 10 to >100 kDa, which means that the alginate molecules could penetrate the pre-coat layer and be adsorbed on/in the active layer of the membrane.

## 4.3.2 Characteristics of flux decreases during alginate fouling
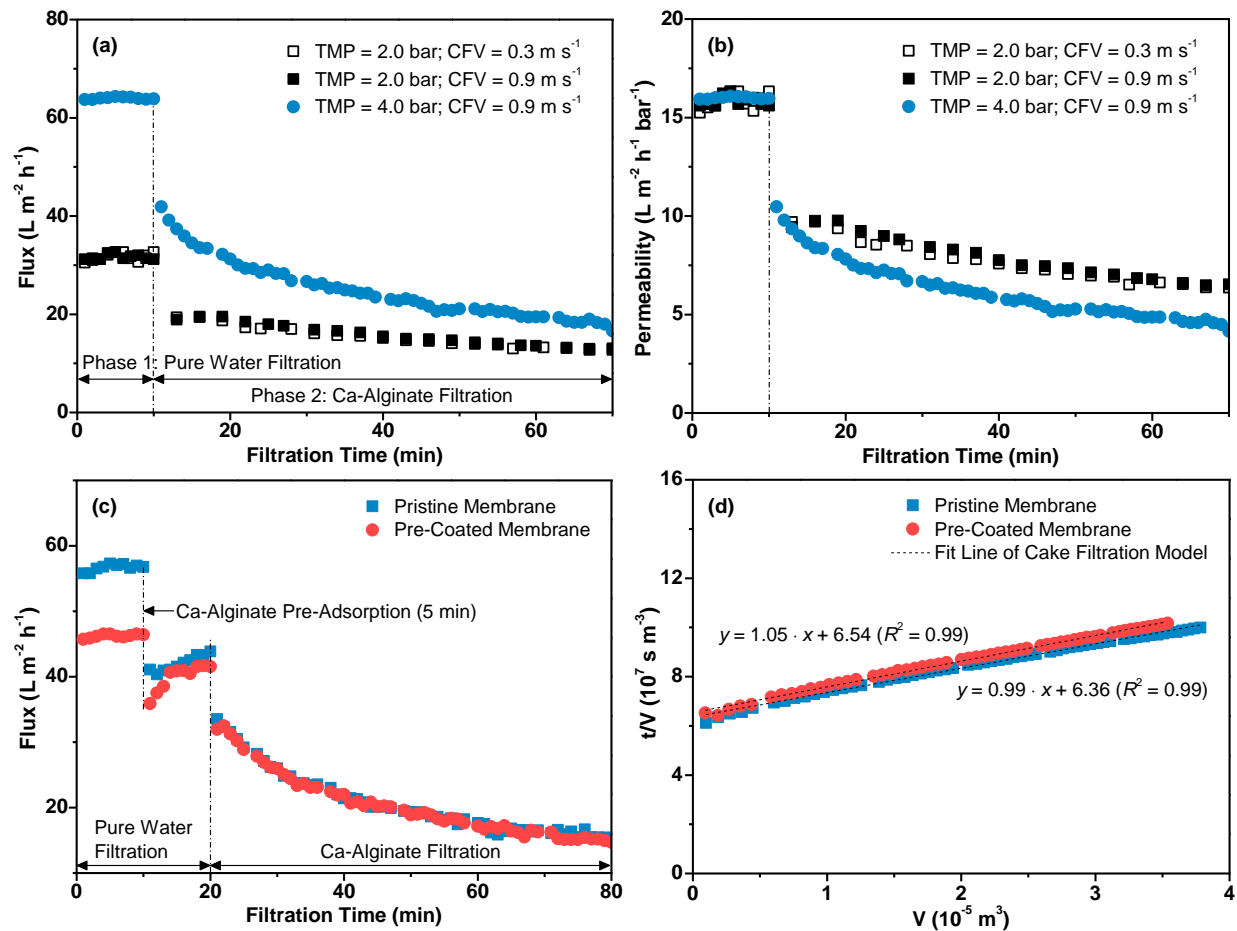
Figure 4.3 *Variations in (a) water flux and (b) membrane permeance during filtration under different transmembrane pressures (TMPs) and cross-flow velocities (CFVs) with pristine ceramic NF membrane. (c) Flux evolution and (d) t/V vs. V variation profiles of pristine and FeOCl pre-coated membranes operated at TMP = 3.0 bar and CFV = 0.9 m s⁻¹. The straight lines correspond to the linear fitting of t/V vs. V profiles to the cake filtration model.*

The pristine membrane first underwent an abrupt decline in the initial pure water flux, whereafter a gradual flux decrease followed (Figure 4.3a), during filtration of the alginate solution. The time-

dependent flux decreases during filtration with the alginate solution were in agreement with the linear relation of the cake filtration model (Section 4.2.3) with a correlation coefficient of R^2 = 0.95–0.99 (Figure S4.3, Supplementary Data), thereby corresponding to the progressive build-up of a cake layer on the membrane (Ognier et al., 2002; Yao et al., 2018). Filtration at a high initial flux (64.0 L m^{-2} h^{-1}) developed a larger flux decline (R_c = 39.5%) with the cake growth, than that (R_c = 20.4%) at a lower initial flux (31.6 L m^{-2} h^{-1}), probably driven by the high permeate drag forces (Miller et al., 2014; Seidel and Elimelech, 2002). The cake fouling at the low initial flux was independent of the CFV, where 0.3 m s^{-1} corresponded to a laminar flow (Re = 2013.0) and 0.9 m s^{-1} to a turbulent flow (Re = 6038.9), respectively. It is thus suggested that the alginate cake layer had a high adhesion affinity towards the pristine membrane and was thus able to resist the crossflow shear forces, presumably resulting from the formation of aggregates with low back diffusion (van den Brink et al., 2009). As depicted in Figure 4.3b, the initial pure water permeabilities at both TMP = 2.0 and 4.0 bar were similar, while, during filtration with the alginate solution, the permeance decreased to a lower level (4.2 L m^{-2} h^{-1} bar^{-1}) at TMP = 4.0 bar compared to TMP = 2.0 bar (6.5 L m^{-2} h^{-1} bar^{-1}). This is likely a result of the formation of a thicker, more compact cake layer at higher fluxes (Jiang et al., 2022). This observation is not in line with the findings of Akamatsu et al. (2020), who demonstrated an unchanged filtration resistance with an increase in permeate flux, during NF of a sole alginate solution, probably due to the lower compressibility of the long-chain alginate molecules they used, while here the coiled Ca-alginate colloids were filtered.

Figure 4.3c displays the flux profiles of the pristine and FeOCl pre-coated membranes operated under initial fluxes of 56.7 and 46.2 L m^{-2} h^{-1}, respectively. The same membrane was used for these comparative experiments (see Section 4.2.3). The pristine and pre-coated membranes developed a sharp decline in the individual pure water flux, after pre-adsorption (5 min), and a progressive flux decrease, during filtration with the alginate solution. Moreover, as illustrated in Figure 4.3d, good linear fits (y = 0.99 x + 6.36 and y = 1.05 x + 6.54, R^2 = 0.99) to the cake filtration model were observed for the progressive flux decreases of both membranes. The results thus indicate that the two stages of the flux reductions were attributed to initial rapid adsorption of the foulants and subsequent gradual cake growth on the membranes, respectively. In addition, the fouling characteristics during cake build-up were independent of the presence of the pre-coat layer, as suggested by the nearly same flux decline curves of the two membranes (Figure 4.3c), which is in agreement with previous studies regarding other pre-coat types (e.g. floc/particulate FeCl$_3$ and Fe$_3$O$_4$ layers) (Kramer et al., 2020; Lin et al., 2021).

4.3.3 Adsorptive fouling as a mechanism for initial rapid flux decline
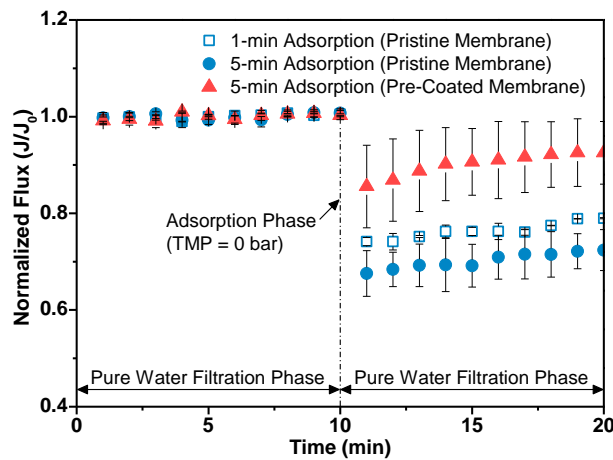
Figure 4.4 *Experimental determination of permeance declines due to foulant adsorption onto pristine and FeOCl pre-coated membranes at pH = 7.0.*

For evaluating the rate of rapid fouling at the start of a filtration cycle, the decline of initial pure water fluxes, caused by membrane fouling in the absence of a permeate flow, was separated from the subsequent gradual flux decrease due to cake build-up. Short contact periods, i.e. 1 and 5 min, were adopted in the adsorption tests, to simulate the early stage of fouling resulting from foulant adsorption. Figure 4.4 depicts the variations of the pure water fluxes over the pristine and FeOCl pre-coated membranes, upon exposure to the alginate solution. The pristine membrane, after 5 min contact with the alginate solution without a permeate flow, displayed a pure water flux reduction of 32.5%, while adsorptive fouling was considered to be the only cause for the flux decline, since no cake layer was able to build up in the absence of a permeate flow (Akamatsu et al., 2020; Miller et al., 2014). The adsorption test with a shorter contact time of 1 min caused a flux decline of 25.9%, which suggests that adsorption of the foulants onto the pristine membrane rapidly took place. However, the FeOCl pre-coated membrane, upon exposure to the alginate solution, within the same time frame (5 min), underwent a smaller decline (14.5%) in the pure water flux compared to the pristine membrane. This is presumably due to the adsorption of foulants on the pre-coat layer without adding to the flux decline, as a result of the large pore sizes of the pre-coat layer. Similar findings have previously been reported for other types of pre-coat layers (e.g. iron oxide and aluminium oxide layers) on ceramic membranes, acting as a pre-filtration media for organic molecules and colloids prior to reaching the active layers of the membranes (Malczewska et al., 2015; Yao et al., 2009).

4.3.4 Dependence of cleaning efficacy on fouling characteristics during a single fouling cycle
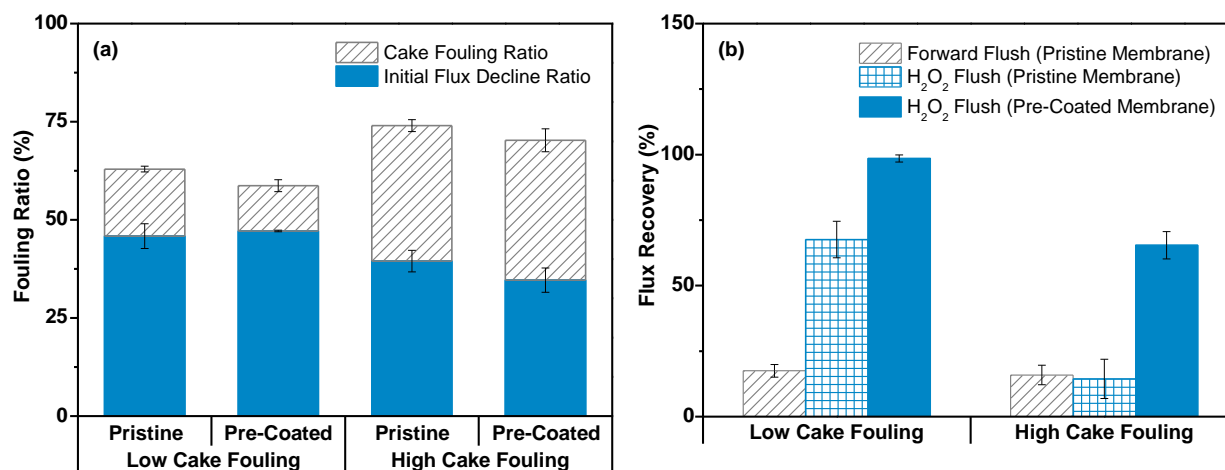
Figure 4.5 *(a) Initial flux decline ratios and cake fouling ratios during thin cake fouling (J_0 = 29.3–40.5 L m^{-2} h^{-1}, fouling duration = 30 min) and during thick cake fouling (J_0 = 46.3–57.2 L m^{-2} h^{-1}, fouling duration = 60 min), respectively, using pristine and FeOCl pre-coated membranes. (b) Cleaning efficiencies of forward flush with demineralized water or H_2O_2 solutions (pH = 3.3) during a single fouling cycle of the membranes.*

As suggested in several studies, a fouling layer on catalytic membranes is likely to behave as a barrier for the diffusion of H_2O_2 onto the active sites, thereby hampering the Fenton oxidation of organic foulants (De Angelis and de Cortalezzi, 2016; Sun et al., 2018c). Therefore, in the present section of this chapter, the efficacy of Fenton cleaning for the FeOCl pre-coated membrane, was assessed for both thin and thick cake fouling, in comparison with using demineralized water forward flush and sole H_2O_2 cleaning of the pristine membrane (Figure 4.5a and b). The thin cake fouling of the membranes was obtained by starting fouling at a comparatively low initial flux (29.3–40.5 L m^{-2} h^{-1}) for 30 min, while for the thick cake fouling an initial flux of 46.3–57.2 L m^{-2} h^{-1} for 60 min, corresponding to cake fouling ratios of R_c = 11.5–17.0% and 34.5–35.6%, respectively (Figure 4.5a). As depicted in Figure 4.5b, forward flush of the pristine membrane slightly recovered the pure water flux, by 17.5% and 15.9%, at the thin and thick cake fouling conditions, respectively, indicating that the majority of the alginate foulants were strongly attached to the membrane surface and could resist hydraulic scouring (Kramer et al., 2020; Zhao et al., 2018). H_2O_2 flush ([H_2O_2]$_0$ = 30.0 mM) of the pristine membrane seemed effective in pure water flux restoration (F_r = 67.6%) for the thin cake fouling, but less effective (F_r = 14.4%) for the thick cake fouling, even at a high dosage of H_2O_2 ([H_2O_2]$_0$

= 60.0 mM). H_2O_2 cleaning in the presence of a FeOCl pre-coat on the membrane, increased the flux recovery to 98.5% for the thin cake fouling, suggesting effective Fenton oxidation during crossflow flush with a H_2O_2 solution. Fenton reactions as indicated in Equation (4.6) and (4.7), were supposed to take place on/within the FeOCl pre-coat layer, accompanied with the generation of $^\bullet OH$ radicals in the presence of H_2O_2 at the catalytic sites of the FeOCl particles (Sun et al., 2018b; Yang et al., 2013; Zhang et al., 2021).

$$FeOCl + H_2O_2 \leftrightarrow Fe_{1-n}^{III}Fe_n^{II} + {}^\bullet OOH + H^+ \tag{4.6}$$

$$\equiv Fe^{II} + H_2O_2 \leftrightarrow \equiv Fe^{III} + {}^\bullet OH + OH^- \tag{4.7}$$

Hence, the adsorptive fouling and the deposited cake layer on/in the FeOCl pre-coat, tended to be degraded by the generated $^\bullet OH$ radicals. However, a lower flux recovery of 65.4% was obtained after Fenton cleaning ($[H_2O_2]_0$ = 60 mM) of the thick cake fouling. The dependence of the Fenton cleaning efficacy on the fouling characteristics, could be ascribed to increased deposition and compacted conformation of cake layers as a result of high-flux convection (as described in Section 4.3.2), which could slow down the diffusion of H_2O_2 through the cake layer into the FeOCl pre-coat (Ricceri et al., 2021; Sioutopoulos and Karabelas, 2015; Soesanto et al., 2019).

4.3.5 Fenton cleaning in relation to fouling types over multiple cycles

Cleaning of cake layer dominated fouling
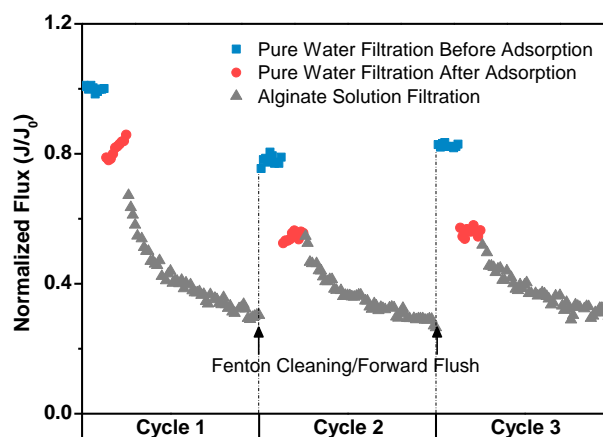
Figure 4.6 *Multiple cycles of pure water filtration (J_0 = 47.1 L m^{-2} h^{-1}) and combined pre-adsorption/filtration with an alginate solution using an FeOCl pre-coated membrane, with periodical Fenton cleaning ($[H_2O_2]_0$ = 60.0 mM, pH = 3.3) followed by demineralized water forward flush.*

To study the efficacy of Fenton cleaning in relation to the type of fouling on the FeOCl pre-coated membrane, combined pre-adsorption/cake filtration/cleaning steps were sequentially executed over three cycles without refreshing the pre-coat layer. The experiment was performed using an initial flux of 47.1 L m^{-2} h^{-1}, corresponding to the relatively thick cake layer fouling as discussed in Section 4.3.4. As presented in Figure 4.6, a sharp flux decline, due to initial fast adsorption of the foulants, and a progressive flux decrease, resulting from subsequent cake build-up, were separately observed at each cycle of adsorption and filtration with the alginate solution. Upon combined Fenton cleaning/forward flush after *Cycle 1* and *2*, the initial pure water fluxes at *Cycle 2* and *3* were recovered to $J//J_0$ = 78.0% and 82.5%, respectively, which represent the cleaning efficacy of the total fouling (i.e. adsorptive and cake fouling) at each cycle. In the meantime, however, the average fluxes during cake filtration at *Cycle 2* and *3* were restored to a larger extent, i.e. by 92.1% and 92.3% (relative to the average cake filtration flux at *Cycle 1*), respectively, corresponding to the cleaning efficacy of the cake layer fouling. The results indicate that the cake layer fouling of the pre-coated membrane was much better cleaned than was the adsorptive fouling. Nonetheless, the removal of the adsorptive fouling seemed to be less important than that of the cake layer fouling, since new adsorptive fouling occurred rapidly on/in the cleaned membrane upon contact with the alginate solution at *Cycle 2* and *3*, as indicated by the abrupt flux declines of 25.5% and 25.3%, respectively. Similar observations have also been reported for other type of oxidative cleaning, such as chlorine cleaning (Kuzmenko et al., 2005).

Cleaning of adsorption dominated fouling
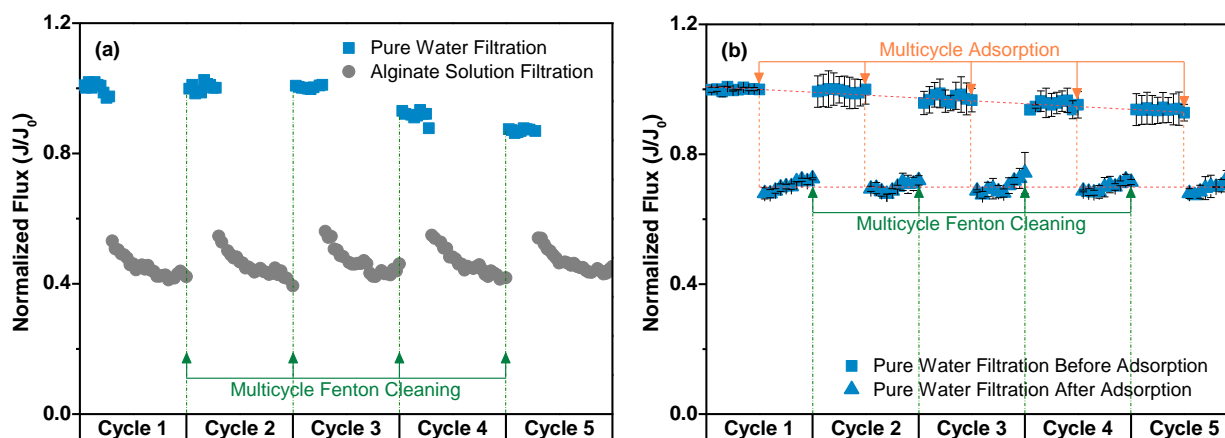
Figure 4.7 *Multiple-cycle (a) filtration (J_0 = 39.5 L m^{-2} h^{-1}) and (b) adsorption with alginate solutions and periodical Fenton cleaning ([H_2O_2]$_0$ = 30.0 mM, pH = 3.3) using an FeOCl pre-coated membrane.*

To further explore the efficacy of Fenton cleaning on adsorptive fouling, interference of cake fouling accumulation over multiple cycles should be excluded. For this purpose, a multicycle filtration/cleaning experiment was done with adsorption-dominated fouling (i.e. thin cake layer fouling, as described in Section 4.3.4), obtained by filtration at an initial flux of 39.5 L m^{-2} h^{-1} for a short period (30 min) at each cycle, in parallel to a multicycle adsorption/cleaning experiment (see Section 4.2.3). As depicted in Figure 4.7a, the flux decrease at each cycle was predominantly attributed to initial flux declines (R_i = 43.9–46.8%) during filtration with the alginate solution, which confirms the dominance of adsorptive fouling. The pure water fluxes at *Cycle 2* and *3* were restored to the same level as the initial baseline flux, i.e. $J//J_0$ = 1, while the pure water fluxes at *Cycle 4* and *5* dropped to $J//J_0$ = 0.91 and 0.87, respectively. Meanwhile, the fluxes during cake filtration over the five cycles, remained similar, decreasing from $J//J_0$ = 0.55 to 0.42, approximately. The results suggest that the cake layer formed at each cycle was entirely removed by Fenton cleaning, whilst some adsorptive fouling progressively accumulated on/within the active layer of the membrane at the later cycles. However, the incomplete removal of the adsorptive fouling after Fenton cleaning, did not influence the fluxes during cake filtration and the total amount of fouling.

The multicycle adsorption/cleaning experiment was performed under the same conditions as the multicycle filtration/cleaning test, without allowing a permeate flow during adsorption. As shown in Figure 4.7b, the pure water fluxes after periodical Fenton cleaning followed a descending trend from $J//J_0$ = 1 to 0.93, indicating that a proportion of the adsorbed foulants were not reversed by the cleaning steps and tended to accumulate on/in the active layer of the membrane. Nonetheless, the pure water fluxes after multicycle adsorption remained stable, in the range of $J//J_0$ = 0.68–0.72, from *Cycle 1* to *5*, implying that the total adsorptive fouling on/within the active layer of the membrane was independent of the progressive accumulation of the residual foulants. It is likely that the limited number of adsorption sites on/in the active layer of the membrane corresponded to the constant amount of the adsorptive fouling during the multiple adsorption/cleaning cycles (Li et al., 2018). The results confirm the aforementioned minimal impact of incomplete removal of adsorptive fouling on the flux evolution during cake filtration over pre-coated ceramic NF membranes, using Fenton cleaning.

4.4 Conclusions

The efficacy of Fenton cleaning of an FeOCl pre-coated ceramic NF membrane was assessed in relation to different fouling types. For this purpose, membrane adsorption and constant-pressure filtration experiments with a model biopolymer solution (i.e. alginate in the presence of calcium ions)

were performed in parallel, to differentiate between permeance decreases during adsorptive fouling and cake build-up.

The main conclusions of this chapter were:

(1) The flux evolution could be divided into an initial sharp flux decline, due to fast adsorption of the foulants, and a subsequent gradual flux decline, resulting from progressive cake growth on the membrane.

(2) During multiple adsorption (without a permeate flux)/cake build-up (at a relatively high flux)/Fenton cleaning cycles, Fenton cleaning was mainly effective for the cake layer fouling compared to the adsorptive fouling.

(3) The total permeate production during ceramic NF was not influenced by the remaining adsorptive fouling (after cleaning), since the adsorptive fouling always only occurs at the beginning of each cycle. As such, the removal of the adsorptive fouling was of minor importance for the overall performance of the coated ceramic NF membrane using Fenton cleaning.

Supplementary data

### Text S4.1 Calculation of temperature-calibrated permeance of membranes

The temperature-calibrated permeance of membranes was calculated with Equation (S4.1):

$$L_{20°C} = \frac{J \cdot e^{-0.0239\cdot(T-20)}}{\Delta P} \tag{S4.1}$$

where $L_{20°C}$ (L m^{-2} h^{-1} bar^{-1}) is the temperature-calibrated permeance at 20 °C, J (L m^{-2} h^{-1}) is the measured water flux, T (°C) is the temperature of water, and ΔP (bar) is the measured transmembrane pressure.

Table S4.1 Permeance loss of ceramic membrane during FeOCl pre-coating
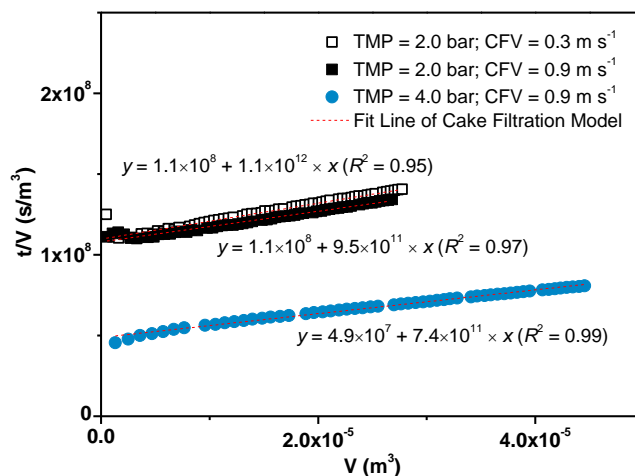
FeOCl dosage (mg L^{-1})	Initial permeance (L m^{-2} h^{-1} bar^{-1})	Transmembrane pressure (bar)	Permeance loss (%)
23.1	12.9±0.7	17.1±0.9	3.4±1.0
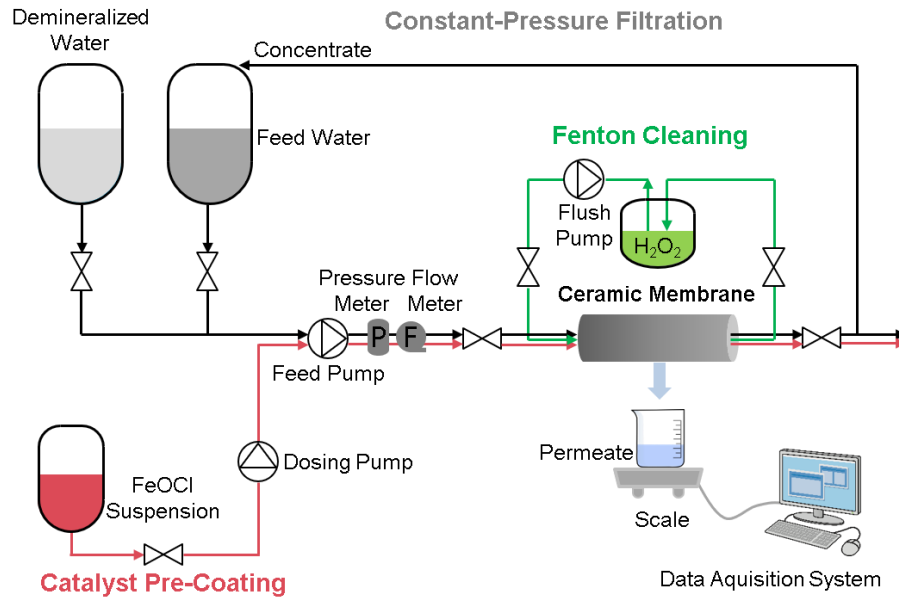
Figure S4.1 *Integrative system of catalyst pre-coating, constant-pressure filtration and Fenton cleaning.*
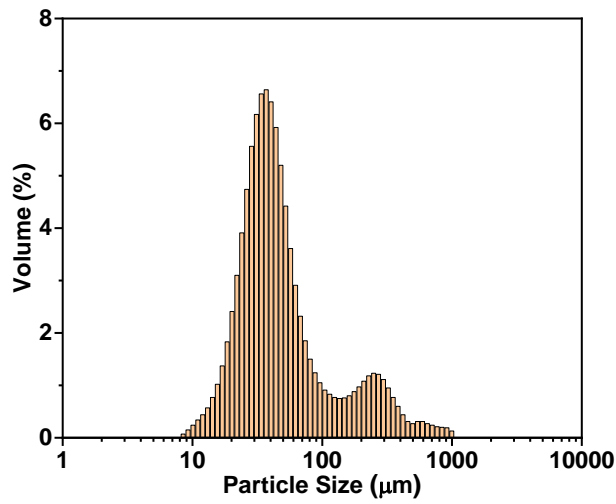
Figure S4.2 *Particle size distribution of alginate in the presence of calcium.*

Figure S4.3 t/V vs. V profiles of pristine ceramic NF membrane operated at TMP = 2.0 or 4.0 bar and CFV = 0.3 or 0.9 m s⁻¹. The straight lines correspond to the linear fitting of t/V vs. V profiles to the cake filtration model.

References

Akamatsu, K., Kagami, Y., Nakao, S.-i., 2020. Effect of BSA and sodium alginate adsorption on decline of filtrate flux through polyethylene microfiltration membranes. Journal of Membrane Science 594, 117469.

Bao, Y., Lee, W.J., Lim, T.-T., Wang, R., Hu, X., 2019. Pore-functionalized ceramic membrane with isotropically impregnated cobalt oxide for sulfamethoxazole degradation and membrane fouling elimination: Synergistic effect between catalytic oxidation and membrane separation. Applied Catalysis B: Environmental 254, 37-46.

Caltran, I., Rietveld, L.C., Shorney-Darby, H.L., Heijman, S.G.J., 2020. Separating NOM from salts in ion exchange brine with ceramic nanofiltration. Water Research 179, 115894.

Chen, Y., Miller, C.J., Collins, R.N., Waite, T.D., 2021. Key considerations when assessing novel Fenton catalysts: Iron oxychloride (FeOCl) as a case study. Environmental Science & Technology 55(19), 13317-13325.

De Angelis, L., de Cortalezzi, M.M.F., 2016. Improved membrane flux recovery by Fenton-type reactions. Journal of Membrane Science 500, 255-264.

Fujioka, T., Hoang, A.T., Okuda, T., Takeuchi, H., Tanaka, H., Nghiem, L.D., 2018. Water reclamation using a ceramic nanofiltration membrane and surface flushing with ozonated water. International Journal of Environmental Research and Public Health 15(4), 799.

Guo, Y., Li, T.-y., Xiao, K., Wang, X.-m., Xie, Y.F., 2020. Key foulants and their interactive effect in organic fouling of nanofiltration membranes. Journal of Membrane Science 610, 118252.

Jiang, S., Xiao, S., Chu, H., Sun, J., Yu, Z., Zhang, W., Chen, Y., Zhou, X., Zhang, Y., 2022. Performance enhancement and fouling alleviation by controlling transmembrane pressure in a vibration membrane system for algae separation. Journal of Membrane Science 647, 120252.

Katsoufidou, K., Yiantsios, S.G., Karabelas, A.J., 2007. Experimental study of ultrafiltration membrane fouling by sodium alginate and flux recovery by backwashing. Journal of Membrane Science 300(1), 137-146.

Kim, B.-C., Nam, J.-W., Kang, K.-H., 2017. Dynamic membrane filtration using powdered iron oxide for SWRO pre-treatment during red tide event. Journal of Membrane Science 524, 604-611.

Kim, H.-C., Dempsey, B.A., 2013. Membrane fouling due to alginate, SMP, EfOM, humic acid, and NOM. Journal of Membrane Science 428, 190-197.

Kramer, F.C., Shang, R., Heijman, S.G.J., Scherrenberg, S.M., van Lier, J.B., Rietveld, L.C., 2015. Direct water reclamation from sewage using ceramic tight ultra- and nanofiltration. Separation and Purification Technology 147, 329-336.

Kramer, F.C., Shang, R., Rietveld, L.C., Heijman, S.J.G., 2020. Fouling control in ceramic nanofiltration membranes during municipal sewage treatment. Separation and Purification Technology 237, 116373.

Kramer, F.C., Shang, R., Scherrenberg, S.M., Rietveld, L.C., Heijman, S.J.G., 2019. Quantifying defects in ceramic tight ultra- and nanofiltration membranes and investigating their robustness. Separation and Purification Technology 219, 159-168.

Kuzmenko, D., Arkhangelsky, E., Belfer, S., Freger, V., Gitis, V., 2005. Chemical cleaning of UF membranes fouled by BSA. Desalination 179(1), 323-333.

Li, N., Tian, Y., Zhao, J., Zhang, J., Kong, L., Zhang, J., Zuo, W., 2018. Static adsorption of protein-polysaccharide hybrids on hydrophilic modified membranes based on atomic layer deposition: Anti-fouling performance and mechanism insight. Journal of Membrane Science 548, 470-480.

Lin, B., Heijman, S.G.J., Shang, R., Rietveld, L.C., 2021. Integration of oxalic acid chelation and Fenton process for synergistic relaxation-oxidation of persistent gel-like fouling of ceramic nanofiltration membranes. Journal of Membrane Science 636, 119553.

Malczewska, B., Liu, J., Benjamin, M.M., 2015. Virtual elimination of MF and UF fouling by adsorptive pre-coat filtration. Journal of Membrane Science 479, 159-164.

Meng, S., Wang, R., Meng, X., Wang, Y., Fan, W., Liang, D., Zhang, M., Liao, Y., Tang, C., 2022. Reaction heterogeneity in the bridging effect of divalent cations on polysaccharide fouling. Journal of Membrane Science 641, 119933.

Miller, D.J., Kasemset, S., Paul, D.R., Freeman, B.D., 2014. Comparison of membrane fouling at constant flux and constant transmembrane pressure conditions. Journal of Membrane Science 454, 505-515.

Mustafa, G., Wyns, K., Buekenhoudt, A., Meynen, V., 2016. Antifouling grafting of ceramic membranes validated in a variety of challenging wastewaters. Water Research 104, 242-253.

Mustafa, G., Wyns, K., Vandezande, P., Buekenhoudt, A., Meynen, V., 2014. Novel grafting method efficiently decreases irreversible fouling of ceramic nanofiltration membranes. Journal of Membrane Science 470, 369-377.

Ognier, S., Wisniewski, C., Grasmick, A., 2002. Influence of macromolecule adsorption during filtration of a membrane bioreactor mixed liquor suspension. Journal of Membrane Science 209(1), 27-37.

Park, H., Kim, Y., An, B., Choi, H., 2012. Characterization of natural organic matter treated by iron oxide nanoparticle incorporated ceramic membrane-ozonation process. Water Research 46(18), 5861-5870.

Ricceri, F., Giagnorio, M., Zodrow, K.R., Tiraferri, A., 2021. Organic fouling in forward osmosis: Governing factors and a direct comparison with membrane filtration driven by hydraulic pressure. Journal of Membrane Science 619, 118759.

Seidel, A., Elimelech, M., 2002. Coupling between chemical and physical interactions in natural organic matter (NOM) fouling of nanofiltration membranes: Implications for fouling control. Journal of Membrane Science 203(1), 245-255.

Shang, R., Goulas, A., Tang, C.Y., de Frias Serra, X., Rietveld, L.C., Heijman, S.G.J., 2017. Atmospheric pressure atomic layer deposition for tight ceramic nanofiltration membranes: Synthesis and application in water purification. Journal of Membrane Science 528, 163-170.

Sioutopoulos, D.C., Karabelas, A.J., 2015. The effect of permeation flux on the specific resistance of polysaccharide fouling layers developing during dead-end ultrafiltration. Journal of Membrane Science 473, 292-301.

Soesanto, J.F., Hwang, K.-J., Cheng, C.-W., Tsai, H.-Y., Huang, A., Chen, C.-H., Cheng, T.-W., Tung, K.-L., 2019. Fenton oxidation-based cleaning technology for powdered activated carbon-precoated dynamic membranes used in microfiltration seawater pretreatment systems. Journal of Membrane Science 591, 117298.

Sun, M., Chu, C., Geng, F., Lu, X., Qu, J., Crittenden, J., Elimelech, M., Kim, J.-H., 2018a. Reinventing Fenton chemistry: Iron oxychloride nanosheet for pH-insensitive H_2O_2 activation. Environmental Science & Technology Letters 5(3), 186-191.

Sun, M., Zucker, I., Davenport, D.M., Zhou, X., Qu, J., Elimelech, M., 2018b. Reactive, self-cleaning ultrafiltration membrane functionalized with iron oxychloride nanocatalysts. Environmental Science & Technology 52(15), 8674-8683.

Sun, S., Yao, H., Fu, W., Hua, L., Zhang, G., Zhang, W., 2018c. Reactive Photo-Fenton ceramic membranes: Synthesis, characterization and antifouling performance. Water Research 144, 690-698.

Van den Brink, P., Zwijnenburg, A., Smith, G., Temmink, H., van Loosdrecht, M., 2009. Effect of free calcium concentration and ionic strength on alginate fouling in cross-flow membrane filtration. Journal of Membrane Science 345(1), 207-216.

Wang, Q., Lu, T.-D., Yan, X.-Y., Zhao, L.-L., Yin, H., Xiong, X.-X., Zhou, R., Sun, S.-P., 2020a. Designing nanofiltration hollow fiber membranes based on dynamic deposition technology. Journal of Membrane Science 610, 118336.

Wang, X., Li, Y., Yu, H., Yang, F., Tang, C.Y., Quan, X., Dong, Y., 2020b. High-flux robust ceramic membranes functionally decorated with nano-catalyst for emerging micro-pollutant removal from water. Journal of Membrane Science 611, 118281.

Wang, Y., Zheng, X., Wang, Z., Shi, Z., Kong, Z., Zhong, M., Xue, J., Zhang, Y., 2021. Effects of –COOH and $–NH_2$ on adsorptive polysaccharide fouling under varying pH conditions: Contributing factors and underlying mechanisms. Journal of Membrane Science 621, 118933.

Yang, X.-J., Xu, X.-M., Xu, J., Han, Y.-F., 2013. Iron oxychloride (FeOCl): An efficient Fenton-like catalyst for producing hydroxyl radicals in degradation of organic contaminants. Journal of the American Chemical Society 135.

Yao, P., Choo, K.-H., Kim, M.-H., 2009. A hybridized photocatalysis–microfiltration system with iron oxide-coated membranes for the removal of natural organic matter in water treatment: Effects of iron oxide layers and colloids. Water Research 43(17), 4238-4248.

Yao, W., Wang, Z., Song, P., 2018. The cake layer formation in the early stage of filtration in MBR: Mechanism and model. Journal of Membrane Science 559, 75-86.

Zhang, S., Gutierrez, L., Qi, F., Croue, J.-P., 2020. $SO_4^{\bullet-}$-based catalytic ceramic UF membrane for organics removal and flux restoration. Chemical Engineering Journal 398, 125600.

Zhang, S., Hedtke, T., Zhu, Q., Sun, M., Weon, S., Zhao, Y., Stavitski, E., Elimelech, M., Kim, J.-H., 2021. Membrane-confined iron oxychloride nanocatalysts for highly efficient heterogeneous Fenton water treatment. Environmental Science & Technology 55(13), 9266-9275.

Zhao, Y.-y., Wang, X.-m., Yang, H.-w., Xie, Y.-f.F., 2018. Effects of organic fouling and cleaning on the retention of pharmaceutically active compounds by ceramic nanofiltration membranes. Journal of Membrane Science 563, 734-742.

Zhu, Y., Chen, S., Quan, X., Zhang, Y., Gao, C., Feng, Y., 2013. Hierarchical porous ceramic membrane with energetic ozonation capability for enhancing water treatment. Journal of Membrane Science 431, 197-204.

Chapter 5

IRON OXYCHLORIDE PRE-COATED CERAMIC NANOFILTRATION MEMBRANE FOR DIRECT SURFACE WATER TREATMENT: FOULING ANALYSIS AND FENTON CLEANING
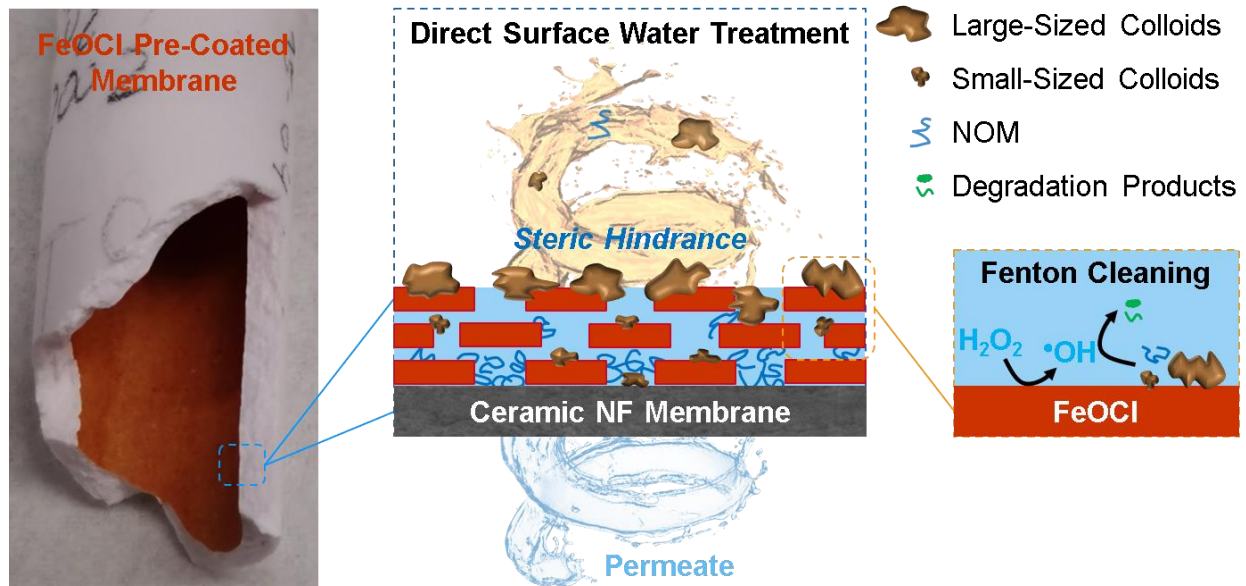
This chapter will be submitted for publication:

Abstract

Single-step nanofiltration (NF) is a promising alternative for direct surface water treatment, but is hampered by severe fouling and the lack of eco-friendly cleaning strategies. In this chapter, an innovative catalytic NF hybrid process, consisting of an iron oxychloride (FeOCl) pre-coat layer on a commercial ceramic NF membrane, was proposed to treat surface (canal) water without pre-treatment. Fenton cleaning with a hydrogen peroxide (H_2O_2) solution was used for the fouled membrane. The catalyst layer was uniformly pre-coated on top of the membrane by means of crossflow pre-filtration with a FeOCl suspension, only resulting in a minimal decrease (<4%) of the membrane permeance. Bench-scale adsorption and constant-flux filtration experiments revealed that the influence of the pre-coat layer and the feed pH (8.5 and 7.0) on the membrane fouling depended on adsorption capabilities of the membrane. An operating flux of around 46 L m^{-2} h^{-1} caused faster fouling for the pre-coated membrane than for the pristine membrane, mainly attributed to aggravated pore clogging in the pre-coat layer by a large-sized fraction (3–30 µm) of the raw water colloids. However, the pristine and pre-coated membranes fouled comparably at a flux of about 23 L m^{-2} h^{-1}, because the cross flow at the lower flux could prevent the large-sized colloid fraction from entering the pores of the pre-coat. During five filtration/cleaning cycles, the catalytic pre-coat layer effectively restored the filtration resistances of the fouled membrane by Fenton cleaning, while the separation layer of the membrane exerted high rejections (approximately 90%) of the natural organic matter, measured as dissolved organic carbon. An acceptable stability of the pre-coat layer (merely a reduction of 15.6% in the thickness), was maintained over five one-day cycles.

5.1 Introduction

Conventional drinking water treatment comprises multiple treatment units involving processes such as coagulation, sedimentation, filtration and disinfection, which results in a large footprint (Ho et al., 2012; Köhler et al., 2016). As a promising alternative, direct nanofiltration (NF) of surface water, without pre-treatment, aims to lower production costs and simplify water treatment with a single-step, chemical-free operation (Futselaar et al., 2002). However, most commercially available NF membranes, e.g. polymeric spiral-wound membranes, are susceptible to biofouling and spacer clogging by colloids in the feed water, which have to be prevented using pre-treatment steps, such as sand filtration or micro-/ultrafiltration (MF/UF) (Dreszer et al., 2014; Wibisono et al., 2015). Alternatively, polyamide thin-film composite membranes can only be operated at a very low flux (e.g. 4 L m^{-2} h^{-1}) to maintain a steady operation during direct surface water treatment (Fujioka et al., 2021).

Ceramic NF membrane is a promising substitute for its polymeric counterparts, due to its robustness and favourable selectivity towards removing natural organic matter (NOM), colloids, pathogens, organic micropollutants and multivalent ions (Árki et al., 2019; Caltran et al., 2020; Fujioka et al., 2014). In constant pressure experiments, various ceramic (e.g. SiO_2, TiO_2 and TiO_2/ZrO_2) NF membranes (Zhao et al., 2018) have shown smaller flux declines (<40%), due to NOM fouling, than polymeric ones (>70%) (Li et al., 2022; Shim et al., 2021). Caltran et al. (2020) found that NOM retention (>90%) by ceramic NF membranes was independent of pH (4–8) and ionic strength (0.1–1 M) of the feed water, while primarily depending on size exclusion. Sentana et al. (2011), however, observed an increase in NOM rejection during ceramic NF, with a reduction of the conductivity (900–4000 $\mu S\ cm^{-1}$), with an increase in the feed pH (4.5–8.3) and with an increase in the flux (9–21 $L\ m^{-2}\ h^{-1}$). Ceramic NF, as a single-step water treatment technology, has only been studied at lab or pilot scale for non-potable water recycling from wastewaters (Cabrera et al., 2022; Kramer et al., 2015).

With respect to cleaning of ceramic NF fouled by NOM in the presence of calcium ions, Zhao et al. (2018) and Mustafa et al. (2016b) reported that forward flush resulted in low flux recovery rates of 30–50%. In addition, it has been observed that hydraulic backwash can break the sealings at both ends of tubular ceramic NF membranes by a back-flow under high pressures (Kramer et al., 2020). Moreover, chemical cleaning of ceramic NF membranes with sodium hypochlorite, has proven to be effective in flux restoration, while damaging end sealing layers of the membranes (Kramer et al., 2019). As an alternative, a catalyst-functionalized ceramic NF hybrid process could enable the membrane to be cleaned through on-site advanced oxidation processes. Studies about ceramic membrane-based oxidation (e.g. Fenton oxidation, peroxymonosulfate activation, catalytic ozonation and photocatalysis) have predominantly been focused on MF and UF processes, having different fouling characteristics (e.g. internal adsorption and pore clogging) than those of NF (Park et al., 2012; Sun et al., 2018b; Zhao et al., 2020b; Zhu et al., 2022). To the best of our knowledge, studies on catalytic ceramic NF membranes for direct surface water treatment do not exist in literature.

Therefore, the present study was dedicated to elucidating fouling characteristics and Fenton cleaning efficacy during direct NF treatment of surface water, using a pre-coated ceramic NF membrane. To this end, the heterogeneous Fenton catalyst, iron oxychloride (FeOCl) (Chen et al., 2021; Yang et al., 2013), was pre-coated on top of a commercial ceramic NF membrane via a crossflow pre-filtration method. Canal water was collected as the feed source for direct NF treatment. Filtration of the membrane was studied in relation to the pre-coat layer, feed pH and fluxes in a constant-flux filtration

mode, to simulate as much as possible potential full-scale application. Underlying fouling mechanisms were studied by membrane adsorption in parallel to filtration experiments with the canal water. The efficacy of separation/cleaning and the stability of the pre-coat layer were evaluated in multiple filtration/cleaning cycles.

5.2 Materials and methods

5.2.1 Surface water and membranes

Table 5.1 *Water quality parameters of Delftse Schie Canal water*

Parameters	Units	Values[a]
pH	/	8.55±0.15
Turbidity	NTU	2.35±0.05
DOC	mg L^{-1}	11.95±0.13
UV$_{254}$	cm^{-1}	0.37±0.01
Conductivity	mS cm^{-1}	2.42±0.02
Ca^{2+}	mg L^{-1}	77.64±0.14
Mg^{2+}	mg L^{-1}	17.71±0.03
Na^{+}	mg L^{-1}	76.16±0.57
K^{+}	mg L^{-1}	12.28±0.14
PO$_4^{3-}$	mg L^{-1}	6.66±0.04
SO$_4^{2-}$	mg L^{-1}	48.14±0.44
Cl^{-}	mg L^{-1}	121.10±0.38
Br^{-}	mg L^{-1}	1.84±0.02

[a] Average ± SD from duplicate measurements

Surface water was collected from the Delftse Schie Canal (Delft, the Netherlands), a moderately contaminated urban canal. The canal water had a dissolved organic carbon (DOC) concentration of 11.95 mg L^{-1} and a UV absorbance at 254 nm (UV$_{254}$) of 0.37 cm^{-1}. Other water quality parameters of the canal water are summarized in Table 5.1.

Commercial ceramic NF membranes (Inopor GmbH, Germany), with nominal molecular weight cut-off (MWCO) of 450 Da (Inopor data), were used. As described by the manufacturer, the membranes have a single-channel tubular configuration with an effective filtration area of 0.00163 m^2 and an

inner diameter of 7 mm. The membranes consist of an active layer of TiO_2 and a support layer of Al_2O_3. The virgin membranes were wetted by soaking in Milli-Q water (18.2 MΩ cm) overnight prior to use.

5.2.2 Experimental methods

Preparation of catalyst pre-coated ceramic NF membranes

A thermal annealing method was used to synthesize FeOCl catalyst (Sun et al., 2018a). The precursor, $FeCl_3 \cdot 6H_2O$ powder, was sealed in a crucible and calcined at a heating rate of 20 °C min⁻¹ to 220 °C and remained for 1 h in a muffle furnace. The resultant FeOCl particles (2.0 g) were ultrasonically dispersed into demineralized water (0.5 L) and left to stand for 10 min to remove the settleable solids. The FeOCl suspension (inset of Figure S5.1a, Supplementary Data) remained stable and was thus favourable for pre-coating through pressure-driven pre-filtration, since undesirable sedimentation in the tubing could be avoided.

A crossflow filtration apparatus (OSMO Inspector 2, Convergence Industry, the Netherlands), with the FeOCl suspension (0.5 L) spiked into the feed mainstream (15 L), was used for membrane pre-coating (Figure 5.1). A laminar cross flow of 0.2 m s⁻¹ (Reynolds number (*Re*) = 1510, Text S5.1, Supplementary Data) and a high transmembrane pressure (TMP = 9–20 bar) were adopted to boost the formation of a uniformly compacted catalyst layer on the membrane. Two pristine membranes, having different permeance of 11.9 and 27.4 L m⁻² h⁻¹ bar⁻¹, were pre-coated at 20.2 and 8.9 bar, respectively, for 30 min, resulting in similar fluxes (233.9–234.8 L m⁻² h⁻¹), to filter comparable amounts of the FeOCl catalyst onto the membranes. Additionally, the effect of FeOCl dosages (0–23.1 mg L⁻¹) in the feed flow on iron loading was studied by changing the flow rate with a peristaltic pump from the concentrated FeOCl tank (4.0 g L⁻¹), during pre-coating (10 min), also at comparable fluxes (213.3–220.3 L m⁻² h⁻¹). The coating efficiency index (α) was calculated as a ratio of the actual loading (M_a, g m⁻²) to the estimated loading (M_e, g m⁻²), as described with Equation (5.1).

$$\alpha = \frac{M_a}{M_e} = \frac{M_a}{C_{Fe} \cdot \int_0^t J_{Fe} \, dt} \tag{5.1}$$

where C_{Fe} (g L⁻¹) is the concentration of the FeOCl suspension in the feed flow, J_{Fe} (L m⁻² h⁻¹) the temperature (20 °C) corrected permeate flux (Text S5.2, Supplementary Data) measured with the feed FeOCl suspension, and t (h) the operational time, during FeOCl pre-filtration. The actual FeOCl loading on the membranes was determined by dissolving the solid iron into an oxalic acid solution (1.0 g L⁻¹) and measuring the ionic iron concentration, while the estimated FeOCl loading was calculated based on a mass balance of FeOCl filtered by the membranes.

Bench-scale experiments of direct NF of canal water and Fenton cleaning
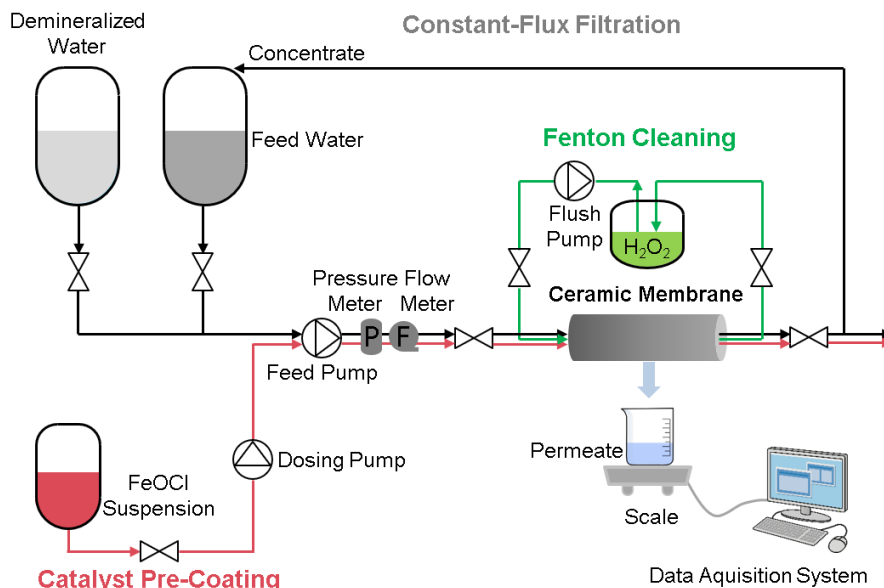
Figure 5.1 *Schematic diagram of the integrative system of catalyst pre-coating, constant-flux filtration and Fenton cleaning for direct ceramic nanofiltration of surface water.*

Bench-scale filtration experiments were performed using the same crossflow filtration setup as the pre-coating tests (Figure 5.1). The pristine and FeOCl pre-coated membranes were tested with demineralized water to determine their initial filtration resistances. Direct NF experiments of the raw canal water (without any pre-treatment) were done in a constant-flux filtration mode through a step-wise increase in TMP (3–22 bar), in order to simulate as much as possible full-scale application. The crossflow velocity was set at 0.9 m s⁻¹ to acquire a turbulent flow (*Re* = 6039) inside the membrane channel. The retentate flow was fed back into the feed tank, while the permeate flux was continuously measured using a scale connected to a data acquisition system. A sodium hypochlorite solution (0.2%) was employed to ensure sufficient cleaning of the fouled membranes after each test. An overview of the performed fouling/cleaning experiments is given in Table S5.1 (Supplementary Data). The filtration/cleaning experiments were done in duplicate.

Single-cycle fouling

Single-cycle fouling (4 h) was executed at fluxes of around 23 and 46 L m⁻² h⁻¹, respectively, to explore the impact of permeate fluxes on fouling of the membranes in the absence or presence of the pre-coat layer. The raw water was subjected to the fouling tests at its original pH (8.5, Table 5.1) and

also at pH = 7.0 (adjusted by a HCl solution of 1.0 M), to gain an insight into the fouling mechanism. In addition, to study the effect of colloids in the feed water on filtration, prefiltered canal water, over a 1.0-µm cartridge filter, was also subjected to the same ceramic NF operations as was the raw water.

Multi-cycle fouling/cleaning

The efficacy of Fenton cleaning for the pre-coated membrane, in comparison with that of sole H_2O_2 cleaning for the pristine membrane, was assessed during repeated constant-flux filtration and cleaning over five cycles (4-h fouling for each cycle). Membrane cleaning (30 min) was carried out by circulating a H_2O_2 solution ($[H_2O_2]_0$ = 10.0 mM, pH = 3.3) inside the membrane channel with a peristaltic pump at a laminar cross flow of 0.16 m s^{-1} (*Re* = 1116) as depicted in Figure 5.1. A longer-term filtration/Fenton cleaning experiment over five cycles (1-d fouling for each cycle), was conducted in a constant-pressure filtration mode. The cleaning agent, i.e. H_2O_2 solution ($[H_2O_2]_0$ = 30.0 mM, pH = 3.3), was repeatedly used throughout the five one-day cycles, to evaluate the stability and sustainability of the Fenton cleaning route.

Determination of hydraulic filtration resistances

The hydraulic filtration resistances were determined using the resistance-in-series model (Choo and Lee, 1996) as described in Text S5.3 (Supplementary Data). The resistances at the varying filtration conditions and stages were calculated with Equations (5.2)–(5.4):

$$R_m = \frac{\Delta P_0}{\eta \cdot J_0} \tag{5.2}$$

$$R_m + R_{pc} = \frac{\Delta P_0}{\eta \cdot J_1} \tag{5.3}$$

$$R_m + R_{pc} + R_f = \frac{\Delta P_2}{\eta \cdot J_2} \tag{5.4}$$

where R_m (m^{-1}), R_{pc} (m^{-1}) and R_f (m^{-1}) are the filtration resistances of the pristine membrane, the pre-coat layer and the fouling layer, respectively. ΔP_0 (Pa) is the applied TMP during pure water filtration over both the pristine membrane and the pre-coated membrane, respectively, ΔP_2 (Pa) the applied TMP during filtration with the canal water using the pre-coated membrane. J_0 (L m^{-2} h^{-1}) and J_1 (L m^{-2} h^{-1}) represent the pure water fluxes before and after FeOCl pre-coating, respectively, J_2 (L m^{-2} h^{-1}) the permeate flux of the pre-coated membrane during filtration with the canal water, η (Pa s) the

permeate viscosity. The filtration resistances during fouling were plotted as a function of the permeate volume per unit filtration area, to compare the fouling status at an equal production.

Membrane adsorption experiments

In order to study the fouling potential and mechanism with respect to foulant-membrane interactions, separate adsorption experiments were performed. Initial fluxes of the pristine and pre-coated membranes were measured with demineralized water at constant pressures of 6–7 bar, to establish a baseline permeance prior to adsorption. The demineralized water in the filtration setup was fully replaced with the canal water samples before the start of the adsorption experiments. Adsorption of NOM/colloids of the canal water onto the membranes was then started by circulating the canal water inside the feed channel, using the same filtration setup and crossflow velocity (i.e. 0.9 m s^{-1}) as the filtration experiments, except without allowing a permeate flow (TMP = 0 bar). The adsorption tests were conducted at the original feed pH (8.5, Table 5.1) and at pH = 7.0 at 20 °C, to better understand the underlying adsorption mechanisms. An adsorption duration of 5 min was adopted to evaluate the potential of rapid adsorption of the foulants on/in the membranes. After adsorption, the feed water was finally switched back to demineralized water to determine fluxes at the same pressures (6–7 bar) as used before adsorption. The contribution to declines in the pure water fluxes before and after adsorption was supposed to be adsorptive fouling, since cake layers are not able to build up in the absence of a permeate flow (Miller et al., 2014).

5.2.3 Characterization and analytical methods

The DOC of the canal water was analysed by a total organic carbon analyser (TOC-VCPH, Shimadzu, Japan). The anions and cations in the canal water were measured with ion chromatography (883 Basic IC plus, Metrohm Instrument, the Netherlands). The UV$_{254}$ was determined by a UV/vis spectrometer (GENESYS 10S UV-Vis, Thermo Scientific, USA) with a quartz cell (1 cm). Prior to all the analyses, the water samples were filtrated through 0.45 μm filters to retain potential impurities. The crystalline profiles of the FeOCl catalyst were analysed between 10° and 110° with a scan step of 0.3° min^{-1} by X-ray diffractometer (D8-Advance, Bruker, USA) under Cu Kα radiation at 45 kV and 40 mA. The zeta potentials of the canal water samples and FeOCl suspensions (0.37 mM) were recorded using a NanoSizer (Nano Series, Malvern Instrument Ltd., UK).

The top-view and cross-sectional mapping of the membranes before and after FeOCl pre-coating was taken by scanning electron microscopy (SEM) (S-3400 N, Hitachi High-Technologies, Japan), equipped with energy dispersive spectroscopy. The top surface and thickness of the remaining FeOCl

pre-coat on the membrane, after the long-term (5 d) multicycle filtration/cleaning, were analysed with the SEM.

The actual MWCO of the membranes was determined by measuring the rejection rates of polyethylene glycols (PEGs) of five molecular weights (200, 300, 400, 600 and 1000 Da) (Sigma-Aldrich, Germany) as tracer compounds, as reported by Shang et al. (2017). The PEG samples were analysed by high-performance size exclusion chromatography (Prominence, Shimadzu, Japan), installed with a gel permeation column (5 mm 30 Å, PSS GmbH, Germany) and a refractive index detector (RID-20A, Shimadzu, Japan).

5.3 Results and discussion

### 5.3.1 Characterization of surface water, FeOCl catalyst and membranes

Surface water
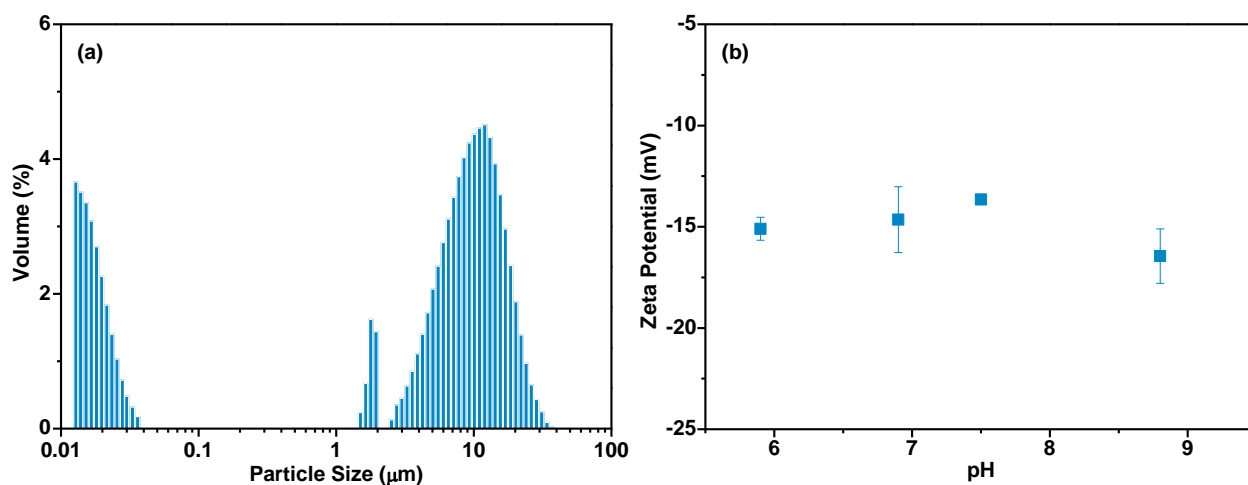
Figure 5.2 *(a) colloidal size distribution and (b) zeta potential of canal water foulants.*

Ceramic NF membranes have abundant porous channels and charged surfaces, and are supposed to intercept large-sized or charged substances via steric hindrance and electrostatic repulsion, respectively (Caltran et al., 2020; Zhao et al., 2018). Figure 5.2a shows that colloidal substances, present in the canal water, were characterized by a bimodal distribution of particle sizes in the range of <0.04 μm and 3–30 μm, as similarly observed in an earlier study (Walther et al., 2006). The zeta potential profiles (Figure 5.2b) imply that NOM/colloids in the canal water were (mostly) negatively charged at pH = 6–9, because particles in surface water adsorb negatively charged humic acids (Xu et al., 2018). The zeta potential of the solution was rather stable, ranging from −15.1 to −16.5 mV, as

a function of the pH (6–9), which is in good agreement with the findings of Zhang and Bai (2003). Apparently, the NOM in the canal water was fully deprotonated above pH = 6.0, since pKa values of the predominant humic/fulvic acid carboxylic groups center around 4.7 and 5.9 (Li et al., 2021).

FeOCl catalyst and membranes
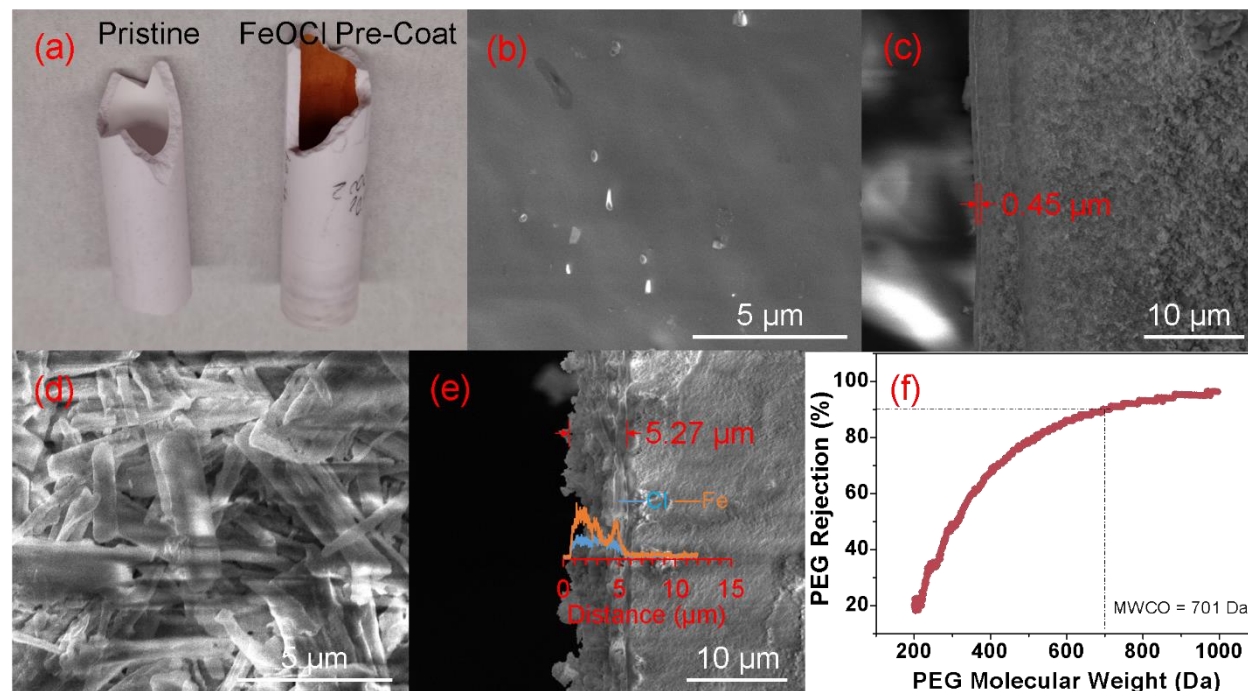
Figure 5.3 *(a) Photograph of pristine (left) and FeOCl pre-coated (right) ceramic NF membranes. (b) Top-view and (c) cross-section SEM images of pristine membrane. (d) Top-view and (e) cross-section SEM images with inset energy dispersive spectroscopy profiles of FeOCl pre-coated membrane. (f) Polyethylene glycol (PEG) rejection curve of ceramic NF membrane. The dashed line shows the PEG molecular weight with a rejection rate of 90%, representing the MWCO.*

The characteristic crystalline phases, i.e. (010), (110), (021) and (111) planes, of the FeOCl catalyst, as measured in Figure S5.1b (Supplementary Data), were in line with the standard XRD pattern of FeOCl in its pure phase (JCPDS No. 72-0619) (Sun et al., 2018a). The profile of the zeta potential as a function of the pH of the FeOCl suspension (Figure S5.1a, Supplementary Data) showed an isoelectric point between pH = 7.0 and 8.1, corresponding to a positively charged surface of the FeOCl particles at pH = 7.0. A comparable isoelectric point (i.e. pH = 8.3) of FeOCl has previously been reported by Chen et al. (2021). As can be observed from Figure 5.3a, the surface of the membrane channel changed from white to homogeneously brownish yellow, upon FeOCl pre-coating, meaning successful

loading of the FeOCl catalyst onto the membrane. The pristine membrane exhibited a dense and smooth surface (Figure 5.3b and c) of the active membrane layer, in accordance with earlier observations (Shang et al., 2017; Voigt et al., 2019). The pre-coated membrane, however, displayed a rougher surface, with the FeOCl particles randomly stacked on the membrane (Figure 5.3d). The FeOCl particles were present as long-strip sheets with dimensions of, approximately, 0.2–0.3 μm in thickness, 0.7–1.2 μm in width and 3.0–5.0 μm in length (inset of Figure S5.1b, Supplementary Data), which enabled the particles to deposit onto the membrane as a pre-coat layer, instead of penetrating into the nano-pores (around 1 nm in diameter). The pre-coat layer had pore sizes ranging from 0.1 to 0.5 μm, as estimated from the top-view SEM image (Figure 5.3d). Therefore, the pre-coat layer was assumed to act as a pre-filtration media to retain the large-sized fraction (3–30 μm, Figure 5.2a) of the colloids from the canal water, while only allowing the small-sized colloid fraction (<0.04 μm, Figure 5.2a) and the dissolved molecules to pass through and reach the surface of the active membrane layer (Malczewska et al., 2015; Zhao et al., 2020a). The pre-coat layer of about 5.3 μm in thickness (Figure 5.3e), appeared to be uniformly coated on the membrane. As indicated by the PEG rejection curve in Figure 5.3f, the measured MWCO of the membrane, i.e. 701 Da, was larger than the nominal MWCO (450 Da, Inopor data), as has also been observed in other studies on similar membranes (Caltran et al., 2020; Mustafa et al., 2016a).
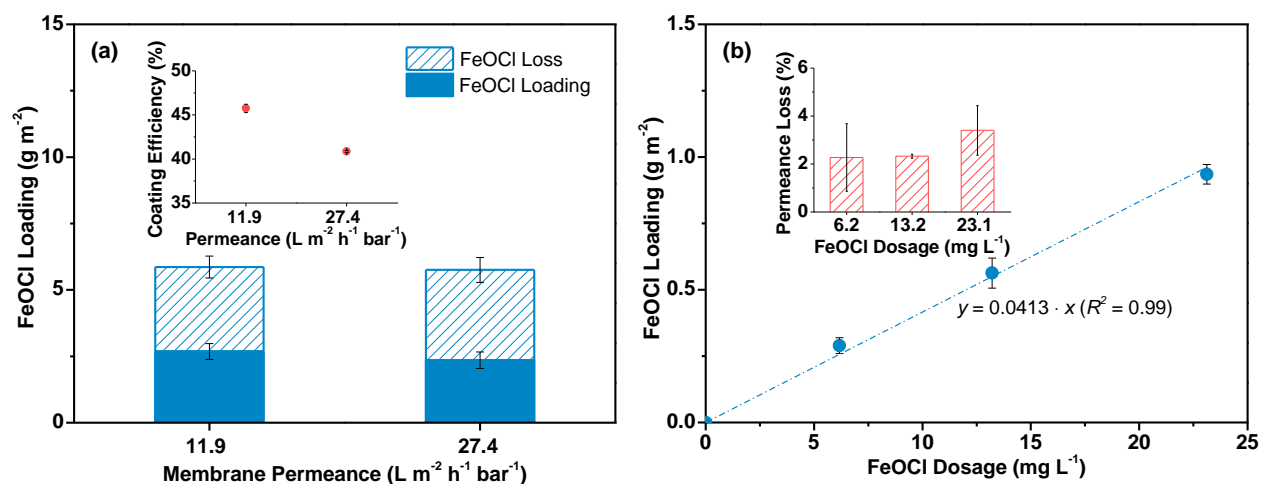

Figure 5.4 *(a) FeOCl loading of ceramic NF membranes with different initial permeance. Inset: FeOCl coating efficiency vs. membrane permeance. (b) Effect of FeOCl dosage on iron loading and permeance loss of ceramic NF membrane.*

In order to test the adjustability of catalyst loading by means of crossflow pre-filtration, loading of the FeOCl particles was studied in relation to different permeance (11.9 and 27.4 L m^{-2} h^{-1} bar^{-1}) of

two pristine membranes and varying FeOCl dosages (0–23.1 mg L^{-1}). Figure 5.4a depicts that the two membranes, when pre-coated at the similar fluxes (see Section 5.2.2), presented comparable FeOCl loading, being 2.7 and 2.4 g m^{-2}, respectively. This thus implies that maintaining the permeate flux at a certain level by tuning the TMP during pre-coating, is a viable method for obtaining the intended catalyst loading on the membranes. The actual loading of the membranes was less than a half (α < 46.0%, inset of Figure 5.4a) of the theoretical loading (5.8–5.9 g m^{-2}), being the total amount of FeOCl filtered by the membranes. It is likely that the cross flow in the membrane channel limited the build-up of the FeOCl pre-coat layer on the membranes, due to a shear-induced diffusion effect (Anantharaman et al., 2020). The FeOCl loading on the membrane was linearly related to the FeOCl dosages ($y = 0.0413 \cdot x$, $R^2 = 0.99$), indicating that the FeOCl loading could also be regulated by changing the FeOCl dosages (Figure 5.4b). The permeance losses of the membranes, as a result of FeOCl pre-coating, were minimal (<4%, inset of Figure 5.4b). This is supposedly because the porous pre-coat layer provided alternative, interconnected channels for water permeation, since intraparticle micropores and particle interspaces (meso/macropores) were abundant in/between the FeOCl particles, as has been verified by prior studies (Luo et al., 2019; Sun et al., 2018a).

5.3.2 Rapid adsorption of foulants on membranes
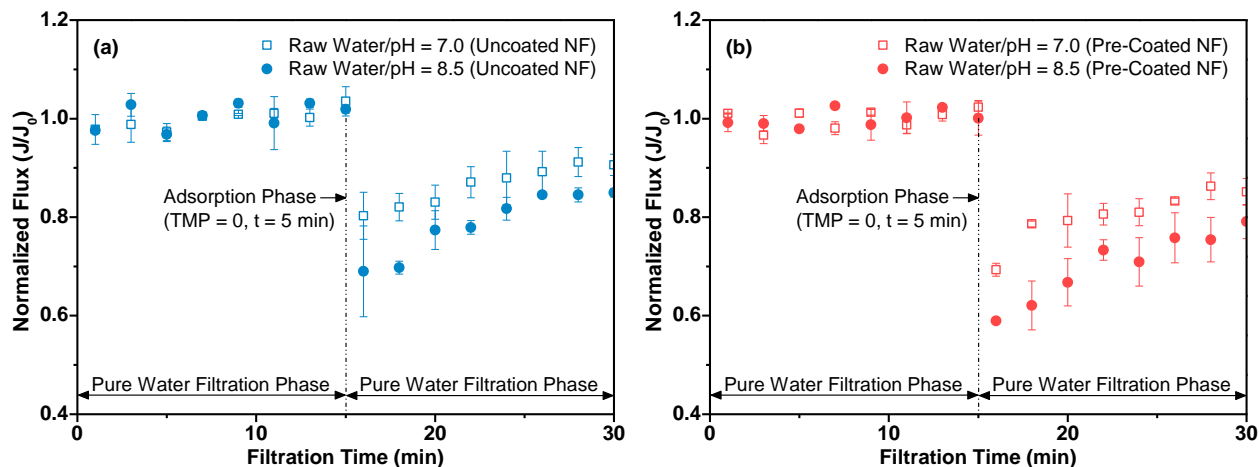
Figure 5.5 *Membrane permeance declines due to adsorption (5 min) of foulants from raw canal water to (a) pristine (uncoated) and (b) FeOCl pre-coated membranes at original (pH = 8.5) and neutral pH (7.0) of the canal water.*

Adsorptive fouling, without a permeate flow through a membrane, provides an insight into solute-membrane interactions (Shao et al., 2011; Zazouli et al., 2009). Figure 5.5a shows that the flux decline of the pristine membrane upon adsorption at pH = 7.0 (19.7%) was much smaller than at pH = 8.5

(31.0%). The same tendency was observed for the FeOCl pre-coated membrane (Figure 5.5b), where the flux decline due to adsorption at pH = 7.0 (30.7%) was also smaller than at pH = 8.5 (41.0%). These findings are in line with the observation of Kim et al. (2009), who have demonstrated that the adsorption capacity of NOM (10 mg L^{-1}) onto TiO_2 particles was increased from 12 to 19 mg g^{-1} with an increase in the solution pH from 5 to 8. They have suggested that NOM-TiO_2 bridging by calcium ions (1 mM) was more prone to occur at pH = 8, where the TiO_2 surfaces were more negatively charged, than at pH = 5. Regardless of the used pH (7.0 and 8.5), the adsorption-induced flux declines of the pre-coated membrane were higher than those of the pristine membrane. Both membranes developed a progressive increase in the fluxes during pure water filtration after adsorption, implying that the adsorbed foulants inclined to be desorbed to some extent during (crossflow) filtration with pure water.

5.3.3 Effect of feed pH, FeOCl pre-coat, foulant sizes and fluxes on filtration resistances

Direct ceramic NF of raw canal water (Figure 5.6a and b) was performed at its original pH (8.5) and at pH = 7.0, using the pristine and pre-coated membranes at a constant flux of 44.7–46.0 L m^{-2} h^{-1}, during a single filtration cycle, to elucidate the underlying fouling mechanisms and influential factors. The mean increase rate of each filtration resistance, represented by the slope of a linear regression of the resistances as a function of the volume per unit area, was used as an indicator for fouling potentials under the various conditions. Both the uncoated NF, at pH = 8.5 and 7.0 (Figure 5.6a), and the pre-coated NF, at pH = 8.5 and 7.0 (Figure 5.6b), developed sharp increases in the initial filtration resistances of 7.2×10^{13}, 6.4×10^{13}, 11.0×10^{13} and 7.5×10^{13} m^{-1}, and afterwards an abrupt transition to slower resistance increases of 0.0561, 0.0241, 0.1418 and 0.0503 (10^{13} m L^{-1}), respectively. Apparently, both membranes fouled more severely at pH = 8.5 than at pH = 7.0, which has been interpreted by increased calcium-bridging between ceramic membranes and NOM at a higher pH in prior studies with consistent findings (Kim et al., 2009; Mustafa et al., 2014). Overall, the increase rates of both the initial and follow-up filtration resistances, at the four combined conditions, followed the same order as the permeance declines during adsorption (Section 5.3.2), i.e. *Uncoated NF/pH7.0 < Uncoated NF/pH8.5 ≈ Pre-Coated NF/pH7.0 < Pre-Coated NF/pH8.5*. This confirms the important role of foulant adsorption in membrane fouling during direct NF of raw (surface) water. Once (some of) the membrane pores were clogged/narrowed by the adsorbed foulants, cake layers started to grow, thereby slowly increasing the resistances, as also observed earlier (Kirschner et al., 2019; Ognier et al., 2004).
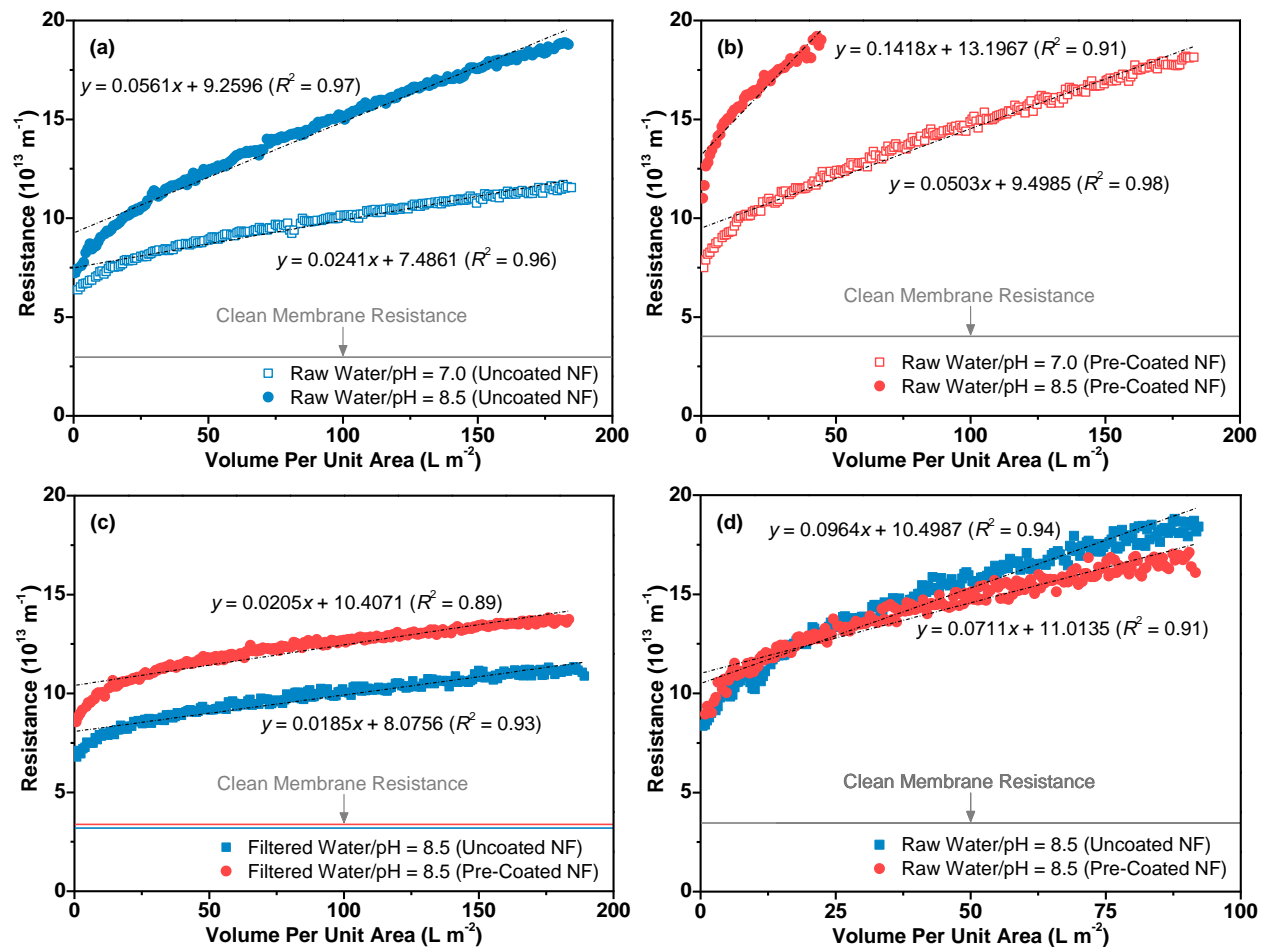
Figure 5.6 *Filtration resistances of (a) pristine and (b) FeOCl pre-coated membranes during direct NF of raw canal water at its original pH (8.5) and pH = 7.0, (c) during NF with pre-filtered canal water (by 1 µm cartridge filter) at pH = 8.5, at constant fluxes of around 46.0 L m⁻² h⁻¹, and (d) during direct NF of raw canal water (pH = 8.5) at constant fluxes of about 23.0 L m⁻² h⁻¹.*

The effect of foulant sizes on filtration resistances was studied using pre-filtered canal water for filtration of the pristine and pre-coated membranes at a constant flux of 45.9–47.5 L m⁻² h⁻¹ (Figure 5.6c). As the raw water colloids had sizes of <0.04 µm and 3–30 µm (Figure 5.2a), the pre-filtered canal water through a 1-µm filter was therefore assumed to only consist of a small-sized fraction (<0.04 µm) of the colloids and dissolved NOM. The pre-coated membrane, during filtration with the pre-filtered canal water, developed a resistance curve nearly parallel to that of the pristine membrane, implying that the membrane fouling by the small-sized colloid fraction and NOM were independent of the presence of the pre-coat layer. It is likely that the small foulants tended to penetrate the pre-coat layer and predominantly fouled the active membrane layer (Yao et al., 2009; Zhao et al., 2020a). The result, however, largely differs from the observations during direct raw water

(pH = 8.5) filtration in Figure 5.6a and b, where the resistance increase rate of the pre-coated membrane was over 2.5 times that of the pristine membrane. The faster fouling of the pre-coated membrane was thus supposedly because the large-sized fraction of the colloids filled and clogged the pores in the pre-coat layer at the flux of 44.7–46.0 L m^{-2} h^{-1} while the pristine membrane tended to develop minor pore clogging due to its small pore sizes (0.9 nm, Inopor data). Likewise, Liu and Benjamin (2016) revealed that fouling of an aluminium oxide pre-coat layer on top of a membrane was dominated by large-sized colloids in surface water, which is in line with our observations. When using the pre-coated membrane, the resistance growth rate (0.0205 [10^{13} m L^{-1}]) during filtration with the pre-filtered canal water (Figure 5.6c), accounted for only 14.5% of that during filtration with the raw canal water (pH = 8.5) (Figure 5.6b), confirming the dominant role of the large-sized colloid fraction in pore clogging of the pre-coat layer.

Figure 5.6d illustrates the resistance evolution of the pristine and pre-coated membranes during direct NF of the raw canal water at a constant flux of 22.8–23.1 L m^{-2} h^{-1}. The pre-coated membrane underwent a resistance increase from 8.9×10^{13} to 16.7×10^{13} m^{-1}, comparable to that of the pristine membrane, from 8.4×10^{13} to 18.4×10^{13} m^{-1}. The result suggests that the pre-coat layer on the membrane, during direct raw water NF at approximately 23 L m^{-2} h^{-1}, did not develop considerable pore clogging, unlike the situation at around 46 L m^{-2} h^{-1}. It is likely that the cross flow (0.9 m s^{-1}) at the lower flux (with a weaker permeation drag force) could, to some extent, prevent the large-sized colloid fraction from entering the pores of the pre-coat layer. In addition, the number of foulants, carried by the lower flux, were fewer, compared to the higher flux, and the foulants might be well dispersed on/within the porous pre-coat layer without causing pronounced clogging of the pores (Soesanto et al., 2019). Similar dependence of fouling potential on the combination of pre-coat layers and filtration fluxes, has been observed for an iron oxide pre-coated membrane, as documented previously (Kim et al., 2017).

### 5.3.4 Filtration/cleaning performance over multiple cycles

Direct filtration of canal water using pristine and FeOCl pre-coated membranes, and membrane cleaning with a H$_2$O$_2$ solution ([H$_2$O$_2$]$_0$ = 10.0 mM, pH = 3.3), were performed over five four-hour cycles, without refreshing the FeOCl pre-coat between the cycles. The fluxes were kept constant at 22.1–22.6 L m^{-2} h^{-1}, to avoid too rapid clogging, as demonstrated in Section 5.3.3. As shown in Figure 5.7, the pristine membrane underwent a continuous increase in filtration resistances from 11.5×10^{13}–21.3×10^{13} (*Cycle 1*) to 18.6×10^{13}–28.9×10^{13} m^{-1} (*Cycle 5*), respectively, while crossflow

flushing with the H_2O_2 solution was done after each filtration cycle. Sole H_2O_2 solutions, in the absence of a Fenton catalyst, have been reported to exert minor oxidative removal of organic foulants from ceramic membranes (De Angelis and de Cortalezzi, 2016; Sun et al., 2018b), which is in accordance with our findings. However, the filtration resistances of the pre-coated membrane only slightly increased at *Cycle 2*, i.e. from 8.9×10^{13}–16.6×10^{13} to 10.8×10^{13}–18.4×10^{13} m^{-1}, respectively, while, thereafter, they remained steady over the following cycles. The chemically irreversible fouling index (*CIFI*) (Text S5.4, Supplementary Data) of the pre-coated membrane was 0.00057 m^{-2} L^{-1}, accounting for less than 25% of the *CIFI* value (0.00231 m^{-2} L^{-1}) of the pristine membrane (Figure S5.2, Supplementary Data). Fenton oxidation reactions, catalysed by the FeOCl pre-coat layer, thus removed the majority of the foulants on/within the pre-coat layer, avoiding aggressive cleaning with strong oxidants (e.g. chlorine) or bases (e.g. caustic soda). The coexistence of Fenton catalyst (i.e. FeOCl), organic foulants (i.e. NOM and colloids) and H_2O_2 was favourable for degradation and removal of the foulants, due to a short mass transfer distance between $^\bullet OH$ radicals and the foulants. Chen et al. (2019b) demonstrated that a MoS_2 coated membrane could provide an active catalyst-contaminant interface with producing radicals in close vicinity to the contaminants, which is a prerequisite for effective oxidation.
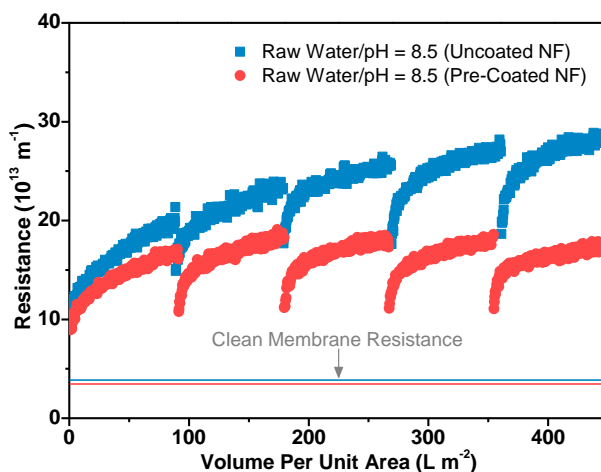
Figure 5.7 *Evolution of filtration resistances of pristine and FeOCl pre-coated membranes during direct filtration of raw canal water (pH = 8.5) at a constant flux of about 22.4 L m^{-2} h^{-1} and periodic H_2O_2 cleaning ([H_2O_2]$_0$ = 10.0 mM, pH = 3.3) over five four-hour cycles.*

5.3.5 Validation of filtration performance and stability of FeOCl pre-coated membrane in long-running operations
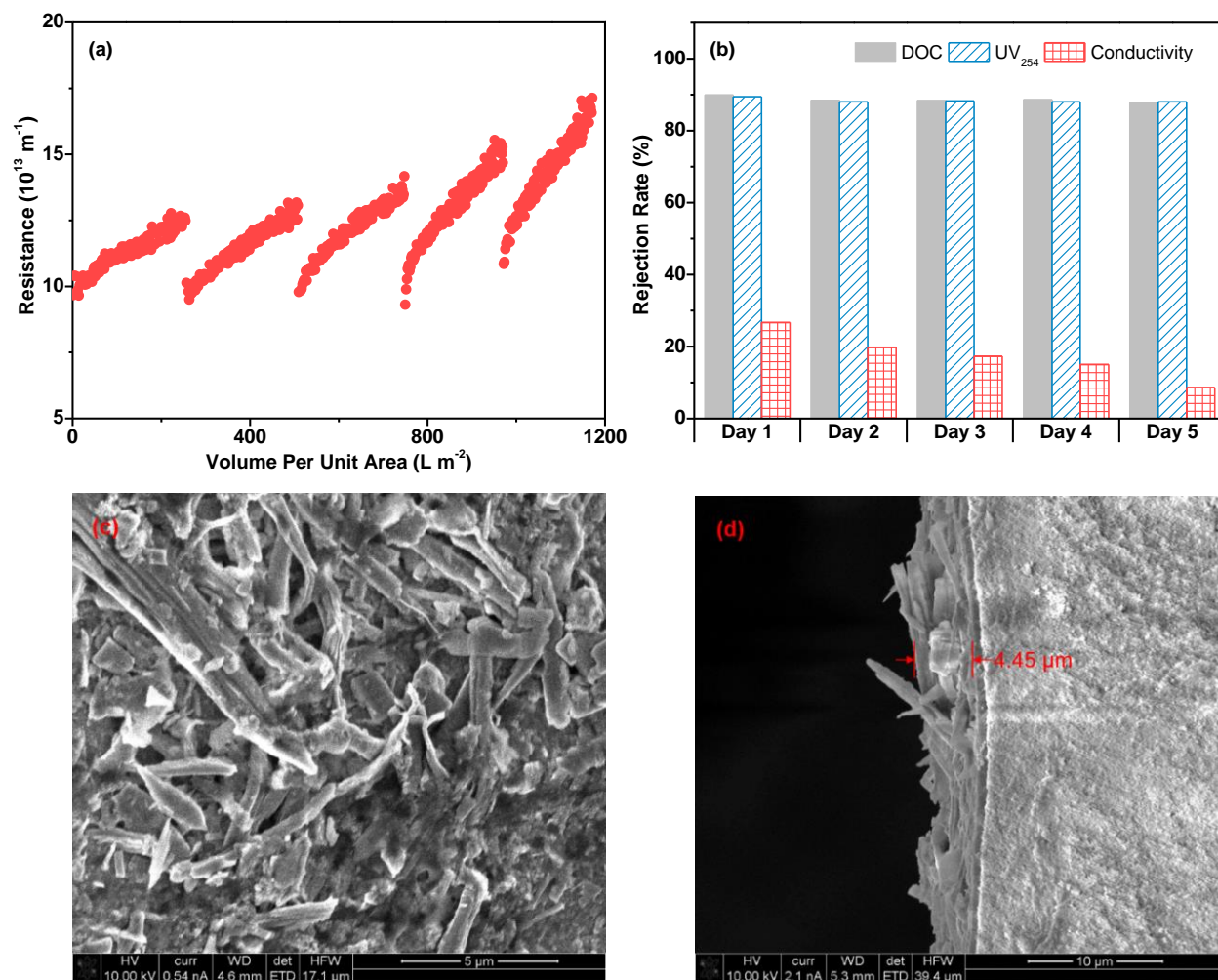
Figure 5.8 *(a) Direct canal water filtration using FeOCl pre-coated membrane at a constant-pressure of 3.0 bar with periodical Fenton cleaning over five one-day cycles. The FeOCl pre-coat and H_2O_2 solution were not renewed between the cycles. (b) Rejection of dissolved organic carbon (DOC), UV absorbance at 254 nm (UV_{254}) and conductivity during five-day filtration. (c) Top-view and (d) cross-sectional SEM images of the membrane after the five one-day cycles.*

Separation/cleaning efficacy and pre-coat stability of the pre-coated membrane, during direct filtration of canal water, were further studied in a longer period, comprising five cycles (1 d for each cycle) of filtration/Fenton cleaning. Constant-pressure filtration (TMP = 3.0 bar) was performed at an initial pure water flux of 21.7 L m^{-2} h^{-1} (Figure S5.3, Supplementary Data), considering its ease in automatic regulation for continuous filtration, over days, at lab scale. As observed in Figure S5.3, the pre-coated membrane experienced an abrupt flux decline by 42.5% at the very beginning of filtration, which was close to the flux decline percentage, i.e. 41.0% (Figure 5.5b, Section 5.3.2), determined by

the adsorption experiment, and was thus assumed to predominantly result from adsorption. Figure 5.8a shows that, following periodical Fenton cleaning, the starting resistances at *Cycle 2*, *3* and *4* were recovered to a level as high as the one at *Cycle 1*, indicating effective removal of the foulants by Fenton cleaning. The multiple cycles presented a gradually rising tendency in the overall filtration resistances, due to accumulation of some irremovable fouling during the longer filtration period (5 d) (Ninomiya et al., 2020).

The rejection percentages of DOC, UV_{254} and conductivity were recorded throughout the five filtration cycles (Figure 5.8b). The rejection percentages in DOC (87.7–89.9%) and UV_{254} (88.0–89.4%) remained high and steady over the multiple cycles, predominantly via steric hinderance acted by the separation layer of the membrane (Caltran et al., 2020; Cheng et al., 2017). Rejection of ions by ceramic NF is mainly governed by electrostatic repulsion, since the sizes of the hydrated ions are much smaller than the pore sizes (Chen et al., 2019a; Wadekar and Vidic, 2018). However, as the charge on the TiO_2 separating layer of the membrane was low and also (negatively) influenced by continuous adsorption of oppositely charged molecules (Caltran et al., 2020), the ions were poorly rejected, as indicated by the small change in water conductivity (8.6–26.7%). As observed in Figure 5.8c and d, the membrane surface after the fifth cycle was still covered with an FeOCl layer with a thickness of approximately 4.5 µm, compared to the initial thickness of 5.3 µm (Figure 5.3e, Section 5.3.1). The aforementioned results, collectively, validate the stability/reactivity of the FeOCl pre-coated ceramic NF membrane during its long-term repeated uses for direct filtration of surface (canal) water and Fenton cleaning.

5.4 Conclusions

A novel catalytic NF hybrid process, comprising a catalyst (FeOCl) pre-coat layer on a ceramic NF membrane, was proposed as a single-step route for direct treatment of surface (canal) water and Fenton cleaning (with a H_2O_2 solution) over the fouled membrane. The ceramic NF fouling was affected by the pre-coat layer and the feed pH (8.5 and 7.0), while the extents varied depending on adsorption capabilities of the membrane under the individual conditions. The main conclusions of this chapter were:

(1) The FeOCl layer was uniformly pre-coated on top of the membrane by means of crossflow pre-filtration with a FeOCl suspension, only causing a minimal decrease (<4%) of the membrane permeance.

(2) A large-sized fraction (3–30 μm) of the colloids in the canal water, in combination with an operating flux of about 46 L m⁻² h⁻¹, contributed to a faster pore clogging in the pre-coat layer than in the pristine membrane. However, the pristine and pre-coated membranes fouled comparably at a flux of around 23 L m⁻² h⁻¹.

(3) The catalytic pre-coat layer facilitated the restoration of filtration resistances of the fouled membrane through Fenton cleaning, while the separation layer of the membrane maintained high rejections (approximately 90%) of the NOM over five one-day fouling/cleaning cycles.

(4) The pre-coat layer remained reproducible over the five long-running cycles, having a minor loss of 15.6% in its thickness.

Supplementary data

Text S5.1 Reynolds number of flows inside a membrane channel

The Reynolds number is an indicator of the flow regime which is calculated with Equation (S5.1):

$$R_e = \frac{v_c \cdot d_h}{v} \tag{S5.1}$$

where R_e is the Reynolds number, v_c the crossflow velocity (m s⁻¹), and d_h the hydraulic diameter of the cross-section of the flow. For tubular membranes, the hydraulic diameter is equal to the inner diameter of the membrane (m). v denotes the kinematic viscosity of the fluid, and it is 1.004×10⁻⁶ m² s⁻¹ for water at 20 °C.

Text S5.2 Temperature-corrected flux of membranes

Real-time variations in solution temperature during filtration were used to calculate the temperature-corrected flux of the membranes with Equation (S5.2):

$$J = J_t \cdot e^{-0.0239 \cdot (T-20)} \tag{S5.2}$$

where J (L m⁻² h⁻¹) is the temperature-corrected flux at 20 °C, J_t (L m⁻² h⁻¹) the measured flux, and T (°C) the temperature of feed solutions.

Text S5.3 Determination of hydraulic filtration resistances

The hydraulic filtration resistances were determined using the resistance-in-series model as described with Equation (S5.3) (Choo and Lee, 1996).

$$J = \frac{dV}{A_m \cdot dt} = \frac{\Delta P}{\eta \cdot R} \tag{S5.3}$$

where J (L m^{-2} h^{-1}) is the temperature-corrected flux at 20 °C (Text S5.2), V (m^3) the cumulative permeate volume, t (s) the filtration time, A_m (m^2) the effective filtration area, ΔP (Pa) the applied TMP, η (Pa s) the permeate viscosity, and R (m^{-1}) the hydraulic filtration resistance.
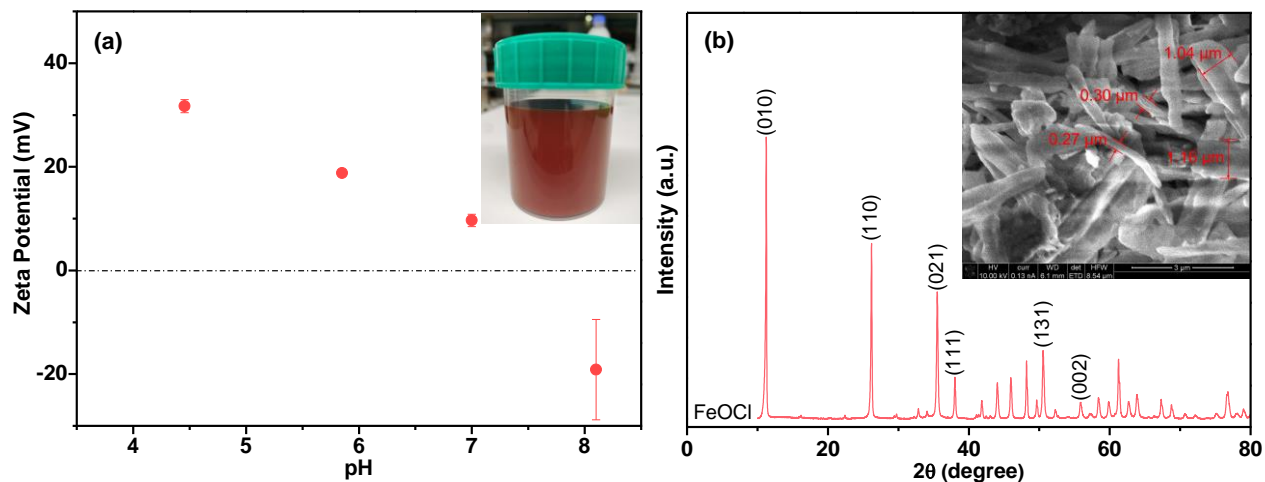
Text S5.4 Chemically irreversible fouling index (CIFI)

Chemically irreversible fouling index (CIFI) was represented by the slope of a line, connecting the starting points of the first and fifth curves of transmembrane pressure vs. permeate volume per filtration area, based on the two-point method (Huang et al., 2009).

Table S5.1 Specifications of performed fouling/cleaning experiments

No.		NF types	Fouling tests					Cleaning tests				
			Canal water	Feed pH	Flux/TMP[c]	CFV[e] $m\ s^{-1}$	t_f[f] h	H$_2$O$_2$ mM	CFV $m\ s^{-1}$	t_c[g] h	pH
Figure 5.6	a	NF$_p$[a]	Raw	7.0 /8.5	46 LMH[d]	0.9	4				
	b	NF$_c$[b]	Raw	7.0 /8.5	46 LMH	0.9	4				
	c	NF$_p$/NF$_c$	Filtered	8.5	46 LMH	0.9	4				
	d	NF$_p$/NF$_c$	Raw	8.5	23 LMH	0.9	4				
Figure 5.7		NF$_p$/NF$_c$	Raw	8.5	23 LMH	0.9	5×4	10	0.16	0.5	3.3
Figure 5.8		NF$_c$	Raw	8.5	3 bar	0.9	5×24	30	0.16	1.0	3.3

[a] NF$_p$: pristine NF; [b] NF$_c$: coated NF; [c] TMP: transmembrane pressure; [d] LMH: L m^{-2} h^{-1}; [e] CFV: cross flow velocity; [f] t_f: fouling time; [g] t_c: cleaning time.

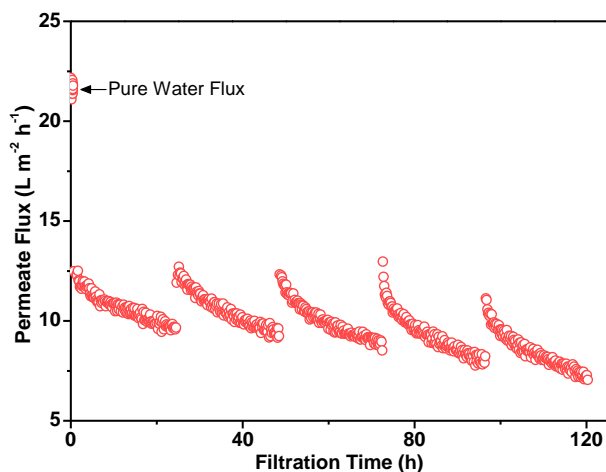***Figure S5.1*** *(a) zeta potential of FeOCl suspension (inset) as a function of pH value. (b) XRD pattern and SEM image (inset) of FeOCl particles.*
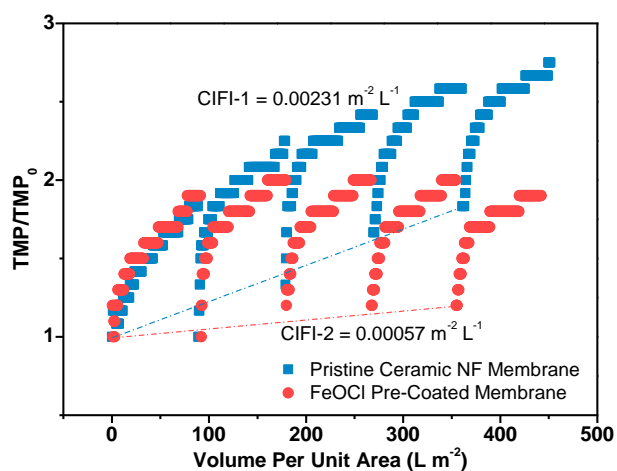
Figure S5.2 *Determination of chemical irreversible fouling indices (CIFI) of pristine and FeOCl pre-coated membranes during multicycle direct NF of canal water and membrane cleaning by H_2O_2 solutions ([H_2O_2]$_0$ = 10.0 mM, pH = 3.3).*

Figure S5.3 *Flux evolution during multicycle filtration with canal water at a constant transmembrane pressure of 3.0 bar using FeOCl pre-coated membrane over five days in combination with periodic Fenton cleaning.*

References

Anantharaman, A., Chun, Y., Hua, T., Chew, J.W., Wang, R., 2020. Pre-deposited dynamic membrane filtration – A review. Water Research 173, 115558.

Árki, P., Hecker, C., Tomandl, G., Joseph, Y., 2019. Streaming potential properties of ceramic nanofiltration membranes – Importance of surface charge on the ion rejection. Separation and Purification Technology 212, 660-669.

Cabrera, S.M., Winnubst, L., Richter, H., Voigt, I., McCutcheon, J., Nijmeijer, A., 2022. Performance evaluation of an industrial ceramic nanofiltration unit for wastewater treatment in oil production. Water Research, 118593.

Caltran, I., Rietveld, L.C., Shorney-Darby, H.L., Heijman, S.G.J., 2020. Separating NOM from salts in ion exchange brine with ceramic nanofiltration. Water Research 179, 115894.

Chen, X., Chen, T., Li, J., Qiu, M., Fu, K., Cui, Z., Fan, Y., Drioli, E., 2019a. Ceramic nanofiltration and membrane distillation hybrid membrane processes for the purification and recycling of boric acid from simulative radioactive waste water. Journal of Membrane Science 579, 294-301.

Chen, Y., Miller, C.J., Collins, R.N., Waite, T.D., 2021. Key considerations when assessing novel Fenton catalysts: Iron oxychloride (FeOCl) as a case study. Environmental Science & Technology 55(19), 13317-13325.

Chen, Y., Zhang, G., Liu, H., Qu, J., 2019b. Confining free radicals in close vicinity to contaminants enables ultrafast Fenton-like processes in the interspacing of MoS_2 membranes. Angewandte Chemie International Edition 58(24), 8134-8138.

Cheng, X., Liang, H., Ding, A., Tang, X., Liu, B., Zhu, X., Gan, Z., Wu, D., Li, G., 2017. Ferrous iron/peroxymonosulfate oxidation as a pretreatment for ceramic ultrafiltration membrane: Control of natural organic matter fouling and degradation of atrazine. Water Research 113, 32-41.

Choo, K.-H., Lee, C.-H., 1996. Membrane fouling mechanisms in the membrane-coupled anaerobic bioreactor. Water Research 30(8), 1771-1780.

De Angelis, L., de Cortalezzi, M.M.F., 2016. Improved membrane flux recovery by Fenton-type reactions. Journal of Membrane Science 500, 255-264.

Dreszer, C., Flemming, H.C., Zwijnenburg, A., Kruithof, J.C., Vrouwenvelder, J.S., 2014. Impact of biofilm accumulation on transmembrane and feed channel pressure drop: Effects of crossflow velocity, feed spacer and biodegradable nutrient. Water Research 50, 200-211.

Fujioka, T., Khan, S.J., McDonald, J.A., Nghiem, L.D., 2014. Nanofiltration of trace organic chemicals: A comparison between ceramic and polymeric membranes. Separation and Purification Technology 136, 258-264.

Fujioka, T., Ngo, M.T.T., Makabe, R., Ueyama, T., Takeuchi, H., Nga, T.T.V., Bui, X.-T., Tanaka, H., 2021. Submerged nanofiltration without pre-treatment for direct advanced drinking water treatment. Chemosphere 265, 129056.

Futselaar, H., Schonewille, H., van der Meer, W., 2002. Direct capillary nanofiltration – a new high-grade purification concept. Desalination 145(1), 75-80.

Ho, L., Braun, K., Fabris, R., Hoefel, D., Morran, J., Monis, P., Drikas, M., 2012. Comparison of drinking water treatment process streams for optimal bacteriological water quality. Water Research 46(12), 3934-3942.

Huang, H., Young, T., Jacangelo, J.G., 2009. Novel approach for the analysis of bench-scale, low pressure membrane fouling in water treatment. Journal of Membrane Science 334(1), 1-8.

Kim, B.-C., Nam, J.-W., Kang, K.-H., 2017. Dynamic membrane filtration using powdered iron oxide for SWRO pre-treatment during red tide event. Journal of Membrane Science 524, 604-611.

Kim, J., Shan, W., Davies, S.H.R., Baumann, M.J., Masten, S.J., Tarabara, V.V., 2009. Interactions of aqueous NOM with nanoscale TiO_2: Implications for ceramic membrane filtration-ozonation hybrid process. Environmental Science & Technology 43(14), 5488-5494.

Kirschner, A.Y., Cheng, Y.-H., Paul, D.R., Field, R.W., Freeman, B.D., 2019. Fouling mechanisms in constant flux crossflow ultrafiltration. Journal of Membrane Science 574, 65-75.

Köhler, S.J., Lavonen, E., Keucken, A., Schmitt-Kopplin, P., Spanjer, T., Persson, K., 2016. Upgrading coagulation with hollow-fibre nanofiltration for improved organic matter removal during surface water treatment. Water Research 89, 232-240.

Kramer, F.C., Shang, R., Heijman, S.G.J., Scherrenberg, S.M., van Lier, J.B., Rietveld, L.C., 2015. Direct water reclamation from sewage using ceramic tight ultra- and nanofiltration. Separation and Purification Technology 147, 329-336.

Kramer, F.C., Shang, R., Rietveld, L.C., Heijman, S.J.G., 2020. Fouling control in ceramic nanofiltration membranes during municipal sewage treatment. Separation and Purification Technology 237, 116373.

Kramer, F.C., Shang, R., Scherrenberg, S.M., Rietveld, L.C., Heijman, S.J.G., 2019. Quantifying defects in ceramic tight ultra- and nanofiltration membranes and investigating their robustness. Separation and Purification Technology 219, 159-168.

Li, D., Lin, W., Shao, R., Shen, Y.-X., Zhu, X., Huang, X., 2021. Interaction between humic acid and silica in reverse osmosis membrane fouling process: A spectroscopic and molecular dynamics insight. Water Research 206, 117773.

Li, S., Meng, H., Wang, H., Vrouwenvelder, J.S., Li, Z., 2022. A sacrificial protective layer as fouling control strategy for nanofiltration in water treatment. Water Research 219, 118554.

Liu, J., Benjamin, M.M., 2016. Effect of water chemistry and operational conditions on μGAF process performance. Water Research 105, 76-84.

Luo, J., Sun, M., Ritt, C.L., Liu, X., Pei, Y., Crittenden, J.C., Elimelech, M., 2019. Tuning Pb(II) adsorption from aqueous solutions on ultrathin iron oxychloride (FeOCl) nanosheets. Environmental Science & Technology 53(4), 2075-2085.

Malczewska, B., Liu, J., Benjamin, M.M., 2015. Virtual elimination of MF and UF fouling by adsorptive pre-coat filtration. Journal of Membrane Science 479, 159-164.

Miller, D.J., Kasemset, S., Paul, D.R., Freeman, B.D., 2014. Comparison of membrane fouling at constant flux and constant transmembrane pressure conditions. Journal of Membrane Science 454, 505-515.

Mustafa, G., Wyns, K., Buekenhoudt, A., Meynen, V., 2016a. Antifouling grafting of ceramic membranes validated in a variety of challenging wastewaters. Water Research 104, 242-253.

Mustafa, G., Wyns, K., Buekenhoudt, A., Meynen, V., 2016b. New insights into the fouling mechanism of dissolved organic matter applying nanofiltration membranes with a variety of surface chemistries. Water Research 93, 195-204.

Mustafa, G., Wyns, K., Vandezande, P., Buekenhoudt, A., Meynen, V., 2014. Novel grafting method efficiently decreases irreversible fouling of ceramic nanofiltration membranes. Journal of Membrane Science 470, 369-377.

Ninomiya, Y., Kimura, K., Sato, T., Kakuda, T., Kaneda, M., Hafuka, A., Tsuchiya, T., 2020. High-flux operation of MBRs with ceramic flat-sheet membranes made possible by intensive membrane cleaning: Tests with real domestic wastewater under low-temperature conditions. Water Research 181, 115881.

Ognier, S., Wisniewski, C., Grasmick, A., 2004. Membrane bioreactor fouling in sub-critical filtration conditions: A local critical flux concept. Journal of Membrane Science 229(1), 171-177.

Park, H., Kim, Y., An, B., Choi, H., 2012. Characterization of natural organic matter treated by iron oxide nanoparticle incorporated ceramic membrane-ozonation process. Water Research 46(18), 5861-5870.

Sentana, I., Puche, R.D.S., Sentana, E., Prats, D., 2011. Reduction of chlorination byproducts in surface water using ceramic nanofiltration membranes. Desalination 277(1), 147-155.

Shang, R., Goulas, A., Tang, C.Y., de Frias Serra, X., Rietveld, L.C., Heijman, S.G.J., 2017. Atmospheric pressure atomic layer deposition for tight ceramic nanofiltration membranes: Synthesis and application in water purification. Journal of Membrane Science 528, 163-170.

Shao, J., Hou, J., Song, H., 2011. Comparison of humic acid rejection and flux decline during filtration with negatively charged and uncharged ultrafiltration membranes. Water Research 45(2), 473-482.

Shim, J., Park, S., Cho, K.H., 2021. Deep learning model for simulating influence of natural organic matter in nanofiltration. Water Research 197, 117070.

Soesanto, J.F., Hwang, K.-J., Cheng, C.-W., Tsai, H.-Y., Huang, A., Chen, C.-H., Cheng, T.-W., Tung, K.-L., 2019. Fenton oxidation-based cleaning technology for powdered activated carbon-precoated

dynamic membranes used in microfiltration seawater pretreatment systems. Journal of Membrane Science 591, 117298.

Sun, M., Chu, C., Geng, F., Lu, X., Qu, J., Crittenden, J., Elimelech, M., Kim, J.-H., 2018a. Reinventing Fenton chemistry: Iron oxychloride nanosheet for pH-insensitive H_2O_2 activation. Environmental Science & Technology Letters 5(3), 186-191.

Sun, S., Yao, H., Fu, W., Hua, L., Zhang, G., Zhang, W., 2018b. Reactive Photo-Fenton ceramic membranes: Synthesis, characterization and antifouling performance. Water Research 144, 690-698.

Voigt, I., Richter, H., Stahn, M., Weyd, M., Puhlfürß, P., Prehn, V., Günther, C., 2019. Scale-up of ceramic nanofiltration membranes to meet large scale applications. Separation and Purification Technology 215, 329-334.

Wadekar, S.S., Vidic, R.D., 2018. Comparison of ceramic and polymeric nanofiltration membranes for treatment of abandoned coal mine drainage. Desalination 440, 135-145.

Walther, C., Büchner, S., Filella, M., Chanudet, V., 2006. Probing particle size distributions in natural surface waters from 15 nm to 2 μm by a combination of LIBD and single-particle counting. Journal of Colloid and Interface Science 301(2), 532-537.

Wibisono, Y., Yandi, W., Golabi, M., Nugraha, R., Cornelissen, Emile R., Kemperman, A.J.B., Ederth, T., Nijmeijer, K., 2015. Hydrogel-coated feed spacers in two-phase flow cleaning in spiral wound membrane elements: A novel platform for eco-friendly biofouling mitigation. Water Research 71, 171-186.

Xu, H., Xu, M., Li, Y., Liu, X., Guo, L., Jiang, H., 2018. Characterization, origin and aggregation behavior of colloids in eutrophic shallow lake. Water Research 142, 176-186.

Yang, X.-J., Xu, X.-M., Xu, J., Han, Y.-F., 2013. Iron oxychloride (FeOCl): An efficient Fenton-like catalyst for producing hydroxyl radicals in degradation of organic contaminants. Journal of the American Chemical Society 135.

Yao, P., Choo, K.-H., Kim, M.-H., 2009. A hybridized photocatalysis–microfiltration system with iron oxide-coated membranes for the removal of natural organic matter in water treatment: Effects of iron oxide layers and colloids. Water Research 43(17), 4238-4248.

Zazouli, M.A., Susanto, H., Nasseri, S., Ulbricht, M., 2009. Influences of solution chemistry and polymeric natural organic matter on the removal of aquatic pharmaceutical residuals by nanofiltration. Water Research 43(13), 3270-3280.

Zhang, X., Bai, R., 2003. Mechanisms and kinetics of humic acid adsorption onto chitosan-coated granules. Journal of Colloid and Interface Science 264(1), 30-38.

Zhao, Y.-y., Wang, X.-m., Yang, H.-w., Xie, Y.-f.F., 2018. Effects of organic fouling and cleaning on the retention of pharmaceutically active compounds by ceramic nanofiltration membranes. Journal of Membrane Science 563, 734-742.

Zhao, Y., Kitajima, R., Shirasaki, N., Matsui, Y., Matsushita, T., 2020a. Precoating membranes with submicron super-fine powdered activated carbon after coagulation prevents transmembrane pressure rise: Straining and high adsorption capacity effects. Water Research 177, 115757.

Zhao, Y., Lu, D., Xu, C., Zhong, J., Chen, M., Xu, S., Cao, Y., Zhao, Q., Yang, M., Ma, J., 2020b. Synergistic oxidation-filtration process analysis of catalytic $CuFe_2O_4$-Tailored ceramic membrane filtration via peroxymonosulfate activation for humic acid treatment. Water Research 171, 115387.

Zhu, L., Wang, W., Zhao, P., Wang, S., Yang, K., Shi, H., Xu, M., Dong, Y., 2022. Silicon carbide catalytic ceramic membranes with nano-wire structure for enhanced anti-fouling performance. Water Research 226, 119209.

Chapter 6

CONCLUSIONS AND OUTLOOK

6.1 Conclusions

In this thesis, studies were conducted on the efficacy and mechanisms of using Fenton-based oxidation for cleaning ceramic nanofiltration (NF) membranes, in relation to their fouling characteristics during filtration with a model biopolymer (alginate) solution and real surface water. A reactive Fenton catalyst layer was pre-coated on top of a commercial ceramic NF membrane by means of crossflow pre-filtration of an iron oxide (Fe_3O_4) or iron oxychloride (FeOCl) suspension. Adsorption (in the absence of a permeate flow) and constant-pressure filtration (with a permeate flow) experiments with the alginate solution were performed to distinguish between decreases in permeance as a result of adsorptive or cake layer fouling. A sole hydrogen peroxide (H_2O_2) solution or hybrid H_2O_2/oxalic acid solution was used during crossflow cleaning of the pre-coated membrane. For the bench-scale application, filtration performance of the pre-coated membrane in combination with Fenton cleaning was evaluated during direct surface water treatment in a constant-flux filtration mode.

Overall, it can be concluded that ceramic NF membranes, having the iron-based catalyst pre-coat layer (i.e. Fe_3O_4 and FeOCl) on the surface of the membranes, were able to effectively remove the fouling, formed by the highly concentrated alginate model solution or natural organic matter (NOM)/colloids in the surface water, on/in the pre-coated membranes by Fenton cleaning. However, the cleaning efficacy was closely related to fouling types (i.e. adsorptive and cake layer fouling) and characteristics of the pre-coated membranes. The cake layer fouling was almost fully removed by Fenton cleaning, while the adsorptive fouling was only partially removed. However, the latter did not influence the long-term performance of the ceramic NF. A combination of Fenton oxidation and oxalic acid relaxation over the fouling layers improved the cleaning efficacy, as a result of potentially enhanced diffusion of H_2O_2 through the fouling layers onto the active sites of the catalyst pre-coat layer. The FeOCl pre-coated ceramic NF membrane was proved applicable in direct surface water treatment in terms of both rejection of NOM and Fenton cleaning.

The specific conclusions with respect to the research questions proposed in Chapter 1 are as follows:

What is the current understanding of fouling characteristics of ceramic membranes and effect of oxidation on fouling mitigation?

The state-of-the-art knowledge on surface interactions in relation to fouling characteristics of ceramic membranes in water treatment and effect of oxidation on fouling mitigation of the

membranes, was reviewed and discussed in Chapter 2. It was concluded that oxidation of organic matter in feed water can mainly mitigate reversible fouling of ceramic membranes while in many cases being ineffective for irreversible fouling, depending on the whole change of different surface interactions between the organic matter and the membranes. However, the present knowledge is mainly limited to microfiltration and ultrafiltration processes, while a clear understanding of fouling characteristics during ceramic NF in water treatment is still lacking. In addition, available studies about using oxidation methods for fouling mitigation of ceramic membranes were predominantly focused on oxidation of organic matter in the feed water, which has a risk of secondary pollution due to a potential passage of the oxidants and/or oxidation by-products into the permeate. Very little attention has been paid to using (catalytic) oxidation during cleaning of, in particular, ceramic NF membranes. Therefore, in future studies, efficacy and mechanisms of applying oxidation for cleaning a ceramic NF membrane, need to be studied based on an in-depth understanding of fouling characteristics of the membrane.

How to improve the efficacy of Fenton cleaning over an alginate fouling layer on ceramic NF membranes?

Chapter 3 describes a synergistic method of integrating oxalic acid chelation and Fe_3O_4-activated Fenton oxidation for cleaning persistent alginate fouling of the ceramic NF membranes. A synergistic effect of oxalic acid relaxation and Fenton oxidation over the alginate fouling layer was found to play a key role in the removal of the fouling layer, presumably attributed to an enhanced mass transfer of H_2O_2 at the interface between the iron-oxide pre-coat layer and the fouling layer. Cleaning of the iron-oxide pre-coated membrane with the oxalic acid/H_2O_2 solution for 15 min achieved stable initial normalized fluxes (83.33–90.15%) during five filtration/cleaning cycles, with no need of refreshing the pre-coat layer between the cycles.

How is Fenton cleaning related to fouling types of ceramic NF membranes?

The efficacy of Fenton cleaning of the FeOCl pre-coated ceramic NF membrane, in relation to its different fouling types during filtration with the alginate solution, was investigated in Chapter 4. The results imply that the flux evolution could be divided into an initial sharp flux decline, due to rapid adsorption of the foulants (i.e. adsorptive fouling), and a subsequent gradual flux decline, resulting from progressive cake build-up on the membrane (i.e. cake layer fouling). The efficacy of Fenton cleaning was predominantly dependent on the thickness of the cake layer fouling (above the adsorptive fouling layer), where the flux recovery at the thin cake fouling (98.5%) was higher than at the thick cake fouling (65.4%). During multiple adsorption (without a permeate flux)/cake build-

up (at a relatively high flux)/Fenton cleaning cycles, Fenton cleaning was mainly effective for the cake layer fouling compared to the adsorptive fouling. However, the total permeate production during ceramic NF was not influenced by the remaining adsorptive fouling (after cleaning), since the adsorptive fouling always only occurs at the beginning of each cycle. As such, the removal of the adsorptive fouling was of minor importance for the overall performance of the pre-coated ceramic NF membrane using Fenton cleaning.

What are the fouling characteristics and Fenton cleaning efficacy of ceramic NF membranes in direct surface water treatment?

A bench-scale application of the FeOCl pre-coated ceramic NF membrane for direct surface (canal) water treatment in combination with Fenton cleaning, was described in Chapter 5. The fouling during ceramic NF was affected by the pre-coat layer and the feed pH (8.5 and 7.0), while the extents varied depending on adsorption capabilities of the membrane under the individual conditions. The FeOCl layer was uniformly pre-coated on top of the membrane by means of crossflow pre-filtration with a FeOCl suspension, only causing a minimal decrease (<4%) of the membrane permeance. A large-sized fraction (3–30 μm) of the colloids in the canal water, in combination with an operating flux of about 46 L m^{-2} h^{-1}, contributed to faster pore clogging in the pre-coat layer than in the pristine membrane. However, the pristine and pre-coated membranes fouled comparably when filtering the canal water at a flux of around 23 L m^{-2} h^{-1}. The catalytic pre-coat layer facilitated the restoration of filtration resistances of the fouled membrane through Fenton cleaning, while the separation layer of the membrane maintained high rejections (approximately 90%) of the NOM, measured as dissolved organic carbon and UV absorbance at 254 nm, over five one-day fouling/cleaning cycles. The pre-coat layer remained reproducible over the five long-running cycles, having a minor loss of 15.6% in its thickness.

6.2 Outlook and recommendations for future research

6.2.1 Potential of catalyst pre-coated ceramic NF membranes for direct water treatment and de-fouling using Fenton cleaning

Conventional drinking water treatment consists of multiple treatment stages including coagulation, sedimentation, filtration and disinfection, causing a large footprint and complicated operations (Ho et al., 2012; Köhler et al., 2016). This thesis provides a single-step, chemical-free ceramic NF method, as a potential alternative, for direct treatment of surface water sources (without pre-treatment), aiming at more compact design of an advanced water supply system than that of the conventional

multi-stage systems. The process, using a catalyst pre-coat layer on top of a ceramic NF membrane, effectively recovers the filtration resistance of the membrane through Fenton cleaning, while the active layer of the membrane maintains a high rejection of NOM via size exclusion. As proved in this thesis, Fenton cleaning of the catalyst pre-coated ceramic NF membranes was also effective for removing the organic fouling formed by the highly concentrated alginate solution up to 0.8 g L^{-1}. Therefore, it is hypothesised that the catalyst pre-coated ceramic NF membranes, in combination with Fenton cleaning, can even be a potential process for direct treatment of wastewaters with a high organic loading, making direct treatment from municipal wastewater to, e.g. industry water in one step possible.

6.2.2 Modification of ceramic NF membranes with better anti-fouling abilities

Rapid adsorption of organic foulants onto (catalyst pre-coated) ceramic NF membranes at the beginning of filtration with a fouling solution has been found to play a key role in an initial permeance decline, leading to a considerable reduction in water production (Chapter 4). It remains, however, yet unknown what type of surface interactions result in the rapid adsorption and how it can be reduced or avoided during ceramic NF. Therefore, identification of the key surface interactions causing the rapid adsorption is still needed. On this basis, during the preparation of catalytic ceramic NF membranes, nano-engineering methods for modifying the surface (e.g. functionality) of the membranes, in order to reduce the adsorption capabilities of the membranes toward foulants, should be studied. As an example, recent research reported that grafting the surface of ceramic NF membranes with non-polar functional groups (e.g. methyl, phenyl and propyl groups) could reduce adsorption of organic matter onto the membranes, while, in the meantime, substantially decreasing the permeance of the membranes (Mustafa et al., 2016a; b; Mustafa et al., 2014).

6.2.3 Improvement of stability of catalysts on/in ceramic NF membranes

By pre-coating ceramic NF membranes with an FeOCl catalyst layer through a crossflow pre-filtration method, around 15% of the particles leached from the pre-coat layers after five one-day filtration/cleaning cycles (Chapter 5). As a result, the pre-coat layer, even without chemical bonding to the membrane surface, was able to resist hydraulic scouring to a large extent caused by a cross flow during filtration. However, the reason for that has not been answered in this thesis, which makes it hard to know how to optimize the pre-coating processes for obtaining a more hydraulically stable pre-coat layer on the membranes. Therefore, the resistance of the pre-coat layer on the membranes against hydraulic scouring during crossflow filtration needs to be further studied in terms of possible

influencing factors, such as sizes and geometric shapes of catalyst particles and operational conditions (e.g. transmembrane pressures and crossflow velocities) during pre-coating. In addition, to further improve the stability of catalysts on/within ceramic NF membranes, methods for immobilizing the catalysts on the surface and/or within the pores of the membranes should be studied.

6.2.4 Development of catalytic ceramic NF membrane reactors

During ceramic NF of surface water, a fraction of organic molecules (about 10%) passed through the membrane, and the rejection of salts (measured as conductivity) was also low (<30%) (Chapter 5). Therefore, for further enhancing the removal of small-sized organics, which can penetrate the membrane, catalytic oxidation reactions within the inner pores of the membrane should be developed through immobilizing nano-sized Fenton catalysts inside the membrane pores. Based on this kind of design of the catalytic ceramic NF membrane reactor, the membrane is expected to selectively expose small-sized organics to $^{\bullet}$OH radicals within the pores under confinement, while rejecting large-sized organic molecules and/or colloids on the surface of the membrane (Zhang et al., 2021). This may broaden the application of the catalytic ceramic NF membrane for advanced treatment of organic pollutants (e.g. organic micropollutants).

References

Ho, L., Braun, K., Fabris, R., Hoefel, D., Morran, J., Monis, P., Drikas, M., 2012. Comparison of drinking water treatment process streams for optimal bacteriological water quality. Water Research 46(12), 3934-3942.

Köhler, S.J., Lavonen, E., Keucken, A., Schmitt-Kopplin, P., Spanjer, T., Persson, K., 2016. Upgrading coagulation with hollow-fibre nanofiltration for improved organic matter removal during surface water treatment. Water Research 89, 232-240.

Mustafa, G., Wyns, K., Buekenhoudt, A., Meynen, V., 2016a. Antifouling grafting of ceramic membranes validated in a variety of challenging wastewaters. Water Research 104, 242-253.

Mustafa, G., Wyns, K., Buekenhoudt, A., Meynen, V., 2016b. New insights into the fouling mechanism of dissolved organic matter applying nanofiltration membranes with a variety of surface chemistries. Water Research 93, 195-204.

Mustafa, G., Wyns, K., Vandezande, P., Buekenhoudt, A., Meynen, V., 2014. Novel grafting method efficiently decreases irreversible fouling of ceramic nanofiltration membranes. Journal of Membrane Science 470, 369-377.

Zhang, S., Hedtke, T., Zhu, Q., Sun, M., Weon, S., Zhao, Y., Stavitski, E., Elimelech, M., Kim, J.-H., 2021. Membrane-confined iron oxychloride nanocatalysts for highly efficient heterogeneous Fenton water treatment. Environmental Science & Technology 55(13), 9266-9275.

ACKNOWLEDGEMENT/致谢

By having the ambitious thought of being a future expert in water treatment, I came to the Netherlands in October 2017, and started my journey as a PhD candidate in TU Delft. The five-year stay in the Netherlands is not only a journey of knowledge learning, but also an experience of touching the fascinating culture of this country. These experiences are valuable memories that will be kept in my mind, forever, as strong power supporting my future career and life. Now, it is time to show my gratitude to all of you who made my stories in the Netherlands happen.

First of all, I would like to express my thanks to my promotors, Bas Heijman and Luuk Rietveld, for enrolling me in TU Delft and sharing knowledge with me. Bas always comes up with smart ideas and suggestions when I encountered problems in my research. I am impressed by his timely presence in the Waterlab for discussing my experiments with me. Luuk often provides very careful and detailed revision of my papers and criticizes my research from a high point of view. His critical mind in doing research makes me always think if I can lead my research toward a more meaningful and practical direction in the field of water treatment. I sincerely thank them for keeping me on track with my research, no matter when confusion and difficulties confronted me.

My deep gratitude should also go to Lu Yao, as my master student, for her great contributions to a part of my experiments, even during the tough period of the COVID-19 pandemic. I am impressed by her careful attitude in doing experiments. I have learned from her when she positively searched for solutions to experimental problems even if difficulties appeared constantly.

I am very grateful for the assistance of the staff in the Waterlab and in the Water Management department. Many thanks to Armand, Jane and Patricia for your kind coaching for properly using the experimental devices in the Waterlab. I appreciate the help of Mariska and Riëlle for timely arranging some daily stuffs for me, which largely saved my time for focusing on my research. I also want to own my thanks to Ran, Franca and Irene, as the early pioneers in our membrane research group. Without the generous sharing of their knowledge and experience with me, it would be more difficult to carry out my research on the right track. Thank my officemates: Emiel, Daniel, Lenno, Sara, Carina, Antonella, Bruno, Javier, Diana, Lihua, and Yuke, and Chinese friends: Zhe, Tianlong, Hongbo, Xuedong, Hongxiao, Nan, Zheyi, Ka Laung, Feifei, Peng, Cuijie, Liangfu, etc. It is the happy time with you making me feel at home and have the amazing memories in the Netherlands. I also appreciate the accompany from Shuo, Max and Mingliang, as we are "comrades-in-arms" in the same research group. It is my valuable memories to stay with you and to share the moments of excitement and depression during my study and life in the Netherlands.

Last but not the least, my deepest gratitude should go to my family. Your unconditional love and accompany are the origin of power, supporting me to go ahead on the way of pursuing happiness and dream.

感谢我的家人在我无数个艰难时刻的陪伴与守护，你们的鼓舞与不弃赋予了我在追求学业的道路上披荆斩棘的信心和勇气。

Bin LIN

Nanjing, 13th March, 2023

CURRICULUM VITAE

Personal information

Bin Lin（林斌）was born in Huangshan, China, on August 29, 1991. He had his four-year (9/2010−6/2014) bachelor study at Anhui University of Science and Technology, and had his three-year (9/2014−6/2017) master study in the School of the Environment, Nanjing University, both majoring in Environmental Engineering. He started his doctoral program in Water Management department at Delft University of Technology on October 25, 2017, working on the topic of fouling and Fenton cleaning of ceramic nanofiltration membranes in water treatment, under the supervision of Prof. Luuk Rietveld and Dr. Bas Heijman. Since then, he was dedicated to his research on catalytic ceramic nanofiltration for direct surface water treatment and Fenton cleaning.

Publication list

[1] **B. Lin**, S.G.J. Heijman, R. Shang, L.C. Rietveld, Integration of oxalic acid chelation and Fenton process for synergistic relaxation-oxidation of persistent gel-like fouling of ceramic nanofiltration membranes, Journal of Membrane Science 636 (2021) 119553.

[2] **B. Lin**, Y. Zhang, F. Shen, L. Zhang, D. Wang, X. Tang, Y. Zhou, X. Nie, L. Lv, W. Zhang, M. Hua, B. Pan, New insights into the fractionation of effluent organic matter on diagnosis of key composition affecting advanced phosphate removal by Zr-based nanocomposite, Water Research 186 (2020) 116299.

[3] **B. Lin**, M. Hua, Y. Zhang, W. Zhang, L. Lv, B. Pan, Effects of organic acids of different molecular size on phosphate removal by HZO-201 nanocomposite, Chemosphere 166 (2017) 422-430.

[4] X. Zhang, L. Zhang, Z. Li, Z. Jiang, Q. Zheng, **B. Lin**, B. Pan, Rational design of antifouling polymeric nanocomposite for sustainable fluoride removal from NOM-rich water, Environmental Science & Technology 51 (2017) 13363-13371.

[5] **B. Lin**, L.C. Rietveld, L. Yao, S.G.J. Heijman, Adsorption and cake layer fouling in relation to Fenton cleaning of ceramic nanofiltration membranes, Journal of Membrane Science, under review.

[6] **B. Lin**, S.G.J. Heijman, L.C. Rietveld, Iron oxychloride pre-coated ceramic nanofiltration membrane for direct surface water treatment: Fouling analysis and Fenton cleaning, to be submitted.

[7] **B. Lin**, S.G.J. Heijman, L.C. Rietveld, Effect of oxidation on surface interactions in relation to fouling behaviour of ceramic membranes: a review, In preparation.